# Human Embryonic Stem Cells as a Predictive Model for Developmental Toxicity and Disease:

***Reducing the use of animal testing in regulatory toxicology***

Tyler Eng, MSc. Candidate

A thesis submitted in partial fulfillment of the requirements for the Master's in Biology, Specialization in Chemical and Environmental Toxicology

uOttawa

Department of Biology

Faculty of Science

University of Ottawa

© Tyler Eng, Ottawa, Canada, 2023

# Abstract

The recent expansion in chemical and manufacturing and innovation has led to a large influx of chemicals to the market, and subsequent release into the environment. Many of these new chemicals, as well as legacy chemicals are untested for their potential developmental toxicity, especially in early embryonic stages. This creates a need for a timely and cost-effective method for screening these chemicals. Furthermore, advances in *in vitro* methods and human pluripotent cell culturing techniques have revealed some weaknesses in our current animal model-based paradigms. Here we tested an *in vitro* model for developmental toxicity screening using human embryonic stem cells (hESCs) for environmental chemicals. In this study, hESCs were exposed to three known developmental toxicants that are prevalent in the environment, bisphenol A (BPA), perfluorooctane sulfonate (PFOS), or lead chloride ($PbCl_2$), at environmentally relevant concentrations of 0-2500 µg/L, 0-2275 µg/L, and 0-6200 µg/L respectively, for 6-days. hESCs were evaluated for dose responses on proliferation level by assaying cell viability, mitochondrial dehydrogenase activity (MDHA), cell confluency, and cell cycle distribution. Differentiation capability was assayed by induction of differentiation into ectoderm, mesoderm, and endoderm; hESCs and differentiated cells were then sequenced for their full transcriptome. Gene expression effects were analyzed by a single cell transcriptome sequencing and analysis of global DNA methylation. Proliferation and methylation effects were tested for all 3 chemicals, while differentiation and single cell sequencing was only tested on $PbCl_2$. Our results show hESCs were able to identify known and novel proliferation effects of BPA, PFOS, and $PbCl_2$, reflect differentiation level effects of $PbCl_2$, and elucidate molecular level drivers of these toxic effects. We also showed that hESCs responded to developmental toxicants at lower doses than *in vivo* models. In conclusion, our hESC-based model could act as an effective developmental toxicity screening tool for pre- peri- and post-implantation stages of embryo development.

# Acknowledgments

I would like to express my deepest appreciation to Dr. Laurie Chan and Dr. Dawn Jin for their academic mentorship and support during my degree. Additionally, many thanks to my thesis committee and chair: Dr. Jenny Bruin, Dr. Jan Mennigen, and Dr. Mark Ekker. Thanks should also go to Christopher Porter for his contribution to this thesis. Lastly, I'd like to mention the support of the Chan Lab and the RTRD teams for their support during my degree.

# Table of Contents

# List of Abbreviations

BPA: Bisphenol-A

ECVAM: European Commission for the Validation of Alternative Methods

EST: Embryonic stem cell test

GD: Gestation day

GM: Geometric mean

hESCs: Human embryonic stem cells

MDHA: Mitochondrial dehydrogenase activity

Pb: Lead

$PbCl_2$: Lead chloride

PBMC: peripheral blood mononuclear cells

PFOS: Perfluorooctane sulfonate

XCI: X-chromosome inactivation

# List of Figures

# List of Tables

# Introduction

The 21st-century world has evolved into a period of great innovation for the development of new chemical compounds. Each year, thousands of new chemicals are released into environment, which will eventually end up in food and drinking water (Kristiansson et al. 2021). However, their potential developmental and health effects remain unclear. Although many existing chemicals have been studied for developmental toxicities, there is still a lack of knowledge of their effects on early embryo development such as the blastocyst stage. To maintain a standard of human safety, extensive and costly testing must be undertaken for new compounds being introduced to the market (Grandjean and Landrigan 2014). Wherein *in vivo* and/or *in vitro* testing occurs (Chapin et al. 2008). Much of this is *in vivo* animal experimentation. However, there are several shortcomings of animal experimentation from the perspective of human health and safety.

The first of these shortcomings is the species difference in the pathogenic process and consequences of chemical exposure. This can lead to a difference in mechanism and adverse outcomes between animals and humans (Bracken 2009; Rydell-Törmänen and Johnson 2019; Shanks, Greek, and Greek 2009). For example, *in vitro* cultures of Sprague-Dawley rat hepatocytes had significant differences in the clearance and metabolism of chlorinated BPA when compared to human hepatocytes (Plattard et al. 2022).

Another disadvantage of *in vivo* testing is the immense financial cost of performing large-scale animal tests. In 2009, the United States spent approximately $12 billion on animal experiments (Akhtar 2012). Whereas it is generally accepted in the scientific community that

a tiered screening method, that uses *in vitro* preliminary screening would be much more cost-effective and timely as opposed to purely animal experimentation (Krewski et al. 2010) Moreover, in furthering our goal of achieving principles of replacement, reduction, and refinement of animal use in science, championed by Russell & Burch in 1959 (Russel and Burch 1959), we are obligated to investigate alternatives to the use of animals in studying toxicology.

New modern paradigms in toxicity testing are rapidly advancing, exposing these gaps and weaknesses of current standards (Krewski et al. 2010). New advances in cellular, molecular, and genomic analyses have created new opportunities for investigating toxicity mechanisms (Choudhuri et al. 2018). In a 21$^{st}$-century toxicity testing framework, these new mechanistic levels are integrated into a toxicity pathway that assumes less uncertainty than traditional animal models in risk assessment (Adeleye et al. 2015). Additionally, these new models provide higher throughput and cost-effectiveness compared to many current standards (Bhattacharya et al. 2011; Buick et al. 2021).

We have long since discovered the vulnerabilities to chemical toxicity during the developmental phase and its life-long impacts (National Research Council 2000). However, many environmental chemicals, that are considered safe for adult exposure remain unknown in hazards for children, the developing embryo and fetus (Louis et al. 2011). Regulatory bodies have been facing the challenge to adapt their standards to rectify this. To ensure public health and safety, many chemicals remain to be screened for developmental toxicities. To accomplish this, a fast and cost-effective screening method must be developed. This role could be filled using human embryonic stem cell (hESC) modelling. hESCs have been available for research for several decades. Interest in their use in therapeutics has led to vast investments in research. More recently, hESCs have seen significant usage in drug testing and toxicology research (Ilic and Ogilvie 2017).

A model for the screening of developmental toxicity has been previously designed using murine embryonic stem cells at the tail end of the 20th century (Scholz et al. 1999). This model was validated by the European Committee for the Validation of Alternative Methods (ECVAM) as being able to identify developmental toxicity in compounds that had known developmental effects *in vivo* (Spielmann et al. 2004). This model used cell proliferation, differentiation into cardiac cells, and proliferation of fibroblasts as endpoints. These endpoints alone are not descriptive enough to identify mechanisms or create an adverse outcome pathway. To bring this model into the 21$^{st}$-century paradigm, additional endpoints for genomic, proteomic, and molecular biomarkers have been recommended (Seiler et al. 2004). Furthermore, using mouse stem cells creates uncertainty for human health in risk assessment (Krewski et al. 2010).

In this thesis, I have attempted to develop and validate an early developmental toxicity screening model using hESCs as an alternative to animal *in vivo* or *in vitro* models. I have used this model to screen the toxicity of three environmentally relevant chemicals: $PbCl_2$, BPA, and PFOS. These chemicals have been shown to cause developmental harm in humans and pose a health risk to Canadians (Arbuckle et al. 2014; Fillion et al. 2014; Juric et al. 2018; Ostertag et al. 2009). Additionally, these chemicals were selected because they have not yet been studied using hESCs, thus creating a research gap. Furthermore, each of the three chemicals represents a different mode of toxic action. BPA is a known endocrine disruptor, that can affect neonate survival, metabolism, sex differentiation, and behavior (Golub et al. 2010). PFOS is an industrial surfactant, that can affect metabolism, insulin cycling, oxidative stress, and lung development (Lau, Butenhoff, and Rogers 2004). $PbCl_2$ toxicity is characterized by acute mortality, neurotoxicity, and behavioral changes (Claudia Gundacker, Forsthuber, et al. 2021). Thus, we want to observe whether hESCs can reflect

different types of developmental toxicity, and if they are able to propose mechanisms that support the known apical toxic endpoints.

## Study Design Rational

This thesis documented the design of a list of experiments to establish a novel screening protocol using hESCs to identify the potential for early developmental toxicity of the 3 reference contaminants based on the murine embryonic stem cell test (EST) developed by Scholz et al.. The EST uses *in vitro* cultures of two mouse cell lines: murine fibroblasts and murine embryonic stem cells. This test uses 2 endpoints to categorize the embryotoxicity of the compound. Those endpoints are: growth inhibition, and inhibition of differentiation (H. Liu et al. 2017; Scholz et al. 1999). The EST model used the 50% response point as a marker for embryotoxicity in all three of its parameters. Thus, the $IC_{50}$ is the assumed threshold for the detection of potential for apical developmental toxicity (Scholz et al. 1999). In the following hESC based developmental toxicity screening protocol, I have used the same over-arching endpoints as the EST (Figure 1). Those being, inhibition of proliferation and inhibition of differentiation. I have also added transcriptomics and epigenetic markers to elucidate the mechanism, as suggested by Seiler et al.. $PbCl_2$ was chosen to investigate the molecular mechanisms of early embryo toxicity using an up-to-date technology: single cell RNA sequencing, in undifferentiated hESCs. Additionally, whole genome next generation sequencing, in hESCs differentiating into three germ layers. This is to determine if the $PbCl_2$ can exert toxic effects through similar or different modes of actions as what has been reported in animal and other *in vitro* models.

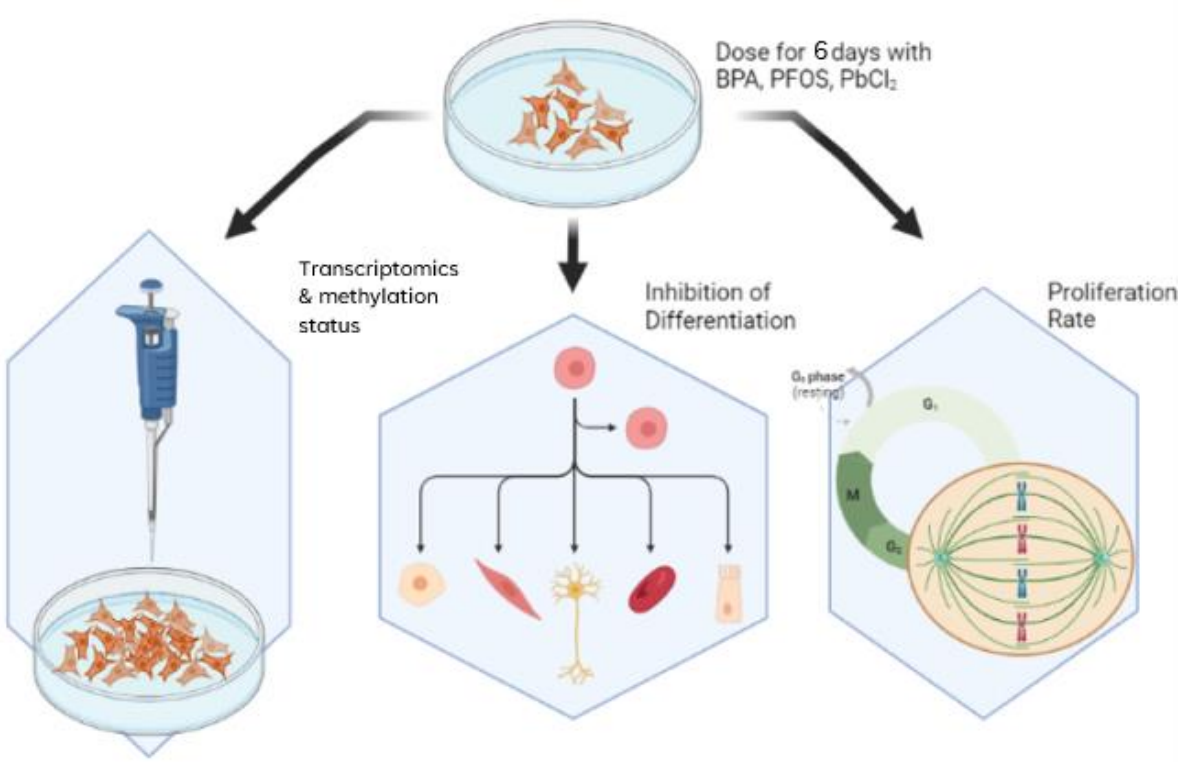


*Figure 1*: The study design of the hESC-based developmental toxicity screening model. This shows the 3 endpoints selected based on the EST with recommended modifications for transcriptomics.

# Literature review

## Human Embryonic Stem Cells (hESCs)

hESCs were first derived from *in vitro* fertilized embryos in 1998. These cells were extracted from the inner cell masses of blastocyst-stage embryos (Thomson et al. 1998). hESCs are pluripotent, and capable of differentiating into the 3 major germ layers: endoderm, mesoderm, and ectoderm. This can occur in serval ways, such as random or directed differentiation of *in vitro* cultures (Odorico, Pedersen, and Zhang 2005). hESCs are also capable of indefinite self-renewal in the undifferentiated state. This action is modulated by the β-catenin protein in hESCs (H. Kim et al. 2013). hESCs can be used *in vitro* to represent the developing embryo in the pre-implantation, implantation, and early post-implantation

phases of development. In these phases, human embryos consist significantly of embryonic stem cells with consistent properties (Giritharan et al. 2011).

hESCs have several major advantages over other types of *in vitro* subjects. The first of which is that: much like how live animals differ mechanistically from humans, so too will animal cell cultures react differently from human cells (Jennings 2015). Additionally, embryonic stem cells can proliferate swiftly and be cultured for indefinite generations (S. Liu, Yin, and Faiola 2017). Additionally, *in vitro* testing allows for more replicates, giving additional statistical power to the model (Sogorb et al. 2014). Finally, hESCs are pluripotent and can be differentiated into many different cell and tissue types, allowing them to be used in the testing of many different bodily systems (Englund, Sartipy, and Hyllner 2011).
The hESC system being used for this study was developed in our lab by Bai Li, a doctoral candidate. It has been used to study the early developmental toxicity of methylmercury (MeHg). The results detected several adverse responses from nanomolar level concentrations of MeHg. The conclusions of the studies reported that low dose toxicity of MeHg and chemical mixtures could be detected *in vitro* by hESCs, and that this suggests potential for embryotoxicity in the pre-, during, and post-implantation stages (B. Li et al. 2021, 2023; B. Li, Jin, and Chan 2023).

## Bisphenol-A

BPA is an organic synthetic compound with the chemical formula $C_{15}H_{16}O_2$. It is a colorless solid that belongs to the group of chemicals known as bisphenols, characterized by having two hydroxyphenyl functional groups. BPA has a molecular weight of 228.29 g/mol and an octanol-water partition coefficient of 3.3. The vapor pressure of BPA is very low, at $4.0 \times 10^{-8}$ mmHg at 25°C (Borrirukwisitsak, Keenan, and Gauchotte-Lindsay 2012). These properties give BPA a high affinity for tissues and sediments. BPA is widely used in the production of polycarbonate plastics and epoxy resins, making it a common component in

consumer products such as food and beverage containers, dental sealants, and thermal paper receipts (Hahladakis, Iacovidou, and Gerassimidou 2023). BPA can find its way into the environment through the disposal of these products, industrial processes, and landfills, leading to its presence in water bodies, soil, and air. The concentration of BPA in the Canadian environment varies by source. Wastewater influent ranges from 34 ng/L to 8000 ng/L, with a median of 400 ng/L (Gewurtz et al. 2021). In untreated landfill leachate, BPA concentrations ranged from 3390 to 1,940,000 ng/L, with a median of 127,500 ng/L (Gewurtz et al. 2021). Canadian surface water samples range in concentration from 3.05 to 1888.51 ng/L BPA (Lalonde and Garron 2020). Human exposure to BPA primarily occurs through dietary sources, as it can leach into food and beverages stored in BPA-containing containers or packaged with BPA-based coatings. Additionally, limited exposure can happen through inhalation in industrial settings, dermal contact with BPA-containing materials, and indirect exposure from dust particles in indoor environments (Hahladakis, Iacovidou, and Gerassimidou 2023).

BPA is rapidly conjugated and excreted in the body. However, maternal transfer through the placental barrier has been demonstrated. Since the predominant exposure route of BPA is ingestion, rate of oral exposure can be translated to fetal exposure. In a study where human participants were given a single dose of 100 µg/kg bw BPA, mean serum total was 390 ng/mL BPA (Thayer et al. 2015). Meanwhile, in a separate study, human placental transfer rate from maternal blood to cord blood was calculated to be a ratio of 1.94 (Zhang et al. 2020). However, transfer rates are related to genetics and highly species dependent (Claudia Gundacker, Graf-Rohrmeister, et al. 2021). For example, Wistar rats given 125 µg/kg bw/day BPA for 35 days, had an average serum concentration of 1130 ng/mL BPA (Kazemi et al. 2016). Additionally, placental transfers in rats was only 0.09% of the maternal blood (Nishikawa et al. 2010).

To confirm if the hESC toxicity screening model can accurately identify the early developmental toxicity of BPA, an understanding of the toxic effects detailed in the published scientific literature must be outlined. Generally, the developmental toxicity of BPA in the literature is focused on BPA's ability to act on estrogenic pathways. Specifically, BPA-induced developmental toxicity endpoints are: embryo, fetal, and neonatal endpoints; postnatal growth; immune responsiveness; effects on sex differentiation of the brain and behavior; and developmental neurobehavioral toxicity. (Golub et al. 2010)

The developmental toxicity effects of BPA on embryo, fetal, and neonatal endpoints are outlined in a number of *in vivo* studies carried out on mice and rats. In a study by Tyr et al. (1987), pregnant CD rats were given 0, 160,320, or 640 mg/kg day of BPA and pregnant CD-l mice 0,500,750,1000, or 1250 mg/kg day of BPA, both by gavage. Exposure took place from gestation day (GD) 6-15. Researchers found that mice exposed to BPA in the 1250 mg/kg/day group showed a significant reduction in gravid uterine weight and average fetal body weight (Morrissey et al. 1987).

An additional study of the developmental effects of BPA was carried out on pregnant Sprague-Dawley rats from GD 1-20. BPA was administered by gavage at 0, 100, 300, and 1000 mg/kg per day. The fetuses were extracted by cesarean section on day 21. Fetuses were examined for external, visceral and skeletal abnormalities. In the 1000 mg/kg day group, an increase in pregnancy failure was found in the successfully mated females. Additionally, increased number of embryonal deaths, increased post-implantation loss, reduced litter size and fetal body weight, and decreased number of fetal ossification centers in several skeletal districts were seen. Moreover, in the 300 mg/kg group, decreased food intake and reduced body weight of male fetuses were seen (J. C. Kim et al. 2001). These effects of BPA on rat and mouse pregnancy outcomes, viability, and weight are consistent with the effects of

known estrogenic compounds on rats (Bartholomeusz, Bruce, and Lynch 1999; Golub et al. 2010; Matsuura et al. 2004).

In a study by Tyl et al., Sprague-Dawley rats were given BPA as a dietary exposure at concentrations of 0, 0.015, 0.3, 4.5, 75, 750, and 7500 ppm (~0.001, 0.02, 0.3, 5, 50, and 500 mg/kg/day of BPA) for 3 generations. Ovarian weights and total pups and live pups/litter on postnatal day (PND) 0 were decreased at 7500 ppm. The study determined the reproductive and postnatal NOAELs = 750 ppm (50 mg/kg/day) (Tyl et al. 2002).

Estrogen receptor activation during development attributed to BPA has been confirmed *in vivo*. A study was conducted using transgenic mice with luciferase-coupled estrogen receptor genes. Pregnant mice were exposed to 10-10,000 µg/kg of BPA at 13.5 GD. Embryos were extracted at 8 or 24 hours. Eight hours after exposure to 1 mg/kg BPA, estrogen receptor transactivation was significantly induced in the embryos. However, when these results were compared to *in vitro* studies with luciferase-coupled estrogen receptors, *in vitro studies* reported much lower sensitivity to BPA compared to the positive control, diethylstilbestrol. This suggests that exposure in utero is more sensitive than *in vitro* assays can report (Lemmen et al. 2004).

At the gene expression level, BPA has been shown to influence the expression of a large number of genes in common with ethynyl estradiol (EE) and genistein. Pregnant Sprague- Dawley rats were given EE, genistein, or BPA from GD 11-20. The uterus and ovaries were extracted, and RNA was analyzed for 7000 genes. The study found that less than 2% of mRNA showed a 2-fold or greater change in expression. Additionally, a dose-dependent analysis of the transcript profile revealed a common set of genes whose expression is significantly and reproducibly modified in the same way by each of the 3 chemicals tested (Naciff et al. 2003). An additional study was performed on the gene expression profile of the testis. Sprague-Dawley rats were dosed via subcutaneous injection with 0.001–10 mg

EE/kg/day, 0.001–100 mg genistein/kg/day, or 0.002–400 mg BPA/kg/day from GD 11-20. Independent dose-response analyses of the three compounds identified 59 genes that are significantly modified by EE, 23 genes by genistein, and 15 genes by BPA, out of 8740, by at least 1.5-fold either up- or down-regulated. Additionally, global analyses aimed at detecting genes consistently modified by all of the chemicals identified 50 genes whose expression changed in the same direction across the three chemicals (Naciff et al. 2005). Additionally, mice were treated with 0.5–5.0 mg/kg BPA on gestational days 9–16. This resulted in a dose-responsive increase in stromal cell HOXA10 expression in 2- and 6-week-old mice exposed in utero. HOXA10 is an important upstream regulator of embryo implantation and is expressed in response to estrogen and progesterone in adult mammals (Zanatta et al. 2010).

Estrogenic effects of BPA during development have also been shown to affect oogenesis. A study conducted by Susiarjo et al. found that exposure to BPA in utero of C57BL/6 inbred strain mice caused aberrations in meiotic prophase, including synaptic defects and increased levels of recombination. In the mature female, these aberrations were translated into increased aneuploid eggs and embryos. Moreover, the same pattern of meiotic defects in the fetal ovaries of mice homozygous for a targeted disruption of ERβ was observed. Furthermore, BPA exposure elicited no additional effects in ERβ null females, suggesting that BPA exerts its effect on the early oocyte by interfering with the actions of ERβ (Susiarjo et al. 2007).

BPA has also been shown to activate other classic toxicity pathways beyond estrogenic signaling. An example of this is the activation of AhR activity. Mouse embryos were exposed in utero to 0.02, 2, 200, and 20,000 μg/kg/day of BPA and 5 μg/kg/day 17β-estradiol, used as a positive control, at 6.5– 13.5 or 6.5–17.5 days post coitum (DPC). All doses increased AhR mRNA expression in the cerebra, cerebella, and testes and ovaries of male and female mid- and late-developmental stage, 14.5- and 18.5-dpc, respectively

embryos. BPA dose-independently up-regulated the expression of AhRR and Arnt in mid- and late-stage embryos (Nishizawa, Imanishi, and Manabe 2005). In a separate study, murine embryos were exposed in utero to 2 µg/kg/day of BPA at 6.5–17.5 DPC. Retinoic acid receptor (RAR) α and retinoid X receptor (RXR) α mRNA levels were observed. In utero BPA reduced the RARα mRNA expression. Moreover, BPA significantly decreased the expression levels of RXRα mRNA in the cerebella of female embryos at 12.5, 14.5 and 18.5 DPC. In utero exposure to BPA decreased levels of RARα mRNA in testes of 14.5- and 18.5-DPC embryos, levels of RXRα mRNA in testes of 14.5-DPC-embryos, and levels of RXRα mRNA in ovaries of 14.5- DPC embryos (Nishizawa et al. 2005a). In a third study by Nishizawa et al., Gonadal mRNA expression of AhR was increased by exposure to BPA in a diphasic manner, as opposed to monotonic effects seen in previous studies (Nishizawa et al. 2005b).

Gene expression patterns can also be affected by DNA methylation status. BPA has been shown to alter the genomic methylation status during developmental windows in exposed organisms. Pregnant mice were given 20 µg/kg/ day of BPA by subcutaneous injection. Dams were exposed from GD 0-12.5 or 14.5. Fetal forebrains were extracted, and observed that low doses of BPA can cause both hyper- and hypomethylation at multiple unique loci in the developing mouse forebrain (Yaoi et al. 2008).

The developmental toxicity effects of BPA also culminate in changes to sex differentiation. In a study by Honma et al. ICR mice were given subcutaneous injections of BPA, 2 and 20 µg/kg, diethylstilbestrol, 0.02, 0.2, and 2 µg/kg or oil vehicle once daily from GD 11–17. Offspring presented vaginal opening was significantly earlier in all exposed females except for 2 µg/kg BPA females than oil controls. Furthermore, body weight at the vaginal opening was lower than controls in all exposed females. Additionally, the first vaginal estrus was earlier in all exposed females except for the 2 µg/kg BPA group females

compared to controls. Finally, anogenital distance (AGD) was significantly higher in all exposed male offspring groups at post-natal day 60 (Honma et al. 2002).

An additional effect of BPA on sexual differentiation in development is the size of the locus coeruleus and sexually dimorphic behaviors. This part of the brain is essential for regulating norepinephrine signaling to the forebrain. The locus coeruleus is typically larger in females. However, in two studies by Kubo et al., pregnant rats were exposed via a dietary route to BPA. Pups were additionally exposed to BPA through breast milk from exposed dams. Also, control female offspring showed a higher activity, a lower avoidance memory, and larger locus coeruleus than the male controls, while the BPA-exposed group did not show any sexual dimorphism between male and female offspring (Kubo et al. 2001, 2003).

BPA toxicity has been tested in several *in vitro* models to confirm mechanisms and adverse outcome pathways. BPA has been shown to affect the rate of embryo development. In a study of two-cell mouse embryos exposed to 100 pM to 100 μM of BPA, rate of blastocyst formation was affected. Findings showed that at 24 h, significantly more embryos exposed to 3 nM BPA had reached the eight-cell stage when compared to the control. Additionally, at 48 h, embryos exposed to 1 nM and 3 nM BPA increased the incidence of blastocyst formation compared to control. At 100 μM, bisphenol A decreased frequency of development to blastocysts occurred. These effects were inhibited by co-exposure to Tamoxifen, an estrogen receptor inhibitor (Takai et al. 2000). Accelerated embryo development effects of BPA were consistent in other models. In a study of medaka fish embryos, low levels of BPA accelerated early embryonic development within 24 h of exposure, attenuated body growth, and advanced the times of hatching and reproductive maturation. However, these effects were inhibited by amiodarone, a thyroid-hormone receptor antagonist (Ramakrishnan and Wayne 2008).

Several *in vitro* gene expression studies have described ER activation to be elicited by BPA in the micromolar range (Bonefeld-Jørgensen et al. 2007; Paris et al. 2002; Vinggaard et al. 2008). Moreover, HOXA10 is a gene that is also vital for uterine development. In a study of Ishikawa cells treated with 0.1 nM to 25 μM BPA, a dose-response increase in HOXA10 mRNA expression was demonstrated. To discern the molecular mechanism of BPA toxicity, the HOXA10 estrogen response element (ERE) and autoregulatory element (ARE) were tested for BPA responsiveness in Ishikawa cells. BPA increased luciferase expression from HOXA10-ERE and ARE reporter constructs (Smith and Taylor 2007).

Using *in vitro* models, SH-SY5Y cells were exposed to BPA at 0.1, 1 and 10 μM concentrations for 48 and 96 h. Exposed cells experienced a 1.3-fold increase in 5-mc% global methylation status (Senyildiz et al. 2017).

Exposure to BPA during fetal development has been demonstrated to cause perturbation of stem cell function. In a study by Calderon-Gierszal & Prins, hESCs were differentiated into prostatic organoids and exposed to 1 nM or 10 nM of BPA during differentiation. Investigators observed disturbed early morphogenesis in a dose-dependent manner, with 1 nM BPA increasing and 10 nM BPA reducing the number of branched structures formed. Additionally, the stem-like cell population increased in treated cultures, appearing as focal stem cell nests that have not properly entered lineage commitment rather than the rare, isolated stem cells found in normally differentiated cultures (Calderon-Gierszal and Prins 2015).

A further example of the effects of BPA on development is the inhibition of proliferation and differentiation of rat fetal neural stem cells. Low doses of BPA were given to pregnant rats at 4, 40, and 400 μg/kg body weight through oral gavage daily from gestational day 6 to postnatal day 21. A group of fetuses at GD 12 were sacrificed to collect neural stem cells (NSC) for culture. Postnatal day 21 pups were dissected to collect brain

samples for immunohistochemical analysis. Investigators found BPA impaired NSC proliferation and neuronal differentiation in the hippocampus and subventricular zones. It significantly altered expression/protein levels of neurogenic genes and the Wnt pathway genes in the hippocampus. BPA reduced cellular β-catenin and p-GSK-3β levels and decreased β-catenin nuclear translocation and cyclin-D1 and TCF/LEF promoter luciferase activity. Activation and inhibition of the Wnt pathway suggested the involvement of this pathway in the inhibition of neurogenesis (Tiwari et al. 2015). Similar effects of neural differentiation inhibition have been documented for mouse embryonic stem cells exposed to BPA (Yin et al. 2019) (Golub et al. 2010).

## Perfluorooctanesulfonic acid

Perflurooctanesulfonic acid (PFOS) is a polyfluorinated persistent organic pollutant (POP) with the chemical formula $C_8HF_{17}O_3S$. PFOS has a molecular weight of approximately 500.13 g/mol. PFOS is a stable, water-repellent fluorinated compound that is highly resistant to degradation, both in the environment and within living organisms. It possesses a very high octanol-water partition coefficient (log Kow) of around 8.0, signifying its strong hydrophobic character and limited solubility in water. PFOS is also characterized by a low vapor pressure, which contributes to its persistence in the environment. These unique chemical properties make PFOS popular in various industrial and consumer applications, particularly in the production of stain-resistant coatings, firefighting foams, and surface treatments. However, these same properties have raised environmental and health concerns due to PFOS's resistance to degradation, resulting in bioaccumulation in organisms and its designation as an environmental pollutant of global concern under the Stockholm Convention. (Jarvis et al. 2021; Uwayezu, Yeung, and Bäckström 2022). PFOS contamination in the environment can be found in soil, groundwater, surface water and organisms. The concentration of contamination varies widely, but tends to accumulate down stream of industrial activities or

areas where firefighting foams have been used (Choi et al. 2017; He 2023; Jarvis et al. 2021). Human exposure to PFOS is often attributed to drinking water contamination and food packaging. However, other exposure pathways such as inhalation of contaminated dust and dermal contact have also been reported (DeLuca et al. 2022). PFOS exposure has been reported as ubiquitous in the population with an average maternal blood concentration of 4.55 ng/L PFOS (Fisher et al. 2016).

PFOS has a high $k_{ow}$ and therefore, strong affinity for tissues and lipids. This gives it a strong ability to pass the placental barrier. In a paired maternal exposure study, pregnant Sprague-Dawley rats were dosed for 42 dayts prior to mating. Maternal serum concentration was 155 µg/mL in the 3200 µg/kg bw/day rats. There was high degree of correlation between maternal serum concentration of PFOS and fetus serum concentration. The concentration of fetus serum on GD21 was 164 µg/mL (Luebker, York, et al. 2005). This results in a maternal transfer ratio of approximately 1.06.

PFOS has been shown to have several toxic effects on *in vivo* neonatal development. Many of these apical toxicities culminate in a birth defect or post-natal mortality. In a study by Thibodeaux et al., Pregnant Sprague-Dawley rats were given 1, 2, 3, 5, or 10 mg/kg PFOS daily by gavage from gestational day (GD) 2 to GD 20. Additionally, CD-1 mice were similarly treated with 1, 5, 10, 15, and 20 mg/kg PFOS from GD 1 to GD 17. Fetuses were extracted, and investigators observed numerous birth defects, including cleft palate, anasarca, ventricular septal defect, and enlargement of the right atrium, were seen in both rats and mice, primarily in the 10 and 20 mg/kg dosage groups, respectively (Thibodeaux et al. 2003).

A continuation of the study by Thibodeaux et al. showed PFOS to be a driver of significant post-natal mortality. Investigators allowed exposed dams to reach parturition. All pups were born alive and appeared similar. However, in the 10 mg/kg for rat and 20 mg/kg for mouse dosage groups, the pups became pale, inactive, and moribund within 30–60 min,

and all died soon afterward. Furthermore, in the 5 mg/kg rat and 15 mg/kg mouse dosage groups, the pups also became moribund but survived between 8-12 hours. Approximately 50% of pups died at 3 mg/kg for rats and 10 mg/kg for mice. Cross-fostering the PFOS-exposed rat neonates to control nursing dams failed to improve survival, suggesting that in utero exposure is the driver of neonatal mortality. Small but significant and persistent growth lags were detected in surviving rat and mouse pups exposed to PFOS prenatally.

Moreover, delays in eye opening were noted in treated pups. Significant increases in liver weight were observed in the PFOS-exposed mouse pups. Serum thyroxine levels were suppressed in the PFOS-treated rat pups, although triiodothyronine and thyroid-stimulating hormone levels were not altered (Lau et al. 2003). These results have been observed in several different research groups (Case, York, and Christian 2001; Luebker, Case, et al. 2005; Luebker, York, et al. 2005).

This post-natal mortality has been explored further and determined to occur only in late developmental windows. Timed-pregnant Sprague-Dawley rats were treated by oral gavage with 25 mg/kg/d PFOS/$K^+$ on four consecutive days GD 2–5, 6–9, 10–13, 14–17, or 17–20) or with 0, 25, or 50 mg/kg/d PFOS/$K^+$ on GD 19–20. Pup survival decreased in groups dosed later during gestation, approaching 100% with dosing on GD 17–20. Maternal serum PFOS levels on GD 21 were higher in groups exhibiting higher mortality. In the GD 19-20 treatment, PFOS groups experienced significant pup mortality by PND 1. Neonatal mortality continued through PND 5, when survival was 98, 66, and 3% for the 0, 25, and 50 mg/kg groups, respectively. Additionally, following gross dissection and histological examination of lungs revealed differences in maturation between control and treated animals on PND 0 (Rayetta C. Grasty et al. 2003).

The mechanism of late gestational exposure-early post-natal mortality is under investigation. Theories relating to PFOS's known metabolic toxicity have been investigated.

PFOS has been shown to attenuate lipid and cholesterol metabolism in Wistar rats (Haughom and Spydevold 1992). This phenomenon has been attributed to peroxisome formation due to PFOS exposure (Berthiaume and Wallace 2002). This peroxisome formation is mediated by peroxisome proliferator-activated receptor-alpha (PPARα). However, in a study by Abbot et al. used wild-type and PPARα knock-out mice to test this mechanism. Both PPARα knockout and wild-type pups suffered from post-natal mortality (Abbott et al. 2009).

The mechanism of lung malformation resulting in early post-natal mortality has been investigated. Pregnant Sprague-Dawley rats were exposed to 0, 25, 0r 50 mg/kg/day from GD 19-20. Dams reached parturition, and pups' lungs were extracted. Pup lung histology revealed thicker alveolar walls and increased tissue to small airway ratio. These results support the hypothesis of arrested fetal lung development due to prenatal PFOS exposure. However, when standard rescue agents were applied, no changes in exposed neonate mortality were observed. Additionally, pulmonary surfactant profiles were normal in exposed neonates. These results contradict the lung immaturity hypothesis (R. C. Grasty et al. 2005).

Further investigations into the mechanism of PFOS toxicity on lung development have been performed at the transcriptome and proteomics levels. Pregnant Sprague-Dawley rats were exposed to 0, 1, or 5 mg/kg/day from GD 12-18. Pup lungs were extracted at 1, 3, 7, and 14 days postnatal. Histological results reported reduced alveolar numbers, simplified structure and thickened alveolar septa. PFOS-treated pups also revealed increased lung inflammation, and up-regulated inflammasome-associated proteins NLRP3, ASC, Caspase-1 and GSDMD and increased inflammatory cytokines IL-18 and IL-1β. Additionally, genes critical for alveolar development and pulmonary angiogenesis, HIF-1α and VEGFA, were significantly down-regulated by PFOS exposure.

Other hypotheses on the mechanism of pulmonary toxicity exhibited by prenatal PFOS exposure is related to apoptosis. Pregnant Sprague-Dawley rats were exposed to PFOS

by oral gavage from GD 1-21 at 0, 0.1, and 2 mg/kg/day. Pups in the 2.0 mg/kg/day group experienced significant histopathological changes along with marked oxidative injuries and cell apoptosis in offspring lungs. Additionally, the ratio of Bax to Bcl-2, release of cytochrome c from mitochondria to the cytoplasm, expressions of Fas and Fas-L, and activities of caspase-3, -8, and -9 were up-regulated by treatment. These results suggest that oxidative stress and intrinsic and extrinsic cell death pathways are involved in pulmonary injury caused by prenatal PFOS exposure. (T. Chen et al. 2012).

These apoptotic effects have also been shown to cumulate in the heart. Briefly, Sprague-Dawley rats were exposed to PFOS prenatally at 0, 0.1, 0.6, and mg/kg/day from GD2-21. Heart tissues were retrieved from pups. Terminal dUTP nick-end labelling staining was performed. Additionally, mRNA was extracted for qPCR analysis and proteins for Western Blotting. The study found that the proportion of cells undergoing apoptosis increased with treatment. Moreover, expression of apoptosis-related genes and proteins associated with mitochondrial-mediated apoptosis pathway, including p53, bax, cytochrome c, caspase-9, and caspase-3 were upregulated, while bcl-2 was downregulated (Zeng et al. 2015).

Prenatal and early-life PFOS exposure has been shown to induce glucose and lipid metabolic disorders. Pregnant Wistar rats were given 0, 0.5, or 1.5 mg/kg/day from GD 0 – PND 20. Offspring were observed to have signs of prediabetes, with elevated fasting serum insulin and leptin levels and impaired glucose tolerance. Additionally, hepatic steatosis and elevated gonadal fat pad weight were observed, suggesting a state of abnormal lipid homeostasis (Lv et al. 2013).

Furthermore, PFOS has been shown to alter global DNA methylation status due to prenatal exposure. Briefly, pregnant Sprague-Dawley rats were exposed to 0, 0.1, 0.6, or 2.0

mg/kg/day of PFOS. Livers of pups were analyzed on PND 21. In the 2 mg/kg/day dose group, global DNA methylation decreased significantly (Wan et al. 2010).

In non-mammalian species models, PFOS has been shown to affect organogenesis due to developmental exposure. In a study by Chen et al., zebrafish were exposed to 16 µM of PFOS at either 0-48 or 48-96 hours post fertilization (hpf). Larvae exposed at 48-96 hpf experienced a significant increase in malformations such as uninflated swim bladder, less developed gut, and curved spines. Zebrafish exposed at 0-48 hpf did not display a significant increase in any malformations. Additionally, whole transcriptome sequencing of larval tissues resulted in a PFOS-induced network of perturbed transcripts relating to swim bladder and gut development, revealing that misexpression of genes were involved in organogenesis (J. Chen et al. 2014).

Moreover, additional studies on the developmental effects of PFOS on zebrafish show transcriptomic effects related to apoptosis, thyroid development, and sex hormone balance. Zebrafish embryos were exposed to 0.1, 0.5, 1, 3 and 5 mg/L of PFOS from 4-132 hpf. Larvae exposed to greater than 1 mg/L displayed significant physical malformations such as: epiboly deformities, hypopigmentation, yolk sac edema, tail and heart malformations and spinal curvature. Genes related to cell apoptosis, *p53* and *Bax*, were significantly upregulated in all treated groups. Furthermore, flow cytometry analysis using acridine orange reported an increase in the proportion of cells undergoing apoptosis, when compared to the control. Additionally, PFOS upregulated *hhex* and *pax8*, genes involved in thyroid development. Genes that regulate androgen and estrogen pathways, *cyp19a* and *cyp19b* were also significantly down-regulated (X. Shi et al. 2008).

Additionally, cardiac effects of PFOS have been shown *in vitro*. In a study by Yang et al., hESCs were exposed to PFOS at concentrations of 0.1-60 µM for 8 days, concurrently with the induction of differentiation into cardiomyocytes. The results showed that PFOS

inhibited the differentiation of hESCs into cardiomyocytes. Additionally, an increase of differentiation in epicardial cells was observed with PFOS treatment. Transcriptomics sequencing attributed this to an upregulation of the WNT signaling pathway.(R. Yang et al. 2020)

## Lead (II)

Lead (Pb) is heavy metal that is number 82 on the periodic table of elements. It is a soft malleable metal that has a molecular weight of 207.2 g/mol. Pb is a naturally occurring element that is often found in several minerals. When these minerals are exposed and weathered during other activities, Pb can leach into the environment (Yu et al. 2021). However, there are also increasing sources of anthropogenic Pb being found in the environment. These sources are often associated with industrial processes such as metal smelting, leaded gasoline use, and e-waste processing (T. Shi et al. 2019).

Pb has a low solubility relatively high affinity for soil (Allison and Allison 2005). This results in an accumulation of lead in agricultural soils that are in the vicinity of heavy industry. This can lead to human exposure through ingestion of food grown in contaminated soils (T. Shi et al. 2019). Anthropogenic Pb has the potential to leach into surface and groundwater sources. Additionally, mining activity can introduce oxygen into otherwise isolated Pb-containing minerals in groundwater sources causing Pb to leach into the water. This can result in human and wildlife exposure to Pb through contaminated water (Raj et al. 2022). Pb also has a high affinity for tissues such as bones, teeth, liver, lung, kidney, brain, and spleen. This causes Pb to rapidly bioaccumulate in food webs, resulting in high levels of exposure to humans and top level predators (Zuluaga Rodríguez, Gallego Ríos, and Ramírez Botero 2015).

Pb kinetics following oral exposure is not related to dose in a linear manner. Rats that were given 1000 µg/kg experienced at 42% transfer to blood. Meanwhile, when given $1x10^6$

µg/kg, blood concentration was only 2% of the dose (Aungst, Dolce, and Fung 1981). Furthermore, Pb has been shown to be capable of placental transfer, albeit at low levels in rats. In a study by McClain et al., pregnant rats on GD17 were given an infusion of lead nitrate at 0.7 mg/kg/min for 64 mins. Maternal blood concentrations reached 425 µg/mL; while whole fetus concentrations were 2.4 µg/g bw (McClain and Becker 1975). In a paired human study, maternal blood concentration had a mean of 40.4 ng/mL, while cord blood had an average concentration of 37.1 ng/mL(Loueniva and Kauppila 1986).

Pb is an environmentally relevant contaminant that has been shown to be developmentally toxic. Pregnant Sprague Dawley rats were exposed to 250 ppm of Pb in drinking water from GD 7-16. Mortality and birth outcome metrics were recorded. The incidence of fetus reabsorption and abortion was significantly increased by treatment. Moreover, fetuses had increased mortality rates, significantly lower body weight, length, and an increase in skeletal/external malformations compared to controls. Histopathological examination of tissues revealed an increase in DNA fragmentation in hepatic tissues with treatment (Aglan et al. 2021).

Sublethal effects of prenatal exposure to Pb are often characterized by neurological disorder resulting in behavioral changes. In pregnant Sprague Dawley rats exposed to Pb at 0, 50, or 150 ppm in drinking water and subjected to a Morris water maze test at postnatal day 56-60. Pb-exposed female mice had significantly higher escape latencies and lower times spent in the quadrant containing the objective. These results suggest that learning and spatial memory are negatively impacted by prenatal exposure to Pb (Betharia and Maher 2012).

In a similar study, behavioral markers were tested on BALB/cAnNTac mice prenatally exposed to 20 ppm Pb from GD 8-21. Various behavioral tests were performed, and gene expression in female brain tissues was analyzed by qRT-PCR. Exposed mice significantly lowered exploratory behavior, and female mice had significantly more anxious

behaviors. Additionally, Pb-exposed male mice showed increased aggressive behaviors. Additionally, exposed groups had poorer performance in a Morris water maze trial. Gene expression results showed significant activation of the focal adhesion and extracellular matrix receptor interaction pathways. These pathways are associated with region formation and growth of the developing brain. Additionally, VEGF and TGF-β perturbation was associated with disrupted vascularization. Furthermore, significant up-regulation of genes associated with pro-inflammatory pathways was measured (Kasten-Jolly et al. 2012).

Alternative mechanisms of toxicity for Pb developmental toxicity are epigenetic and DNA methylation effects. Female C57/Bl6 mice were exposed to 0 or 100 ppm of Pb 2 months prior to mating until weening. Female pups experienced a significantly higher level of serum corticosterone, a stress response molecule. Additionally, several DNA methyltransferases were significantly altered, suggesting effects on genomic DNA methylation status (Sobolewski et al. 2018). Additionally, in a study by Montrose et al., novel intracisternal A particle retrotransposons displayed reductions in methylation in a dose-dependent manner with Pb perinatal exposure. Intracisternal A particle retrotransposons are retrovirus transposable elements that can induce gene mutations (L. Montrose et al. 2017). Moreover, in human studies, neonate blood spots were retrieved at birth. Results showed a decrease in methylation from increasing Pb exposure (Luke Montrose et al. 2020).

Another reported mechanism of Pb developmental toxicity is attributed to oxidative stress. neuroblastoma SH-SY5Y cells were exposed to 0, 2, 10, or 50 µM Pb for 48 hours. Results showed that Pb increased the incidence of reactive oxygen species in a dose-dependent manner. Furthermore, glutathione and mitochondrial calcium uniporter (MCU) abundance were both significantly reduced. Co-exposure to spermine, an MCU activator, significantly reduced the effects of Pb-related oxidative stress and increased mitochondrial

calcium uptake. Conversely, Ru360, an MCU inhibitor, potentiated the effects of Pb (X. Yang et al. 2014).

Pb has been shown to have an impact on differentiation of stem cells into neurons. P19 stem cells were exposed to Pb at 0, 1, 2, or 3µM for 4 days. Pb exposure significantly inhibited the determination of cells into neuronal lineage. Gene expression analysis revealed a significant increase in Sox2 expression and a decrease in N-cadherin. Additionally, neural and glial cell differentiation was reduced by Pb treatment in a dose-dependent manner (Mansel et al. 2019). Similar studies found that hESC differentiation into neurons was affected by Pb exposure. hESCs that were differentiated into neural progenitor cells and exposed to 1.9 µM Pb, generated significantly more TUJ1-positive neurons. Moreover, hESCs exposed to Pb during neural rosette formation had gene expression profiles with a significant decrease in Pax6 and MSI1. This resulted in neurons with shorter neurites and less branching structures. Concurrently, global methylation status analysis showed that Pb treatment modulated the methylation status of genes involved in several neurogenetic signaling pathways (Senut et al. 2014).

# Goals and Objectives

The main goal of this thesis was to develop a model to detect the early developmental toxicity of toxicants using hESCs, by screening 3 environmentally relevant chemicals. The results could lead to an effective, efficient, and relatively inexpensive method to screen toxicants for early developmental effects, that does not involve animal testing. This methodology could also provide novel insights into the mode of action for developmental toxicity of these compounds.

## Research Questions

To achieve the goal of this thesis, I will need to identify the dose-response relationships between the 3 selected reference contaminants and many markers of toxicity and cellular health in hESCs *in vitro.* Subsequently, I will compare these relationships to the observations reported in *in vivo* and other species *in vitro* studies to determine the relative sensitivity and effectiveness of our hESC-based developmental toxicity screening model. The thesis is designed to answer 2 main research questions:

1. Which of the selected endpoints are most predictive of the risk of developmental toxicity for the selected compounds? This will be determined by whether the dose-response relationships of the selected compounds in hESCs and observed biological responses lead toward the known apical toxic endpoints.
2. Can toxicity screening with hESCs *in vitro* models detect developmental toxicity? This will be determined by whether observed biological responses can be related to known adverse developmental outcomes.

## Specific Objectives

The previously stated research questions were addressed with the following objectives:

1. To review the scientific literature for assays previously used to detect cytotoxicity/ inhibition of growth, and inhibition of differentiation *in vitro*. Identify which assays best deliver data that suggest towards known developmental effects.
2. To perform the selected *in vitro* embryotoxicity assays using hESC cultures and the 3-reference compound and identify the dose-response relationships.
3. To compare and contrast the data collected to those reported in other *in vivo* or *in vitro* testing models and identify the relationship between the biological responses and the

known apical developmental toxic endpoints. Additionally, whether our data provides insights to the molecular mode of action using genomic, transcriptomic, and epigenetic assays.

# Hypothesis

The overall hypothesis is that our hESC based developmental toxicity screening protocol will be able to detect a dose-response relationship of the developmental toxicity endpoints of the 3 selected contaminants. Additionally, these dose-response relationships will be reflective of the apical developmental toxicity endpoints in *in vivo* and non-hESC *in vitro* studies. Moreover, we will be able to identify crucial components of the developmental toxicity mode of action.

The specific hypotheses of the three compounds are:

Exposure of BPA to hESCs at concentrations from 0.25-2500 µg/L for 6 days will increase the proliferation rate, and cell population in a dose-dependent manner when compared to hESCs dosed with the solvent control. There will be no observed effect on cell death rate. Additionally, exposure to BPA will cause global hyper-methylation of 5'-mc genomic DNA.

Exposure of PFOS to hESCs concentrations from 0.455-2275 µg/L for 6 days will decrease the proliferation rate in hESCs in a dose-dependent manner when compared to solvent control. PFOS will cause an increase in cellular death rate at high doses. Moreover, exposure to PFOS will cause global hyper-methylation of 5'-mc genomic DNA.

Exposure of $PbCl_2$ to hESCs for 6 days at concentrations from 0.62-6200 µg/L will decrease the proliferation rates and increase death rate in a dose-dependent manner. Concurrently, Pb exposure will cause an inhibition of gene expression for hESC differentiation markers in ecto-, meso-, and endoderm. Additionally, Gene expression of Pb

affected hESCs will show down regulated expression of neurogenesis genes and cell survival pathways. Furthermore, exposure to $PbCl_2$ will cause global hyper-methylation of 5'-mc genomic DNA.

# Materials and Methods

## Ethics Review and Approval

This project was reviewed and approved by the Health Canada and Public Health Agency of Canada's Research Ethics Board (File No. REB 2016-027H) and by the Office of Research Ethics and Integrity of the University of Ottawa (File No. H-05-19-4084).

## Human Embryonic Stem Cell Culturing

Human embryonic stem cells (hESCs) (H9 line; passage 23) were acquired from WiCell Research Institute (Madison, WI). These cells were adapted to the laboratory conditions using Matrigel™ (Catalogue no. CB-40234A; Fisher Scientific) and Essential 8™ Flex Medium (Catalogue no. A2858501; ThermoFisher). Due to supply shortages and incompatibility with other reagents, the culture matrix was changed from Matrigel™ to Vitronectin XF™ (Catalogue no. 07180; STEMCELL Technologies).

Vitronectin XF™ was aliquoted and frozen to reduce freeze-thaw cycles. Vitronextin XF™ was then diluted with CellAdhere™ Dilution Buffer (Catalogue no. 07183; STEMCELL Technologies) to a concentration of 10 or 20 µg/mL. If diluted to 10 µg/mL, 1 mL was added to each well of a Nunclon Delta 6-well treated culture plate (Catalogue no. 140675; ThermoFisher); if diluted to 20 µg/mL, 0.5 mL was added to each well and 0.5 mL of CellAdhere™ Dilution Buffer was also added to the well to result in a concentration of 10 µg/mL. Plates with diluted Vitronectin XF™ were incubated for 60 minutes at room temperature. After incubation, the Vitronectin XF ™ was removed with a VACUUBRAND™ BVC Control fluid aspirator (Catalogue no. 13-688-008; Fisher

Scientific). Culture plate wells were then washed with 1 mL of CellAdhere™ Dilution Buffer per well.

H9 hESCs, suspended and frozen in mFreSR™ cryopreservation medium (Catalogue no. 05855; STEMCELL Technologies), were then thawed at 37°C until fully liquid. The cell suspension was diluted with 9mL of Essential 8™ Flex medium and centrifuged in a Thermo Scientific™ Sorvall™ ST 40 Centrifuge (Catalogue no. 75-257-406; FisherScientific) at 1000 RPM for 5 minutes to remove the cells from suspension. The supernatant was aspirated, and the cell pellet was resuspended in 12 mL of Essential 8™ flex medium. Subsequently, 2mL of cell suspension was then added to each well of a Nunclon Delta 6-well treated culture plate. Y-27632 dihydrochloride, otherwise known as RHO/ROCK inhibitor (Catalogue no. 72304; STEMCELL Technologies) was diluted with distilled water to a stock concentration of 0.01M. Following this, 2µL of ROCK inhibitor stock was added to each well containing 2mL of cell suspension. This is to improve cell attachment and survival. Plates containing hESCs were then incubated in a Heracell™ VIOS 160i Tri-gas Incubator (Catalogue no. 51030406; ThermoFisher) for 48 hours at 37°C, 4% oxygen, and 10% $CO_2$. Following this, the cells were observed for attachment, colony formation and morphology under a 10 × objective on a Zeiss Axiovert 40 CFL inverted microscope (Carl Zeiss Microscopy LLC) with a SPOT RT3 digital camera and SPOT basic software. The medium and cell debris was then aspirated, and 2mL of 37°C Essential 8™ flex medium was added. The culture plate was returned to the tri-gas incubator, and the medium was changed every 24 hours.

Once the hESCs have reached a confluence of 80-90%, cells were seeded at densities appropriate for a 7-day dosing regimen. To do this, hESCs were dissociated with ReLeSR™ cGMP, enzyme-free human pluripotent stem cell selection and passaging reagent (Catalogue no. 05872; STEMCELL Technologies). This was done by adding 1 mL of ReLeSR™ to each well of the culture plate. The dissociation reagent was then immediately aspirated and the

plate was returned to the tri-gas incubator for 5 minutes. After incubation, 2 mL of warmed Essential 8™ flex medium was added to each well. The culture plate is placed on a Labline 4625 Titer Shaker (Catalogue no. LA-TS; Marshall Scientific) for 5 minutes. Subsequently, cell suspension from 2 of the 6 wells was then collected in a 15 mL centrifuge tube. This cell suspension was then centrifuged at 1000 RPM for 5 minutes. The supernatant is then aspirated, and the cell pellet is resuspended in 6 mL of Essential 8™ flex medium. A 10 µL sample of the cell suspension was taken and added to 10 µL of 0.4% Trypan Blue stain (Catalogue no. T10282; ThermoFisher). Then, 10 µL of this stained cell suspension was then loaded into a chamber slide and placed into a Countess™ II Automated Cell Counter (Catalogue no. AMQAX1000; Invitogen). Cells were counted, and the original cell suspension was then added to the warmed essential 8™ flex medium to acquire a concentration of $1x10^4$ cells/mL. This concentration was selected to optimize colony formation and prevent overcrowding during the 7-day treatment. Subsequently, 2 mL of diluted cell suspension was added to each well. Additionally, 2 µL of ROCK inhibitor was added to each well. Cells were left to incubate undisturbed for 48 hours.

## Toxicant Preparation and Dosing

Analytical grade bisphenol A (BPA), perfluorooctane sulfonate (PFOS), and lead chloride ($PbCl_2$), were acquired from Sigma-Aldrich (Cat. #239658, Oakville, ON, Canada), AA Blocks Inc. (Cat # AA0024HO, San Diego, CA, USA), and Sigma-Aldrich (Cat# 203572, Oakville, ON, Canada), respectively. Chemicals were delivered in solid granular/powdered form. Chemicals were dissolved in type 1 water, produced with a Synergy Water Purification System (Cat# SYNSVR0US, Millipore-Sigma, Oakville, ON, Canada) by stirring in glass beakers and filtered through a Thermo Scientific™ Nalgene™ Rapid-Flow™ Sterile Disposable Filter Units (Fisher Scientific, Ottawa, ON, Canada) to prepare 250 or 500

mL of 100x stock solutions of the highest dose required for each toxicant. Serial dilutions were performed in 10-fold increments to achieve 5 different stocks.

Concentrations of BPA, PFOS, and $Pb^{2+}$ used in this study were chosen based on their reported geometric mean (GM) concentrations (2.5 µg/L for BPA, 4.55 µg/L for PFOS, 6.2 µg/L for Pb), in human maternal blood (Arbuckle et al. 2016; Chou et al. 2011; Fisher et al. 2016). Serial dilutions were prepared around the GM maternal blood concentrations. Three increments higher and one increment lower than GM maternal blood concentration were prepared. The highest concentration dose for PFOS was halved due to extreme acute toxicity, being nearly 100% lethal. The doses can be seen in table 1.

*Table 1:* The toxicants selected for dosing and the concentrations used. Stock solutions were prepared to 100x the dose by dilution in type-1 water.

**Indicates the reported GM maternal blood concentration from the chosen study*

| **Toxicant** | **Dose 1** | **Dose 2** | **Dose 3** | **Dose 4** | **Dose 5** | **Source** |
|---|---|---|---|---|---|---|
| **BPA** | 0.25 µg/L | 2.50 µg/L* | 25.0 µg/L | 250 µg/L | 2500 µg/L | (Chou et al. 2011) |
| **PFOS** | 0.455 µg/L | 4.55 µg/L* | 45.5 µg/L | 455 µg/L | 2275 µg/L | (Fisher et al. 2016) |
| **$Pb^{2+}$** | 0.62 µg/L | 6.20 µg/L* | 62.0 µg/L | 620 µg/L | 6200 µg/L | (Arbuckle et al. 2016) |

HESCs were dosed with toxicants following the daily medium change. To achieve the target concentrations, 20 µL of the 100x stock was added to each well containing 2 mL of medium. A solvent control group was dosed with 20 µL of type 1 water to simulate any effects of the solvent. Dosing occurred after the 48-hour undisturbed plate adhesion period, every 24 hours for 6 days. 6-day was selected as the dosing period after optimizing the seeding density to the size of the Nunclon Delta 6-well treated culture plate. It was found this period would result in a high confluency without overcrowding or multi-layering of hESCs.

## Inhibition of Proliferation Endpoint

### WST-1; Metabolic Activity Assay

The activity of metabolic dehydrogenase was assessed to estimate cell viability and proliferation. In principle, this is done by measuring the absorbance of formazan dye, which is created by the cleavage of the tetrazolium salt WST-1 by cellular mitochondrial dehydrogenases. Therefore, a higher absorbance of formazan dye indicates higher levels of cellular activity of mitochondrial dehydrogenases, indicating higher cell viability.

Dosed hESCs exposed to the reference contaminants at the concentrations and exposure length stated above are assessed using the WST-1 assay kit (Cat # ab155902, Abcam Inc. Toronto, ON. Canada). WST-1 reagent is added, 20 µL of reagent per 2 mL of medium. Plates are agitated for 10 seconds to distribute the reagent. Kinetic absorbance over time at 420-480 nm wavelength is measured using a BioTek™ Cytation™ 5 Cell Imaging Multi-Mode Reader (Agilent, Santa Clara, CA, USA) over a 2-hour period of incubation at 37°C. Measurements are taken every 5 minutes over the period.

### Assessment of Rates of Cell Death

The rate of hESC death was estimated over 6-days of BPA, PFOS and $PbCl_2$. Daily medium changes were performed at 2 mL of Essential 8™ per well. The expended medium

was sampled daily. The number of dead cells in suspension were measured using a Countess™ II Automated Cell. Daily cell deaths were recorded.

Additionally, daily live cell population counts were performed. To do this, 7 replicates of each sample were treated in parallel. Each day, a replicate was dissociated using Accutase™ to bring live cells into suspension. Essential 8™ was added to each sample to deactivate the dissociation medium and bring the volume to 2 mL, to match the volume of sampled expended medium. Live cell suspensions were sampled using the Countess™ II, and live cells were recorded. The number of dead cells was normalized to the live cell population size each day.

*Table 2*: The cell identification parameters optimized to identify live/ dead hESCs dyed with trypan blue on the Countess™II cell counter.

| | **SIZE** | **COLOUR INTENSITY** | **ROUNDNESS** |
|---|---|---|---|
| **LIVE** | 5-50 | 0-255 | 70 |
| **DEAD** | 5-50 | 30-200 | 100 |

## Cell Colony Growth

Cell population growth was recorded over the 6-day dosing period for hESCs exposed to BPA, PFOS, and $PbCl_2$. Cells were seeded and dosed using the protocols previously described. Plates were loaded into a Cellcyte X (Cytena; Freiburg, Germany). A protocol was designed to image each well at 10x magnification, in a 6x6 grid. Images were stitched together to create a single continuous image. Images were taken using the bright field filter

every 6 hours for 6 days. A training set of 10 images were selected from the pool of images taken over the 6-day period. These images allow the software to identify cells by shape and colour. A cell confluence analysis was run to show changes in confluence over time. Cell identification parameters were created by the user to ensure adequate cell identification apart from debris and background.

## Cell Cycle Assay

The effects of toxicant dosing on hESC cell cycle phases were assessed using a Cell Cycle Assay Kit- Green Fluorometric (Cat no. ab112116; Abcam). This kit uses Nuclear Green CCS1 dye to determine the cell cycle phase using a flow cytometer.

Cells were seeded and dosed with BPA, PFOS, and $PbCl_2$ as described previously. After 6 days of exposure, cells were washed with 2 mL of DPS per well. Cells were then dissociated with ReLeSR™ and resuspended in 2 mL of Essential 8™. Cell suspensions were then transferred to 15 mL conical centrifuge tubes. Cell suspensions were centrifuged at 1000 RPM for 5 minutes, and the supernatants were aspirated. Cells were resuspended in 500 µL of Essential 8™ and 2.5 µL of 200X Nuclear Green CCS1 dye was added. Dyed cells were placed in the tri-gas incubator for 1 hour at 37°C, 4% oxygen, and 10% $CO_2$. After incubation, cells were centrifuged at 1000 RPM for 5 minutes. The supernatant and dye were aspirated, and cells were washed with 2 mL of medium. Cells were centrifuged and washed 2 more times for a total of 3 washings. Cells were then resuspended in 500 µL of assay buffer provided in the kit.

Cells were analyzed for dye emission using a BD LSRFortessa™ Cell Analyzer (BD Bioscience; San Jose, CA, USA). Cells were analyzed with the blue laser settings (Ex/Em= 490/525 nm). A minimum of 10,000 events were recorded for a sample to be considered valid.

# Inhibition of Differentiation Endpoint

## Stem Cell Differentiation Assay

Due to logistic and time constraints, only 1 of the 3 reference chemicals was selected for the inhibition of differentiation screening. The effects of dosing on pluripotency and the ability to differentiate of hESCs were determined for $PbCl_2$. $PbCl_2$ was selected due to the large magnitude of its effect and the biphasic effect it had in the WST-1 assay. This was done by inducing hESCs to differentiate into the 3 primary germ layers: mesoderm, ectoderm, and endoderm. To do this, a STEMdiff™ Trilineage Differentiation Kit (Cat no. 05230; StemCell Technologies) was used. Due to sample size constraints, only 2 relevant doses of $PbCl_2$ were selected; These doses were the GM maternal blood concentration and 118.1 µg/L $Pb^{2+}$. 118.1 µg/L $Pb^2$ was selected due to its likelihood to illicit sublethal effects, as determined in the WST-1 assay. A solvent control dose was also tested. This consisted of filtered type-1 water.

To test the effects of dosing on differentiation, hESCs were dosed concurrently with differentiation. Differentiation was induced as per the kit instructions. Cells were seeded at $1x10^4$ live cells per mL, as described previously. Dosing and differentiation did not begin until 48 hours after seeding. After 48 hours, the medium was changed with a differentiation induction medium, 3mL per well. Additionally, 30 µL of stock or control solvent was added to achieve the concentrations described above. Medium change and dosing were repeated every 24 hours for 6 days for ectoderm and 4 days for mesoderm and endoderm. Each germ layer was tested for each of the 3 treatment concentrations. Additionally, an undifferentiated group, treated with only a control solvent, was also created. This resulted in 10 different treatment conditions. This was replicated 3 times with different hESC generations.

Ribonucleic acids (RNA) were extracted from differentiated/dosed cells and the undifferentiated control. This was done using a Total RNA Purification Kit (Cat no. 79040; StemCell Technologies). RNA sample concentrations and purity was assessed using a

NanoDrop ND-1000 spectrophotometer (Thermofisher Scientific). Only samples with a concentration greater than 20 µg/µL and a 260/280 wavelength ratio greater than 1.8 was accepted for analysis. Whole transcriptome sequencing was performed by the company Novogene. RNA concentration differences were analyzed by the Ottawa Hospital Research Institute (OHRI) Bioinformatics services.

# Transcriptomic/Genomic Endpoint

## Single Cell Transcriptome Sequencing

A single-cell transcriptome sequencing was done for hESCs exposed to $PbCl_2$. Again, $PbCl_2$ was selected due to the large magnitude of effects and the biphasic effect it had in the WST-1 assay. Doses were amended to focus on sub-lethal doses that may have an effect on RNA based on the results of the WST-1 and cell death assays. For this 118.1, 6.2, and 0.62 µg/L $PbCl_2$ were selected. 118.1 µg/L was selected because it is approximately one-sixth of the molarity of the 620 µg/L concentration that elicited significant acute mortality. A new stock solution was created for this dose by diluting 190.5 µL of the 620,000 µg/L stock with 9809.5 µL of type 1 water. Cells were seeded using the protocol described previously and dosed for 6 days as previously described.

Single-cell transcriptomes were captured using a BD Rhapsody™ Single-Cell Analysis System (Becton, Dickinson; Franklin Lakes, New Jersey, USA). Briefly, treated hESCs were dissociated into single-cell suspension using Accutase™ as described above. A BD Rhapsody™ Cartridge Reagent Kit (Cat no. 633731; BD) was retrieved, and components were equilibrated to room temperature or placed on ice, as per kit instructions. A 5 mL LoBind Tube (Cat. no. 0030108310; Eppendorf) and BD Rhapsody™ Cartridge Kit (Cat no. 633733; BD) was loaded into the Rhapsody™. Subsequently, 700 µL of 100% ethanol, 700 µL of air and 700 µL of Cartridge Wash Buffer 1 (PN 650000060) was loaded into the cartridge.

To treat the cartridge surface, 700 µL of air and 700 µL of Cartridge Wash Buffer 1 were added to the cartridge. This was allowed to incubate at room temperature for 10 minutes. An additional 700 µL of air was added to the cartridge along with 700 µL of Cartridge Wash Buffer 2 (PN 650000061).

Cell suspensions from each sample were aliquoted to contain $1x10^6$ hESCs. Cell suspensions were centrifuged at 1000 RPM for 5 minutes, and the supernatant was discarded. Cells were then resuspended in 200 µL of BD Stain Buffer. Subsequently, 180 µL of cell suspension was transferred to a Sample Tag tube for each sample. Tagged cell suspensions were allowed to incubate at room temperature for 20 minutes. Afterward, 200 µL of BD Stain Buffer was added to the cell suspension and mixed by gentle pipetting. Cells were centrifuged at 300 x *g* for 5 minutes, and the supernatant was discarded. Cells were resuspended in 500 µL in BD Stain Buffer and centrifuged at 300 x *g* for 5 minutes; the supernatant was discarded. Cells were then resuspended in 500 µL of Sample Buffer from BD Rhapsody™ reagents.

Cell viability was confirmed by staining with Calcein AM and DRAQ7™ fluorescent stains. These stains identify live and dead cells, respectively. Briefly, 2.5 µL of 2 mM Calcein AM and 2.5 µL of 0.3 mM DRAQ7™ were added to 500 µL of hESC suspension. The dyes were mixed by pipetting and incubated for 5 minutes at 37°C on a heating block. Subsequently, 10 µL of cells were loaded into an INCYTO™ disposable hemocytometer (Cat no. 82030-480; VWR). The hemocytometer was placed into the hemocytometer adaptor, allowed to incubate at room temperature for 1-5 minutes and counted in the Rhapsody™.

A dilution of the tagged cell suspension was made with cold Sample Buffer (PN 650000062) as the diluent. This was prepared to a volume of 650 µL containing 10,000 cells. This cell volume was selected because it is the maximum range validated for sequencing with the Rhapsody™ device. The cell suspension was filtered with a Falcon® Tube with Cell

Strainer Cap (Cat. no. 352235; Thermo Fisher Scientific). The cartridge on the tray was loaded with 700 µL of air. Subsequently, 40 µL of air and 575 µL of cold cell suspension were loaded into the cartridge. Cells in the cartridge were incubated at room temperature, away from light, for 15 minutes.

Cell capture beads were prepared before imaging. To do so, Cell Capture Beads (PN 650000089) were placed on the 1.5 mL tube magnet for 1 minute. The storage buffer was then discarded while retaining the beads. The tube was separated from the magnet, and 750 µL of cold Sample Buffer was added to suspend the beads.

To load beads into the cartridge, 700 µL of air was loaded into the cartridge. The even suspension of cell capture beads was ensured via gentle pipetting. The cartridge was then loaded with 630 µL of bead suspension. The beads were allowed to settle into the cartridge for 3 minutes at room temperature. The cartridge was then imaged in the Rhapsody ™scanner.

The cartage is washed with 700 µL of air, then 700 µL of cold Sample Buffer. These wash steps were repeated an additional 2 times. The cartridge was imaged again in the Rhapsody™ scanner.

Cells were then lysed, and the beads were removed to extract mRNA. To do this, 75.0 µL of 1 M DTT (PN 650000063) was mixed with 15 mL of Lysis Buffer (PN 650000064). Afterward, 550 µL of Lysis Buffer/DTT solution was loaded into the cartridge and incubated at room temperature for 2 minutes. The cartridge and scanner were moved into the bead retrieval position and allowed to magnetize the beads for 30 seconds. Then, 4950 µL of Lysis Buffer/DTT solution was loaded into the cartridge. The beads were captured in a 5 mL LoBind tube and set on the magnetic separation stand for 1 minute. The cartage was then imaged on the scanner.

The supernatant was aspirated using a pipette without disturbing the beads. Approximately 1 mL of supernatant was left in the LoBind tube. The beads were resuspended in the supernatant by pipetting and transferred to a 1.5 mL LoBind tube. The tube was placed on the 1.5 mL tube magnet for 2 minutes, and the supernatant was discarded. Afterward, 1.0 mL of cold Bead Wash Buffer (PN 650000065) was added to the tube. The beads were then suspended by gentle pipetting. The beads were then magnetized for 2 minutes, and the supernatant was discarded. The beads were again suspended with 1.0 mL of cold Bead Wash Buffer and transferred to a new 1.5 mL LoBind tube and placed on ice.

The cDNA mixture was prepared in a new LoBind tube on ice. Briefly, 128 µL of nuclease-free water (PN 650000076), 48 µL of RT Buffer (PN 650000067), 24 µL of dNTP (PN 650000077), 12 µL of RT 0.1 M DTT (PN 650000068), 4 µL of RT/PCR Enhancer (PN 650000070), 12 µL of RNase Inhibitor (PN 650000078), and 12 µL of Reverse Transcriptase (PN 650000069) are vortexed then centrifuged to mix. Beads were then magnetized for 2 minutes, and the supernatant was discarded. Beads were resuspended in 200 µL of cDNA mix and suspended via pipetting. The bead suspension was transferred to a new 1.5 mL LoBind tube and incubated on a thermomixer at 1200 RPM for 20 minutes at 37°C.

The Exonuclease I mix was prepared in the pre-amplification workspace. Briefly, 204.0 µL of nuclease-free water, 24.0 µL of 10X Exonuclease I Buffer (PN 650000071), and 12 µL of Exonuclease I (PN 650000072) were mixed in a 1.5 mL LoBind tube. The beads were magnetized for 2 minutes, and the supernatant was discarded. The beads were then resuspended in 200 µL of Exonuclease I mix. The bead suspension was then incubated in a thermomixer at 37°C for 30 minutes at 1200 RPM. Exonuclease 1 was inactivated by incubating at 80°C in a heating block for 20 minutes. The beads were chilled on ice for 1 minute. The bead suspension was then magnetized for 1 minute until the solution became

clear; the supernatant was discarded. The beads were resuspended in 200 µL of cold Bead Resuspension Buffer (PN 650000066).

PCR I reaction mix was prepared in the pre-amplification workspace. Briefly, 34.6 µL of nuclease-free water (PN 650000076), 120 µL of PCR MasterMix (PN 650000073), 24 µL of Universal Oligo (PN 650000074), 12 µL of RT/PCR Enhancer (PN 650000070), 48 µL PCR1 primer panel, 12 µL of PCR 1 panel supplement, 1.4 µL of Sample Tag PCR1 Primer was mixed by vortex and centrifugation in a 1.5 mL LoBind tube.

Subsequently, the beads were magnetized for 2 minutes, and the supernatant was discarded. Beads were resuspended in 200 µL of PCR I reaction mix. The bead suspensions were then separated into 50 µL aliquots in 0.2 mL PCR tubes. Tubes are placed in a thermocycler that has been heated to 95°C. The thermocycler program can be seen in table 3.

*Table 3*: The thermocycler program for the PCR 1 & PCR2 phase of library preparation for the single cell transcriptome sequencing.

| **Step** | **Cycles** | **Temperature (°C)** | **Time** |
|---|---|---|---|
| **Hot Start** | 1 | 95 | 3 mins |
| **Denaturation** | 15 | 95 | 30 sec |
| **Annealing** | | 60 | 3 mins |
| **Extension** | | 72 | 1 min |
| **Final Extension** | 1 | 72 | 5 mins |
| **Hold** | 1 | 4 | ∞ |

After the PCR I reaction, beads were resuspended by pipetting and suspensions were pooled into a 1.5 mL LoBind tube. The bead suspensions were magnetized for 2 minutes. The

supernatant was transferred to a new 1.5 mL LoBind tube. Beads were resuspended in 200 µL of cold Bead Resuspension Buffer and were stored at 5°C.

To prepare 80% ethanol, 1600 µL of 100% ethanol was diluted with 400 µL of nuclease-free water. AMPure XP beads were vortexed for 1 minute and 140 µL was added to the tube of PCR I supernatant. The solution was mixed by vortex and centrifugation, then incubated for 5 minutes at room temperature. The solution was then magnetized for 5 minutes, and the supernatant was discarded. Subsequently, 500 µL of 80% ethanol is added to the tube and incubated for 30 seconds on the magnet. The supernatant was discarded and the ethanol wash was repeated 2 times. The residual ethanol is allowed to air dry for 5 minutes at room temperature.

Afterward, 30 µL of Elution Buffer (PN 650000075) was added to each tube. The beads were resuspended by gentle pipetting. Cell suspensions were allowed to incubate at room temperature for 2 minutes. Samples were then centrifuged and magnetized for 30 seconds. Eluate was transferred to a new 1.5 mL LoBind tube.

The PCR2 reaction mix was prepared as follows: 9.6 µL of nuclease-free water, 30 µL of PCR MasterMix (PN 650000073), 2.4 µL of Universal Oligo (PN 650000074), 12 µL of PCR2 Primer Panel and 3 µL of PCR2 panel supplement were combined by vortex and centrifuge in a 1.5 mL LoBind tube. Additionally, a Sample Tag PCR2 reaction mix was prepared by mixing 18 µL of nuclease-free water (PN 650000076), 30 µL of PCR MasterMix (PN 91-1052), 2.4 µL of Universal Oligo (PN 91-1054) , and 3.6 µL of Sample Tag PCR2 Primer (PN 91-1061). Then, 5 µL purified PCR1 eluent was mixed with 45 µL of the PCR2 reaction mix. Moreover, 5 µL of the purified PCR1 eluent was mixed with 45 µL of the Sample Tag PCR2 reaction mix. Both samples were mixed by vortex and centrifugation. The sample solutions were placed in the thermocycler and reacted according to the program described in table 3.

The products of the PCR2 reaction were then purified. Briefly, AMPure XP beads were vortexed for 1 minute. Subsequently, 35 µL of AMPure XP beads were added to each sample containing the PCR2 products; this was mixed by vortex and centrifugation. The samples were incubated at room temperature for 5 minutes and magnetized for 3 minutes. The supernatant was discarded, and beads were washed with 200 µL of 80% ethanol. The beads were incubated with 80% ethanol for 30 seconds on the magnet. The supernatant was then discarded. Ethanol washing was repeated 2 additional times. The beads were allowed to air dry for 3 minutes at room temperature. The beads were then resuspended in 30 µL of Elution Buffer and mixed by vortex and centrifugation. The beads were allowed to elute at room temperature for 2 minutes. Samples were then magnetized for 30 seconds, and the eluent was collected into a new 1.5 mL LoBind tube. The concentration of RNA was measured using a Nanodrop ND-1000 Spectrophotometer. The sample concentration was diluted to 10 ng/µL and 0.5 ng/µL for the Targeted PCR2 products and the Sample Tag products, respectively. Dilution was done with nuclease-free water.

The Targeted final amplification mix was prepared by mixing 21.6 µL of nuclease-free water (PN 650000076), 30 µL of PCR MasterMix (PN 650000073), 2.4 µL of Library Forward Primer (PN 650000079), and 2.4 µL of Library Reverse Primer 1-4. (PN 650000080, 650000091–93). Additionally, a Sample Tag final amplification mix was prepared. This was done by mixing 21.6 µL of nuclease-free water, 30 µL of PCR MasterMix, 2.4 µL of Library Forward Primer, and 2.4 µL of Library Reverse Primer. Solutions were mixed by vortex and centrifuge.

Afterward, 3.0 µL of diluted and purified Targeted PCR 2 and Sample Tag PCR2 products were added to 0.2 mL PCR tubes, and 47 µL of Targeted final amplification or Sample Tag final amplification mix was added. The sample was placed in the thermocycler and reacted using the program described in table 4.

*Table 4*: The thermocycler program for the final amplification phase of library preparation for the single-cell transcriptome sequencing.

| Step | Cycles | Temperature (°C) | Time |
|---|---|---|---|
| **Hot Start** | 1 | 95 | 5 mins |
| **Denaturation** | 8 | 98 | 15 sec |
| **Annealing** | | 60 | 30 sec |
| **Extension** | | 72 | 30 sec |
| **Final Extension** | 1 | 72 | 1 min |
| **Hold** | 1 | 4 | ∞ |

To begin purification of the final amplification products, AMPure XP beads were homogenized by vortex for 1 minute. Then, 30 µL of AMPure XP beads were added to the Targeted final amplification products, and 50 µL was added to the Sample tag final amplification products. The solutions were mixed by vortex and centrifugation and incubated at room temperature for 3 minutes. The samples were then magnetized for 3 minutes, and the supernatant was discarded. While still on the magnet, 200 µL of 80% ethanol was added and incubated for 30 seconds. The supernatant was discarded. The ethanol wash was repeated 2 additional times. The residual ethanol was allowed to air dry at room temperature for 3 minutes. Then, beads were resuspended in 30 µL of Elution Buffer was added and allowed to elute for 2 minutes at room temperature. The sample was magnetized for 30 seconds, and the eluent was collected into new 1.5 mL LoBind tubes.

The concentration of RNA in the library was measured using a NanoDrop ND-1000 Spectrophotometer. The library size was measured using an Agilent Bioanalyzer with the

High Sensitivity Kit (Cat. no. 5067-4626; Agilent) for 50–7,000 bp, 5–1,000 pg/µL. The samples were then sequenced with an Illumina™ Sequencer.

## DNA Methylation Assay

The degree of genomic DNA methylation in hESCs exposed to BPA, PFOS, and $PbCl_2$ was assessed. Cells were seeded and expanded using the protocols described previously. Cells were dosed for 7 days with the reference chemicals at the doses described previously. After 6 days of exposure, cells were dissociated from the matrix using ReLeSR™ as described above.

Collected cells were extracted for genomic DNA using a FlexiGene DNA Kit (Cat no. 51206; Qiagen). In brief, cell suspensions were centrifuged at 1000 RPM for 5 minutes to form a pellet. The supernatant was aspirated, and the pellet was resuspended in 300 µL of FG1 buffer provided by the FlexiGene Kit. Next, 300 µL of FG2 buffer mixed with Qiagen Protease was mixed into each sample. Samples were mixed via inversion and incubated at 65 °C for 10 minutes on a VWR Scientific Standard Heat Block (Cat no. 13259-030; American Laboratory Trading). After incubation, 600 µL of ice-cold 100% isopropanol was added and mixed by inversion. Samples were centrifuged for 3 minutes at 10,000 x g, and the supernatant was aspirated. DNA pellets were washed with ice-cold 70% ethanol and vortexed for 5 seconds using a Fisherbrand™ Analog Vortex Mixer (Cat no. 02-215-365; Fisher Scientific). Samples were then centrifuged for 3 minutes at 10,000 x g. The supernatant was aspirated and the pellets were allowed to air dry. Pellets were then dissolved in 200 µL of FG3 buffer, vortexed, and incubated for 30 minutes at 65°C in a VWR Scientific Standard Heat Block.

DNA methylation was quantified using a MethylFlash Global DNA Methylation (5-mC) ELISA Easy Kit (Colorimetric) (Cat no. P-1030-96; Epigentek). Briefly, the concentration of genomic DNA extracted in each sample was determined on NanoDrop ND-

1000 Spectrophotometer. The volume of sample required to acquire 100 ng of DNA (or 8 µL, whichever was smaller) was determined. A standard curve dilution of the positive control provided by the kit was prepared as per the kit instructions. Next, 80 µL of binding buffer was added to each well of the provided treated microwell plate.

The negative control and diluted positive controls were added in duplicate to the plate. Following this, 100 ng of genomic DNA from each sample was added in duplicate to the necessary wells. The plate containing DNA samples was covered and incubated at room temperature for 90 minutes, away from light. The solution was removed from each well and washed 3 times with 150 µL of wash buffer, provided with the kit. Subsequently, capture antibody was prepared as per kit specifications, and 50 µL was added to each well. The plates were then incubated for 60 minutes at room temperature, covered and away from light. Wells were then washed 3 times as described above. Detection antibody was then prepared to kit specifications and 50 µL was added to each well. Plates were then incubated for 30 minutes at room temperature, covered and away from light. Wells were then washed 4 times with wash buffer. Enhancer solution was prepared to specifications and 50 µL was added to each well. Plates were then incubated for 30 minutes at room temperature, covered and away from light. Wells were then washed 5 times with wash buffer. Subsequently, 100 µL of developer solution was added to each well. Plates were incubated for 8 minutes at room temperature, covered and away from light. Next, 100 µL of stop solution was added to each well. Plates were incubated for 2 minutes at room temperature, covered and away from light. Absorbance of light was recorded using a Cytation 5 Cell Imaging Multimode Reader at 450 nm for each well.

To quantify the amount of methylated DNA, a calculation was performed using the following formula:

$$5 - mC\ (ng) = \frac{Sample\ OD - NegOD}{Slope\ \times 2}$$

*Formula 1: The estimation of 5-mC methylated genomic DNA from DNA samples with absorbances read at 450 nm. SampleOD= sample absorbance at 450nm, NegOD= negative control absorbance at 450nm, Slope= Slope of the 450nm absorbance of the positive control standard curve, determined by linear regression.*

# Statistical Analysis

## Analysis of WST-1, cell death rate, cell population, colony growth, cell cycle and DNA methylation in Prism

Statistics for the WST-1, cell death rate, cell population, colony growth, cell cycle and DNA methylation assays were performed on GraphPad Prism 10. In all cases, recorded measurements were normalized by taking a ratio of their respective batch control measurements. Normal or log-normal distribution of the data was ensured using Shapiro-Wilk and Kolmogorov-Smirnov tests. If a set of results failed the normality tests, it would be $\log_{10}$ transformed or ranked. Data that contained points with extreme values was tested for outliers. This was done using a Grubb's test with an $\alpha$=0.05. Outliers identified this was were excluded from the analysis. This data was then ranked in ascending order in Microsoft Excel. A one-way ANOVA of the average ranks was then performed in Prism.

## Analysis of single-cell RNA sequencing data in R

Raw single cell data were processed through the BD Rhapsody data analysis pipeline by BD scientists, and the processed data were made available through the SevenBridges distribution platform, from where they were downloaded for analysis.

Single cell data analysis was carried out within the R software environment (R Core Team 2018) using the Seurat package (Hao et al. 2021). The cell barcode × gene unique molecular index (UMI) count matrix (Combined_583389_RSEC_MolsPerCell.csv) was

loaded into R, the cell barcodes moved to the row names of the matrix, and the matrix was converted into a Seurat object of 28,904 cells.

As a standard quality control measure, the fraction of UMIs derived from mitochondrially-encoded genes was calculated from each cell; it is common practice to remove cells with an extremely high fraction of mitochondrial transcripts as these are understood to derive from low viability or dying cells. This enabled identification of a small group of cells with high mitochondrial content and a low number of detected genes, a typical signature for filtering.

The cells used to generate the single cell library were taken from eight samples (two replicates of each of the four conditions) and were labelled to allow each cell to be assigned to its sample of origin. The sample barcode data was loaded from the file '583389_Sample_Tag_Calls.csv', providing an association between each cell barcode and its sample tag and sample name. In addition to the eight original samples, cells can be labelled as 'Multiplet' (more than one sample tag was detected at a rate that exceeds a threshold for detection, resulting from more than one cell being deposited in a single well) or as 'Undetermined' (no sample tag detected above the threshold limit). Of the 28,904 cells, 8,296 (28.7%) were assigned the 'Undetermined' tag, and 360 (1.2%) were identified as multiplets. The remaining 20,248 cells were assigned to one of the eight original samples. The data set was filtered to retain only those cells of known origin, and thus with a known lead chloride dose.

The read count data was then normalized using the SCTransform procedure (Hafemeister and Satija 2019), and dimensional reduction of the normalized matrix was performed using principal component analysis (PCA). A Uniform Manifold Approximation and Projection (UMAP) projection of the cells was generated from the first twenty principal components (PCs) for visualization purposes, and the same 20 PCs were used to generate a

nearest neighbor graph with the Seurat 'FindNeighbors' function using otherwise default parameters. The neighbor graph was passed to the 'FindClusters' function to identify clusters using Louvain clustering with the resolution parameter set to 0.2.

To investigate gene expression differences between clusters and between $PbCl_2$ doses the original UMI count matrix was normalized using the Seurat 'NormalizeData' function, which performs per-cell scaling to UMIs per 10,000, and log(n+1) transformation of the transformed value. These normalized count values were used to identify marker genes for each of the identified clusters using the 'FindAllMarkers' function using the Wilcoxon rank sum test to determine significant differences in expression. Further to identifying cluster markers, the 'FindMarkers' command was used to identify gene expression differences within each cluster between each of the three $PbCl_2$ doses and the control cells without $PbCl_2$ treatment, and additionally comparing all control cells to all cells at each of the three doses.

To compare the expression of a set of pluripotency genes between clusters we employed the UCell package (Andreatta and Carmona 2021) to calculate an aggregate expression score for the set of genes in each cell in the dataset. For this scoring we used a list of human genes annotated with the Gene Ontology (GO) (Ashburner et al. 2000) term "Stem cell maintenance" from the AmiGO database (Carbon et al. 2009) (GO ID GO:0019827 downloaded from http://amigo.geneontology.org/amigo/term/GO:0019827 on May 24th, 2022). The list was deduplicated and filtered to retain only genes present in the dataset prior to scoring cells for expression of these markers. After scoring each cell, the UCell scores were compared visually on violin plots to determine if any cluster contained cells with higher or lower scores.

## Analysis of RNA sequencing data of differentiated and undifferentiated cells

Raw sequences for the 30 RNA-seq libraries were processed using the nf-core (Ewels et al. 2020) to generate transcript quantifications for each of the samples. The pipeline was

configured to run Fastp (v0.23.2) (S. Chen et al. 2018) for sequence quality and adapter trimming, aligned sequences to the human genome reference version GRCh38 using HISAT2 (v.2.2.1) (D. Kim et al. 2019), and quantified transcripts using Salmon (v1.10.1) (Patro et al. 2017).

The data were analyzed as a whole to identify patterns across the whole dataset, and with each lineage (endoderm, mesoderm, ectoderm) analyzed separately alongside the undifferentiated hESCs (i.e. endoderm + ESC, mesoderm + ESC, ectoderm + ESC) to obtain better expression models for each lineage. Each of the four groups was analyzed using the same approach. Data were loaded into R using the tximport library (Soneson, Love, and Robinson 2016), and the gene/count matrix was filtered to retain only genes with five or more mapped reads in two or more samples. Initial analysis indicated a strong batch effect from the passage number of the hESCs cells, so the passage number was incorporated in the expression model, specified as '~ generation + condition' where generation is the passage number, and condition is the combination of cell type (ectoderm, mesoderm, endoderm, or undifferentiated hESCs) and $PbCl_2$ dose (C (control), L (low), or H (high)). Differential expression was assessed using DESeq2 v1.38.3; expression differences were calculated using an alpha (FDR cut-off) value of 0.05, and fold changes were shrunk using lfcShrink() function to apply the apeglm method (v 1.20.0) (Zhu, Ibrahim, and Love 2019). Multiple testing correction was performed using the Benjamini Hochberg method, and lists of significantly DE genes were identified using a q-value (i.e. a corrected p value) cut-off of 0.05.

PCA plots were generated using the DESeq2 plotPCA function, which runs PCA using the top 500 most variable genes. Heatmaps were plotted using normalized read counts for the samples and genes of interest, with each heatmap row (gene) scaled to a Z-score to show variability between replicates rather than absolute expression values across genes.

# Results

## Inhibition of Proliferation Endpoint

### Cell Proliferation and Metabolic Rate of hESCs exposed to BPA, PFOS, or $PbCl_2$ for 6 days

The proliferation rate was estimated by measuring the mitochondrial dehydrogenase activity (MDHA). After 6 days of exposure hESCs exposed to BPA showed a monotonic dose-dependent decrease in MDHA rate. Cells dosed at 2500 µg/L had a significantly lower MDHA rate compared to solvent control (Figure 2a & 3a). Additionally, BPA-treated hESCs showed increased MDHA rate per live cell at 2500 µg/L compared to 0.25 µg/L cells (Appendix 1).

Furthermore, PFOS-treated hESCs after 6 days of exposure showed a monotonic reduction in MDHA rate in a dose dependent manner. Both 455 µg/L and 2275 µg/L treated hESCs had significantly lower proliferation rates than the solvent control (figure 2b & 3b). When normalized against cell number per well, the differences in MDHA rate between PFOS-treated and control cells vanished (Appendix 2).

$PbCl_2$ exposure to hESCs for 6 days displayed a significant diphasic change in MDHA rate. The 6.2 µg/L treated hESCs had a significantly higher MDHA rate than solvent control hESCs, and 620 µg/L hESCs had a significantly lower MDHA rate than the control (Figure 2c & 3c). Additionally, when normalized per live cell showed a significant increase in MDHA between the 0.62 µg/L and 620 µg/L treated hESCs (Appendix 3).

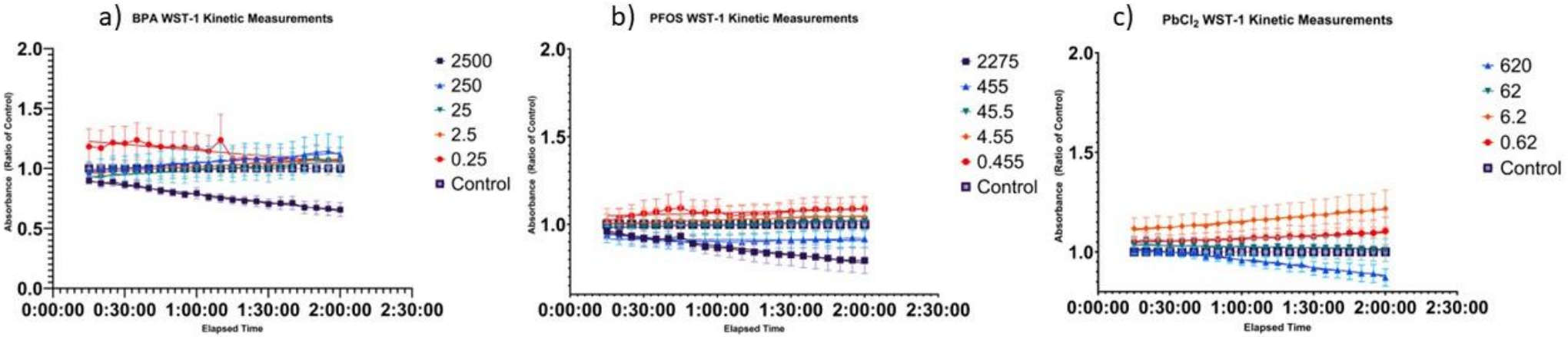


*Figure 2*: a) The effect of BPA or type-1 water on MDHA rate in hESCs. N=6. b) Effects of PFOS or type-1 water on MDHA kinetics of hESCs. N=6. c) Effects of $PbCl_2$ or type-1 water on MDHA kinetics of hESCs. N=7. MDHA activity was measured after 6 days of exposure. MDHA was measured as the absorbance of light emitted at 450 nm by formazan dye. Measurements are taken every 5 minutes over 2 hours. Values are shown as the ratio of each respective replicate control. Error bars represent standard error.

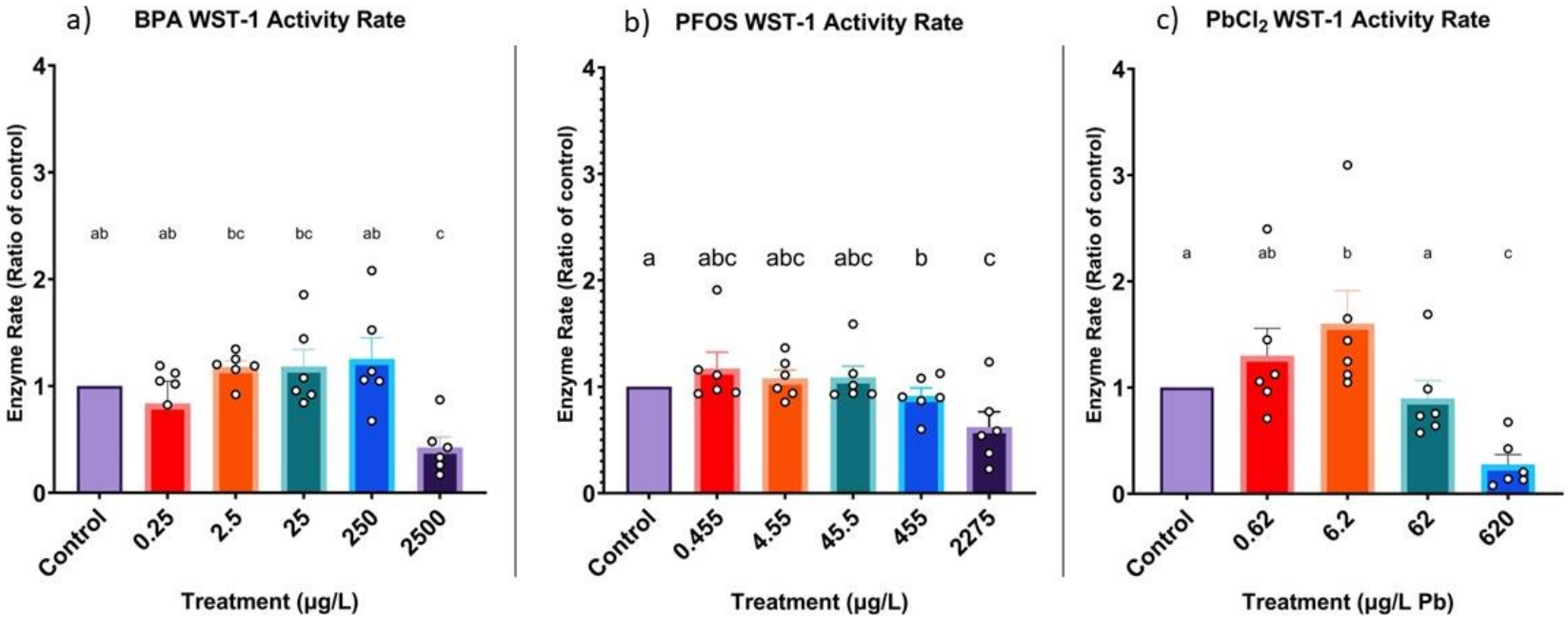


*Figure 3:* a) The effect of BPA or type-1 water on MDHA rate in hESCs. N=6. b) Effects of PFOS or type-1 water on MDHA kinetics of hESCs. N=6. c) Effects of $PbCl_2$ or type-1 water on MDHA kinetics of hESCs. N=7. MDHA activity was measured after 6 days of exposure. Values were obtained from the slope of the absorbance kinetics of 450nm emmision light over time. Measurements were recorded every 5-minutes, over 2-hours. Values are shown as ratios of control of each respective replicate. Error bars represent standard error. Letters with no overlap indicate comparisons with a significant p-value, below 0.05.

## Rate of Cell Death and Measurement of Final hESC Population and Viability After 6 Days of Exposure to BPA, PFOS, or $PbCl_2$

BPA-exposed hESCs at the 0.25 µg/L level showed the greatest total number of cells after 6 days of dosing. However, this was not significantly higher than control, it was significant compared to the 2500 µg/L treatment group (Figure 4a). Additionally, the 25 µg/L dose group displayed a significantly higher number of total cells compared to the 2500 µg/L group, but not when compared to control (Figure 4a). There were no significant effects of BPA dose on cell viability (Figure 5a). Additionally, day-1 of exposure to BPA at 0.25 µg/L showed a significant increase in dead cells in the medium when compared to the 2.5, 25, and 250 µg/L treatments (Figure 6a). Moreover, no significant treatment effects were seen on the overall cell death over the 6-day dosing period (Figure 7a).

PFOS-exposed hESCs showed a diphasic dose response in the total population size after 6-days of exposure. The 45.5 µg/L treatment group had a significantly higher proportion of total and live cells. Meanwhile, the 2275 µg/L group had significantly lower populations in total hESCs compared to both 45.5 µg/L and solvent control groups (Figure 4b). Furthermore, PFOS exposure did not have any significant effects on hESC viability (Figure 5b). PFOS-treated cells did not have a significantly different number of dead cells measured on any day of exposure or overall (Figure 6c & 7c).

PbCl2-treated hESCs displayed a diphasic dose-response effect on the total population size of total cells after 6-days of exposure. The 0.62 µg/ L group had a significant increase in population size compared to the control. Meanwhile, the 620 µg/L group showed a significantly lower population size of total cells compared to the control (Figure 4c). Furthermore, the 6200 µg/L group had a zero population on day 6 (not shown). No dose-response effects were observed on cell viability after 6 days of exposure (Figure 5c). Additionally, a significant decrease in dead cells was observed in the 6200 µg/L Pb treatment

on day 6 (Figure 6c). No significant difference in overall cell deaths was observed between $PbCl_2$ treatment and control groups (Figure 7c).

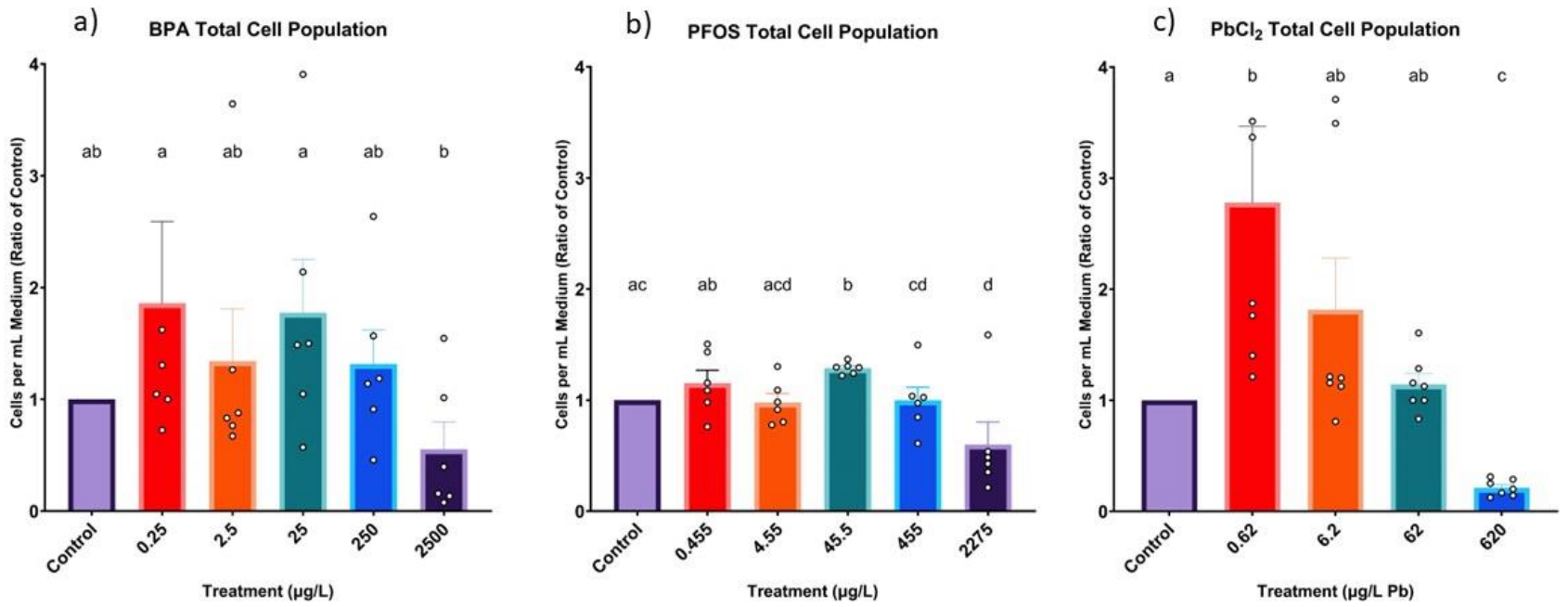


*Figure 4*: a) The effects of BPA on cell population size in hESCs, n=6. b) The effects of PFOS on cell population size in hESCs, n=6. c) The effects of $PbCl_2$ on cell population size in hESCs, n=7. Values are presented as ratios of treatment to control. Population size was measured after 6 days for exposure. Error bars represent standard error. Letters with no overlap represent comparisons with a p-value less than 0.05 when computed by ANOVA on rank.

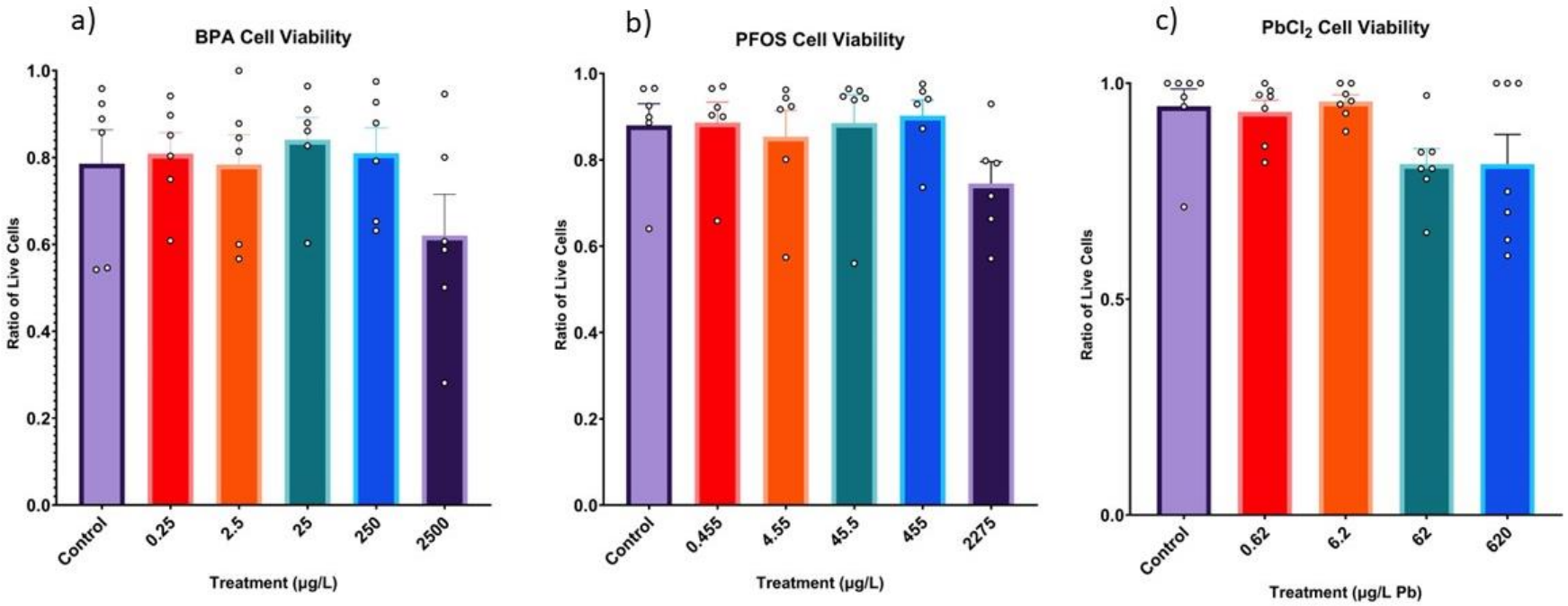


*Figure 5:* a) Effects of BPA on live/ total cell ratio in hESCs, n=6. b) Effects of PFOS on live/ total cell ratio in hESCs, n=6. c) Effects of $PbCl_2$ on live/ total cell ratio in hESCs, n=7. Live, dead, and total cell populations per well were counted in hESCs after 6 days of exposure. The values are shown as ratios of treatment to control. Error bars represent standard error.

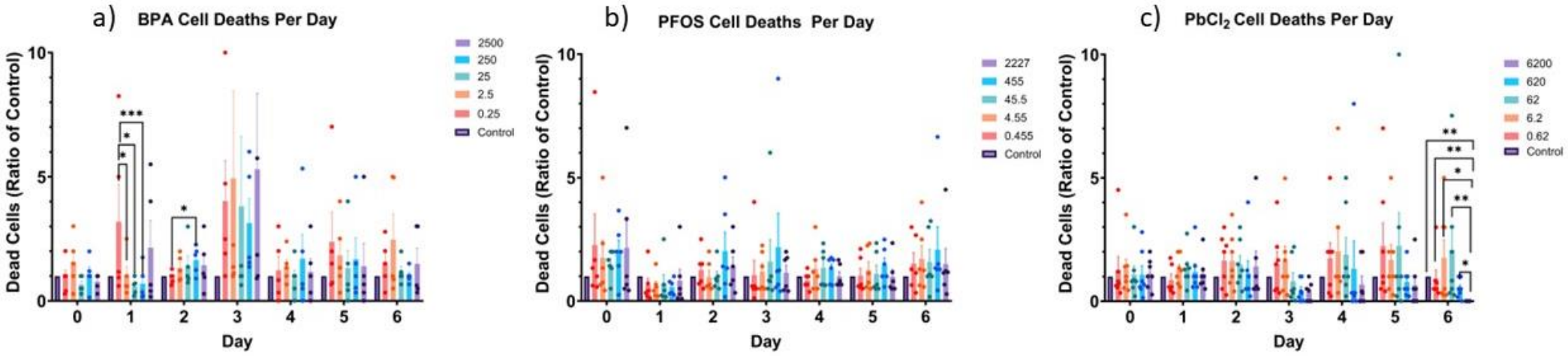


*Figure 6*: a) The effect of BPA on daily number of dead cells in suspension in the medium. b) The effect of PFOS on daily number of dead cells in suspension in the medium c) The effect of $PbCl_2$ on daily number of dead cells in suspension in the medium. Data is presented as a ratio of each batch control each day over the 6-day exposure. Error bars represent standard error. Asterisks represent comparisons with a p-value less than 0.05 computed by ANOVA on rank.

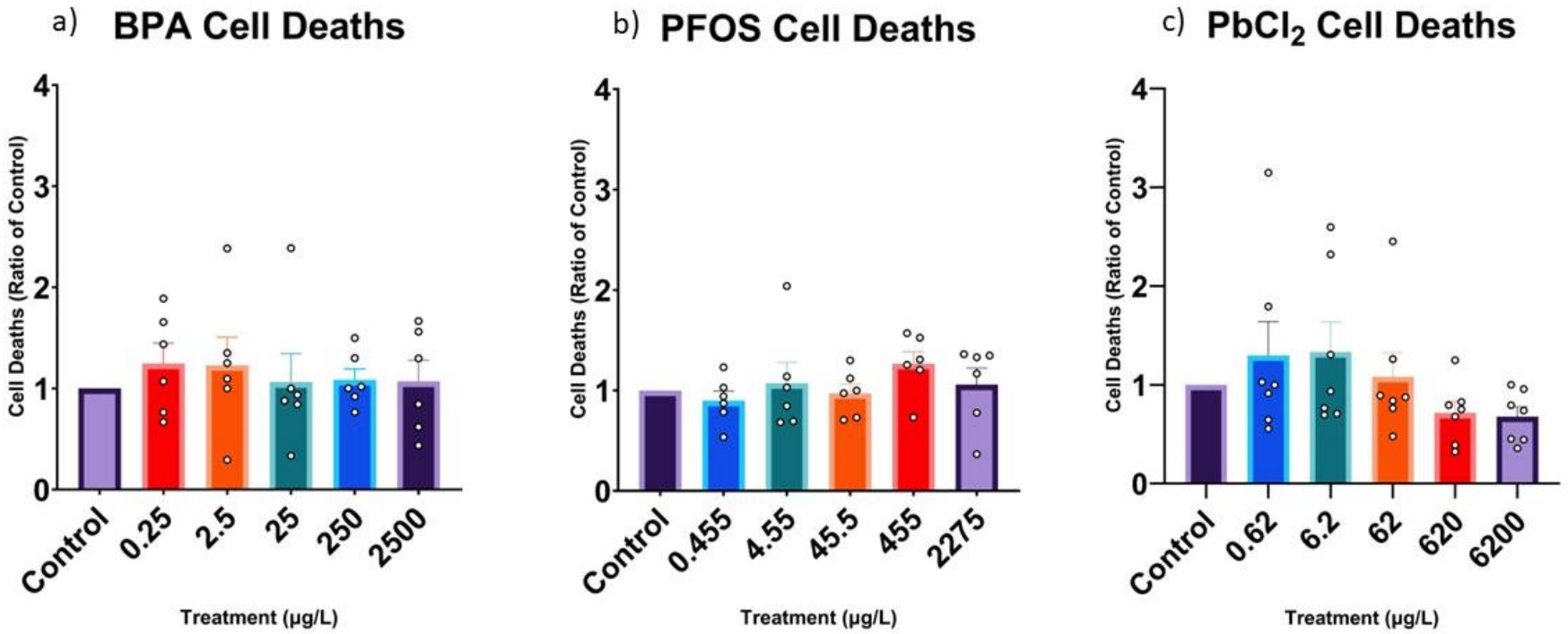


*Figure 7:* a) The effects of BPA on total number of dead cells in hESCs, n=6. b) The effects of PFOS on total number of dead cells in hESCs, n=6. c) The effects of $PbCl_2$ on total number of dead cells in hESCs, n=7. Values are given as a ratio of treatment to control. hESCs were exposed to contaminants or type-1 water as a solvent control. Dead cells floating in culture medium were collected and counted every day during 6 days of exposure. Error bars represent standard error.

## Cell Confluency of hESCs After 6 Days of Exposure to BPA, PFOS, or $PbCl_2$

hESCs treated with type-1 water or BPA showed increased confluency over time. However, there was no significant dose-response relationship from exposure to BPA compared to control (Figure 8a & 9a).

PFOS-treated cells showed a significantly reduced confluence on day 6 in the 45.5 µg/L and 2275 µg/L groups compared to solvent controls. PFOS-treated cells in the 45.5 µg/L and 455 µg/L groups also had lower confluences than control on day 2. Additionally, the 455 µg/L treated group had significantly lower confluency than control on day 3 (Figure 9b).

There were no significant differences in the confluence between any $PbCl_2$ treated groups or with control (Figure 8c & 9c).

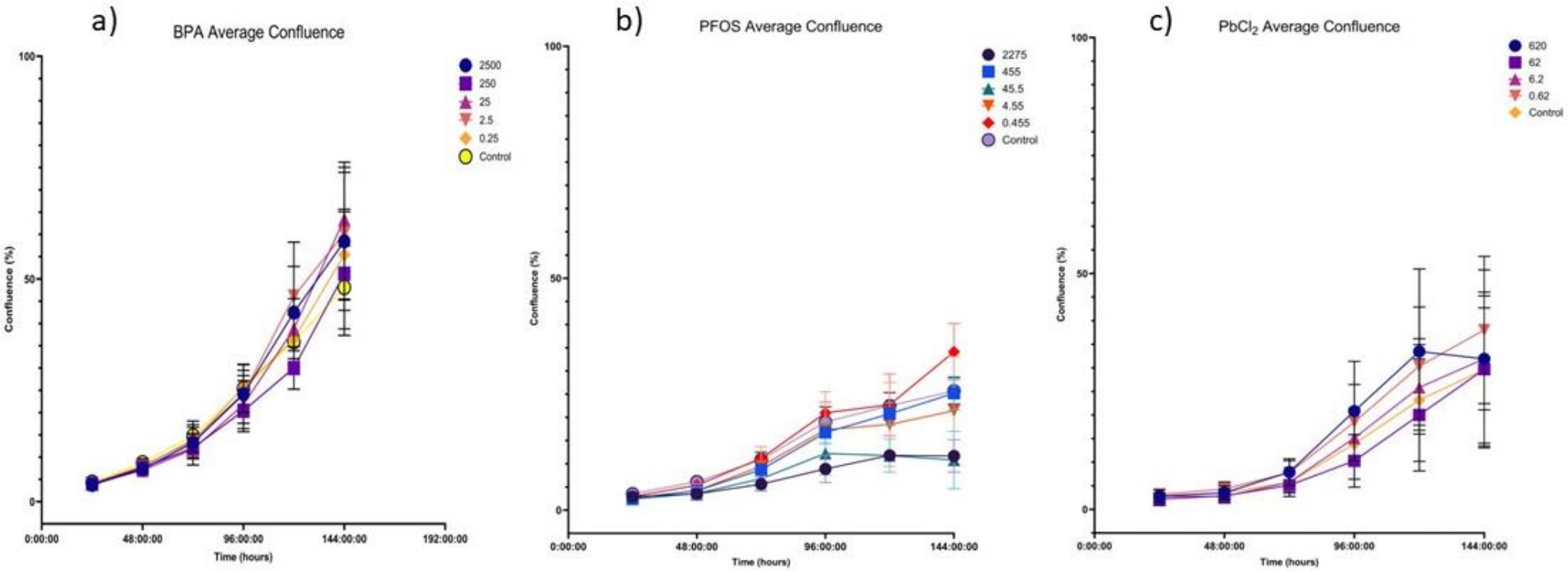


*Figure 8*: a) Effects of BPA on culture confluency in hESCs, n=4. b) Effects of PFOS on culture confluency in hESCs, n=4. c) Effects of $PbCl_2$ on culture confluency in hESCs, n=3. The culture confluency was measured as percentage of cell coverage per field of view in culture plate. Measurements were taken every 6 hours each day during 6-days of exposure. hESCs were exposed to contaminant or type-1 water. Average proportions were calculated daily by taking the mean of the 4 measurements taken every 6-hours each day. Error bars represent standard error.

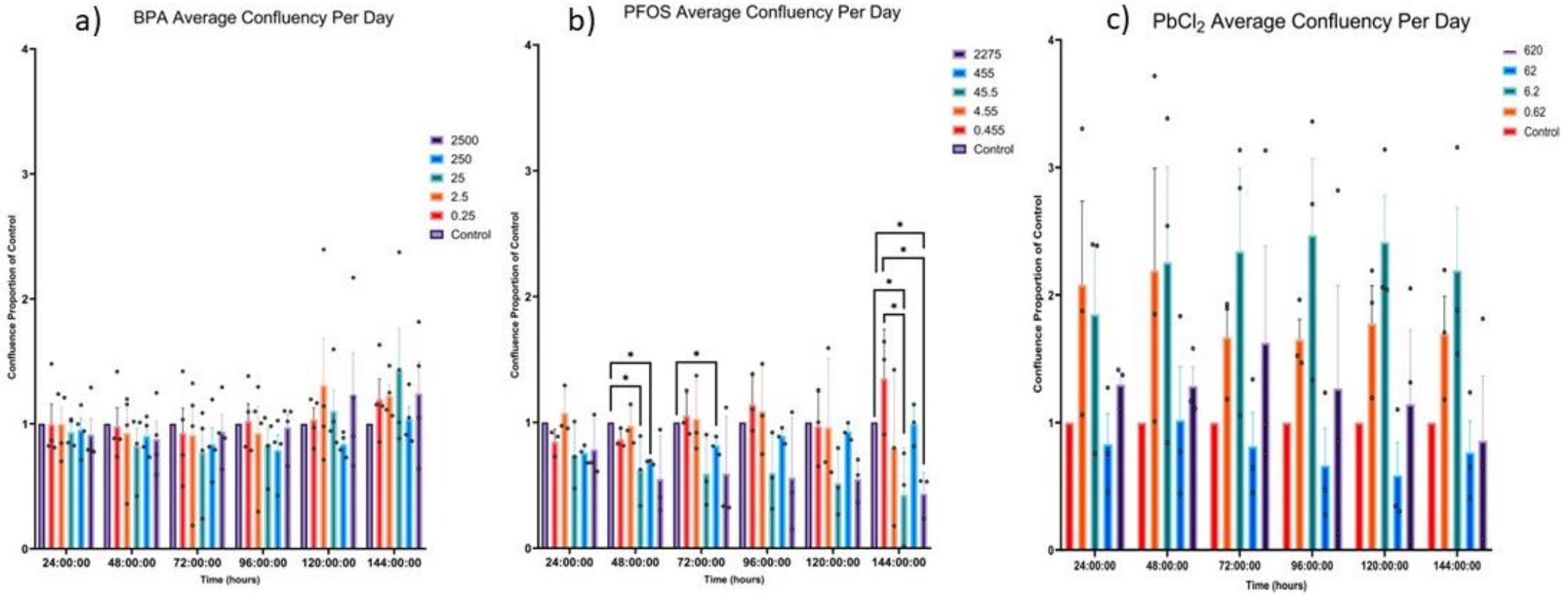


*Figure 9*: a) Effects of BPA on relative culture confluency in hESCs, n=4. b) Effects of PFOS on relative culture confluency in hESCs, n=4. c) Effects of $PbCl_2$ on relative culture confluency in hESCs, n=3. Culture confluency was measured as percentage of cell coverage per field of view in culture plate. Measurements were taken every 6 hours each day during 6 days of exposure to contaminant or vehicle. Four measurements were averaged to represent culture confluency of the day. Values are shown as ratios of treatments to control. Error bars represent standard error.

## Cell Cycle Phase Analysis of hESCs exposed to BPA, PFOS, or $PbCl_2$ for 6 Days

hESCs exposed to BPA showed a biphasic dose response in the proportion of cells in the G2/M phase. Cells exposed to 25 µg/L and 250 µg/L BPA had significantly lower proportions of G2/M phase cells compared to control. Meanwhile, the 2500 µg/L dose group had a significant increase in G2/M cells compared to control. Conversely, 250 µg/L or 2500 µg/L BPA groups had significantly lower proportions of G0/G1 phase cells than the 2.5 µg/L dosed cells. In S-phase proportions, there was a significant decrease in the 2500 µg/L BPA group compared to the 25 µg/L BPA group (Figure 10a).

PFOS-exposed hESCs showed no significant changes in G2/M proportion compared to the control. However, there appears to be a monotonic increase in proportion due to the dose. The 45.5 µg/L group had a significantly higher G2/M proportion than the 0.455 µg/L group. Moreover, the 2275 µg/L exposed group had a significantly higher proportion of cells in the G2/M phase than the 4.55 µg/L group. S-phase proportions showed a monotonic dose-dependent increase. The 0.455 µg/L, 45.5 µg/L, and 455 µg/L groups all had a significantly higher proportion of S-phase cells when compared to control. In G0/G1 phase proportions, 2275 µg/L exposed cells had a significantly lower proportion of cells when compared to the 4.55 µg/L dosed group (Figure 10b).

There was a significant enrichment of S-phase hESCs in the 62 µg/L and 620 µg/L $PbCl_2$ groups when compared to control (Figure 10c).

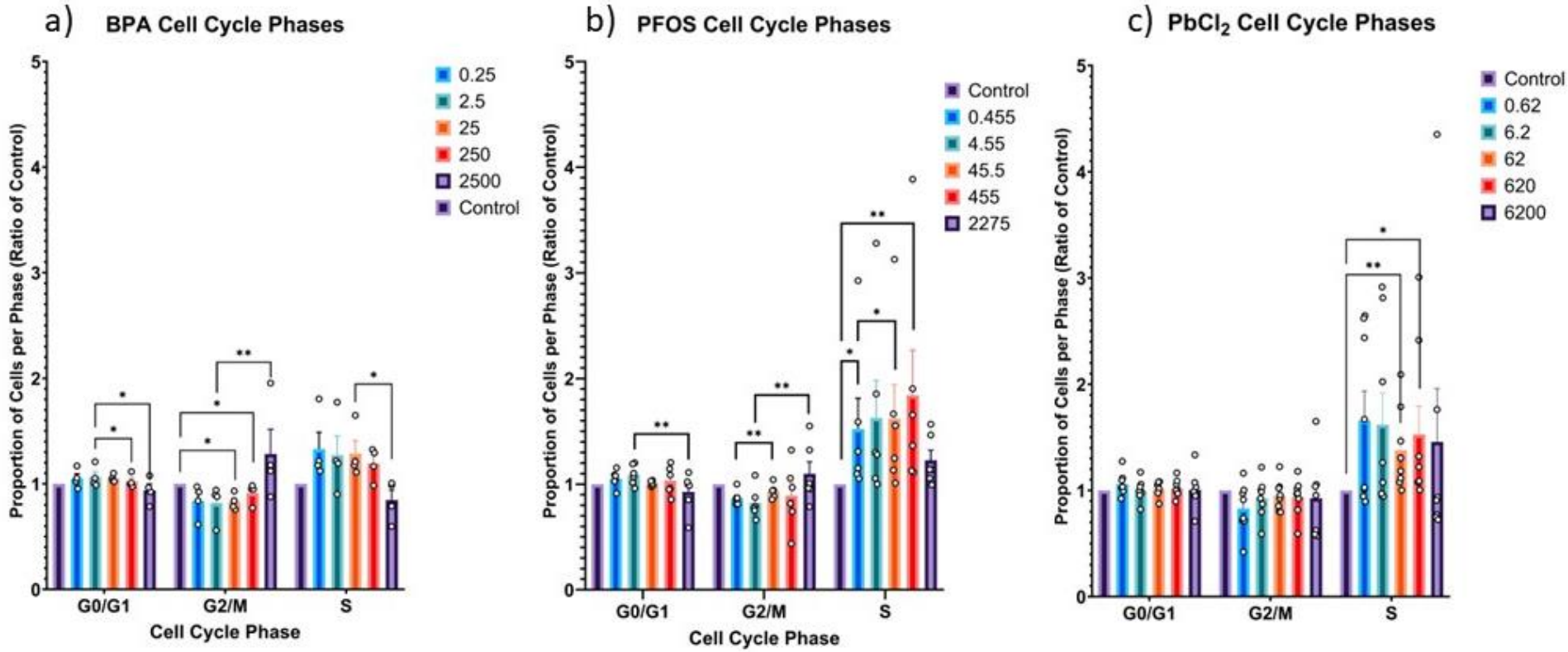


*Figure 10:* a) Effects of BPA on cell cycle phases in hESCs, n=4. b) Effects of PFOS on cell cycle phases in hESCs, n=6. c) Effects of $PbCl_2$ on cell cycle phases in hESCs, n=8. Cellular DNA was labeled with fluorescent dye and measured by flow cytometer after 6 days of exposure to contaminant or type-1 water. Levels of DNA content was used to differentiate cell cycle phases Doses are given in µg/L. Values are given as a ratio to the control of each batch. Error bars represent standard error. Asterisks indicate comparisons with significant differences when computed in an ANOVA on ranks.

## Inhibition of Differentiation Endpoint

### Differentiation Induction and Transcriptome Sequencing of hESCs exposed to BPA, PFOS, or $PbCl_2$ for 5-7 days.

$PbCl_2$ exposure to hESCs and induction of differentiation into ectoderm, mesoderm, and endoderm showed a dose-dependent modulation of several lineage marker genes. In ectoderm, STMN4, WNT1, FABP7, OLIG2, and TUBB3 had a significant increase in expression from dose compared to control (Figure 11a). Within mesoderm lineage markers, HAND1 increased significantly with dose, and TAGLIN decreased significantly only in the 6.2 µg/L group compared to control (Figure 11b). Of the measured endoderm markers, only CDH1 increased significantly with treatment, while GATA4 had lower expression only in the 6.2 µg/L treatment (Figure 11c).

Pluripotency genes seemed to be highly depressed in differentiated samples compared to undifferentiated controls (Figure 12). Some pluripotency genes remain expressed in some differentiated samples, however, there are no significant dose-response relationships observed.

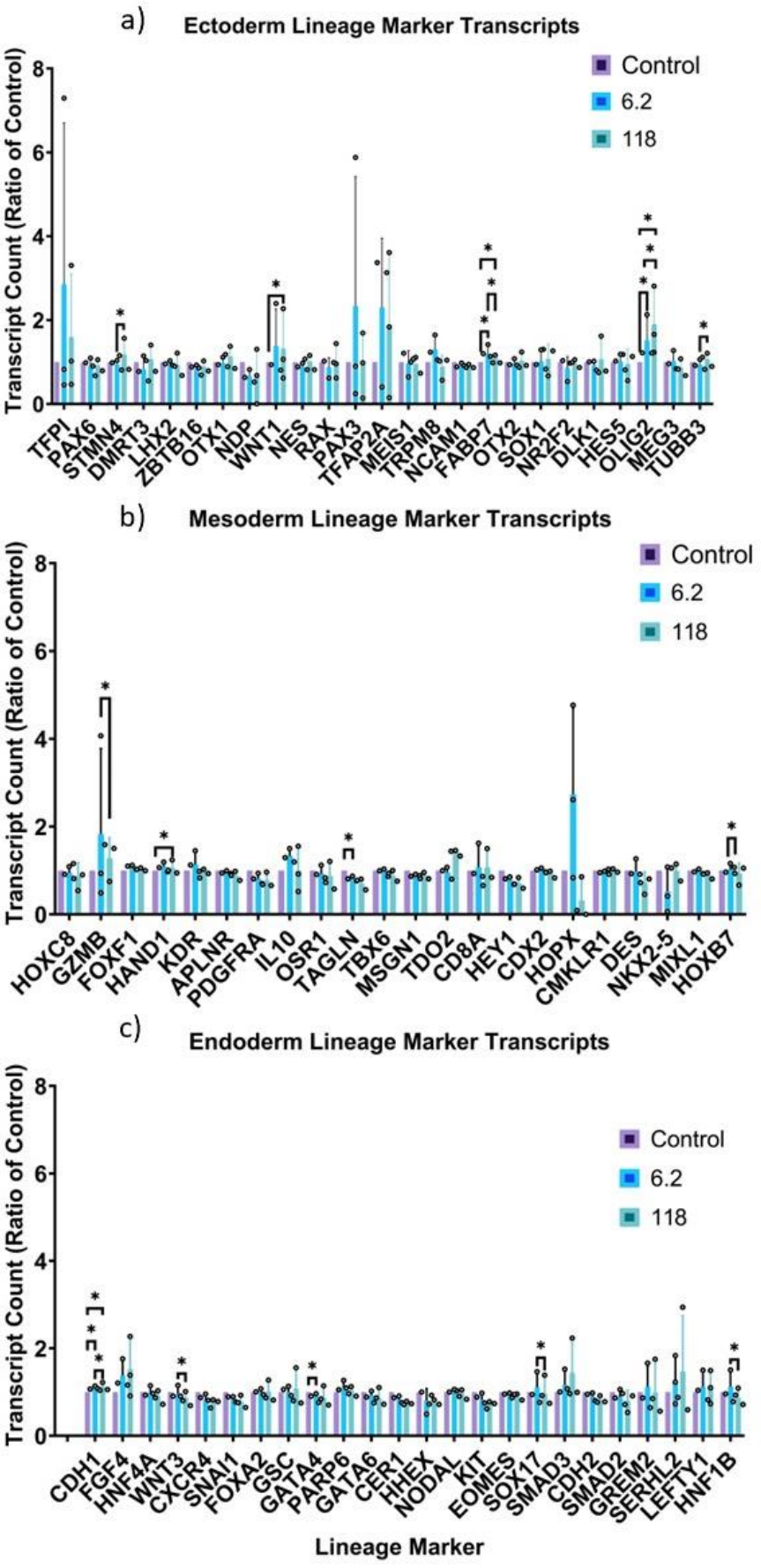


*Figure 11:* a) Effects of $PbCl_2$ on the expression of ectoderm marker genes in hESCs. b) Effects of $PbCl_2$ on the expression of mesoderm marker genes in hESCs. c) Effects of $PbCl_2$ on the expression of endoderm marker genes in hESCs. Cells were exposed to $PbCl_2$ or type-1 water for 7 days for ectoderm and 5 days for meso- and endoderm. hESCs were induced to differentiate during exposure. Gene expression is represented as a ratio of each replicate control. Error bars represent standard error, n=3. Asterisks indicate comparisons with significant differences when computed in an ANOVA on ranks (p=value < 0.05).

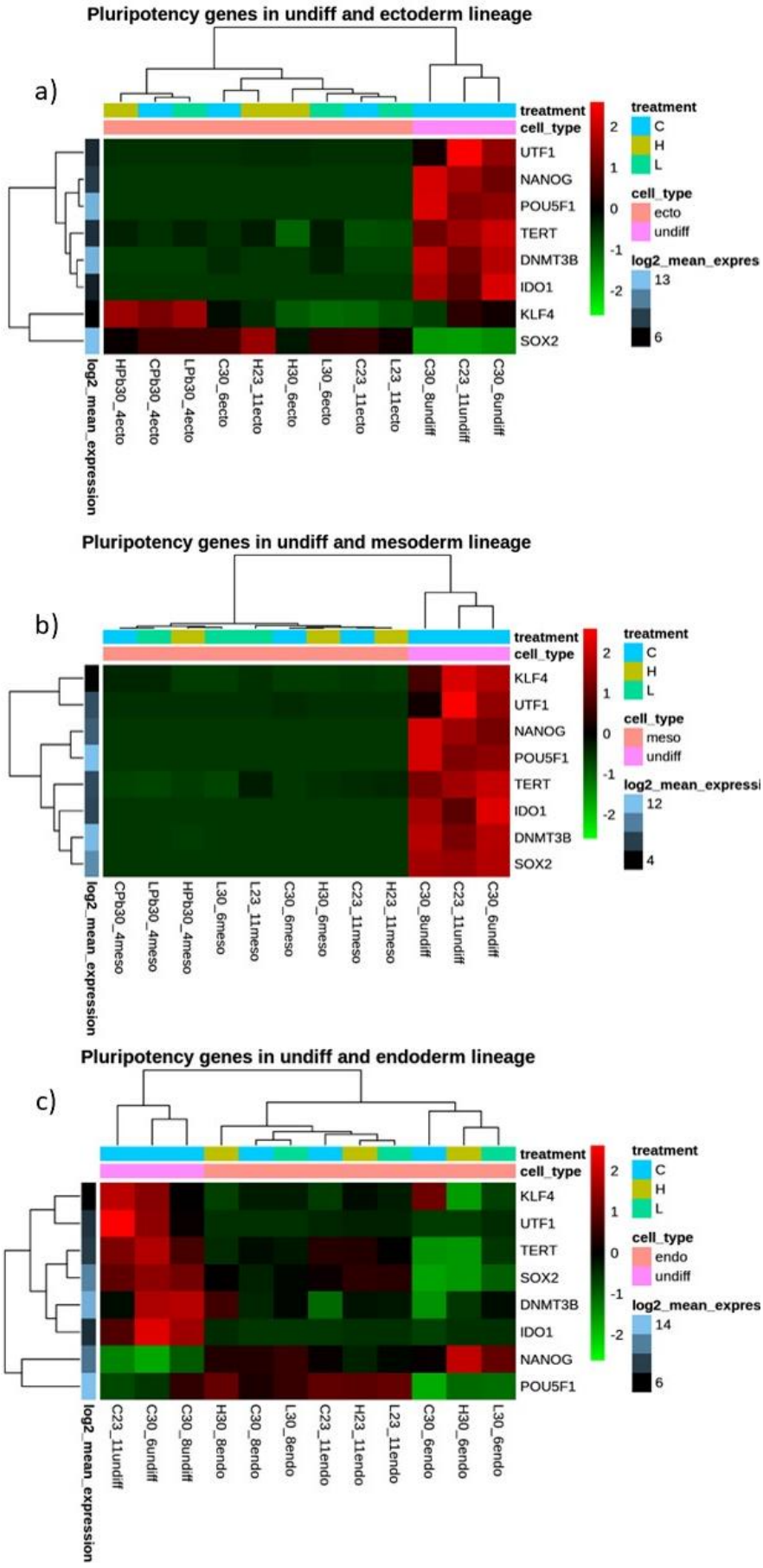


*Figure 12:* a) A heatmap revealing expression profile of pluripotency genes in undifferentiated and differentiated hESCs to ectoderm b) A heatmap revealing expression profile of pluripotency genes in undifferentiated and differentiated hESCs to mesoderm. c) A heatmap revealing expression profile of pluripotency genes in undifferentiated and differentiated hESCs to endoderm. hESCs were exposed to $PbCl_2$ or type-1 water.

The number of genes significantly differentially expressed by $PbCl_2$ treatment is listed in Table 5. $PbCl_2$ 6.2 µg/L exposure group had significantly altered more gene expression during the differentiation of hESCs to ectoderm than to mesoderm or endoderm. In contrast, $PbCl_2$ exposed at 118 µg/L significantly affected more gene expression during the differentiation of hESCs to mesoderm than ectoderm and endoderm. The expression of five genes, including GSTT2/GSTT2B, INE2, PAK6-AS1, PDXDC2P, and TEX13C was affected by both doses of $PbCl_2$ during the differentiation of hESCs to ectoderm (Table 6). The expression of five genes, including ANKRD36BP1, INE2, PWAR1, PCDHA1, and SMG1P2 were altered by both doses of PbCl2 during the differentiation of hESCs to mesoderm. The expression of two genes, INO80B-WBP1 and SPCS2P4 were changed by both doses of $PbCl_2$ during differentiation of hESCs to endoderm. Expression of INE2 (a long-non-coding RNA gene) was altered by both doses of $PbCl_2$ during the differention of hESCs to both ectoderm and mesoderm, suggesting that this gene could be a biomarker of lead exposure during early embryo development.

*Table 5:* Number of genes significantly affected by $PbCl_2$ treatment

| *PbCl2 vs Control* | *Endoderm* | | *Ectoderm* | | *Mesoderm* | |
|---|---|---|---|---|---|---|
| | identified | unknown | identified | unknown | identified | unknown |
| *Low vs. Ctl* | 4 | 13 | 20 | 18 | 12 | 12 |
| *High vs. Ctl* | 8 | 16 | 18 | 14 | 25 | 15 |

*Table 6*: Name of identified genes significantly affected by $PbCl_2$ treatment. Bold genes indicate significance in both 0.62 and 118 µg/L Pb treatments. Red genes are significant in multiple lineages (ectoderm, mesoderm, or endoderm).

| Ecto-LPb/C | Ecto-HPb/C | Meso-LPb/C | Meso-HPb/C | Endo-LPb/C | Endo-HPb/C |
|---|---|---|---|---|---|
| C1QTNF3-AMACR | **ANKRD36BP1** | **ANKRD36BP1** | **ANKRD36BP1** | CERS6-AS1 | C5orf63 |
| LOC643201 | ATM | CALB1 | CERS6-AS1 | GOLGA8Q | **INO80B-WBP1** |
| GSTM3P1 | EWSAT1 | CALB2 | CBY3 | **INO80B-WBP1** | MFSD1P1 |
| **GSTT2/GSTT2B** | **GSTT2/GSTT2B** | **INE2** | CCDC39 | **SPCS2P4** | **NAV2-AS1** |
| H4C12 | **INE2** | NOL4 | COLEC12 | | RGPD4 (includes others) |
| HSPE1-MOB4 | LST1 | NPM1P9 | DNAJB14 | | RHEBP2 |
| **INE2** | MATR3 | PTX4 | GUSBP17 | | **SPCS2P4** |
| IKBKGP1 | MT1E | **PWAR1** | **INE2** | | SNRPGP15 |
| KBTBD11-OT1 | MT1X | **PCDHA1** | **IKBKGP1** | | |
| LKAAEAR1 | MT2A | SLC5A4-AS1 | IGFBP5 | | |
| LY75-CD302 | **PAK6-AS1** | **SMG1P2** | **MT1E** | | |
| LCP2 | **PDXDC2P** | UTP14C | MT1G | | |
| MESP2 | ARHGAP8/PRR5-ARHGAP8 | | **MT1X** | | |
| NAV2-AS1 | RPL41 | | **MT2A** | | |
| **PAK6-AS1** | RN7SL2 | | NQO1 | | |
| PSMB9 | STC2 | | OTUD7A | | |
| **PDXDC2P** | **TEX13C** | | **PWAR1** | | |
| RASGRF2-AS1 | TUBA1B-AS1 | | **PCDHA1** | | |
| SPDYE14 | | | RPL23AP60 | | |
| **TEX13C** | | | **SMG1P2** | | |
| | | | UQCC5 | | |
| | | | LOC100652999 | | |
| | | | LOC118567325 | | |
| | | | ZNF737 | | |
| | | | ZNF883 | | |

PCA analysis showed clustering of genes in all three lineages (endoderm, ectoderm, and mesoderm) distinct from undifferentiated hESCs and from each other, regardless of $PbCl_2$ treatment. This suggests successful differentiation into the 3 germ lineages (Figure 13). PCA analysis also identified significant passage (batch) effects on gene expression profiles. After correcting for this effect, gene expression in the 118 µg/L dose $PbCl_2$ group clustered

away from the solvent control in cells differentiated into ectoderm and mesoderm but not in endoderm.

IPA analysis identified multiple canonical pathways that were significantly affected in cells differentiated into endoderm, ectoderm, and mesoderm as compared to undifferentiated hESCs (Figure 14). Some effects on pathways were conserved across lineage, such as Cholesterol Biosynthesis Pathway. Meanwhile, pathways such as NRF2-Regulated Oxidative Stress had opposing trends among the three lineages. $PbCl_2$ treatment either intensified, such as in Gustation Pathway, weakened, such as in NRF2-Regulated Oxidative Stress, or had no effects, such as in Cholesterol Biosynthesis Pathway, on gene expression within each lineage.

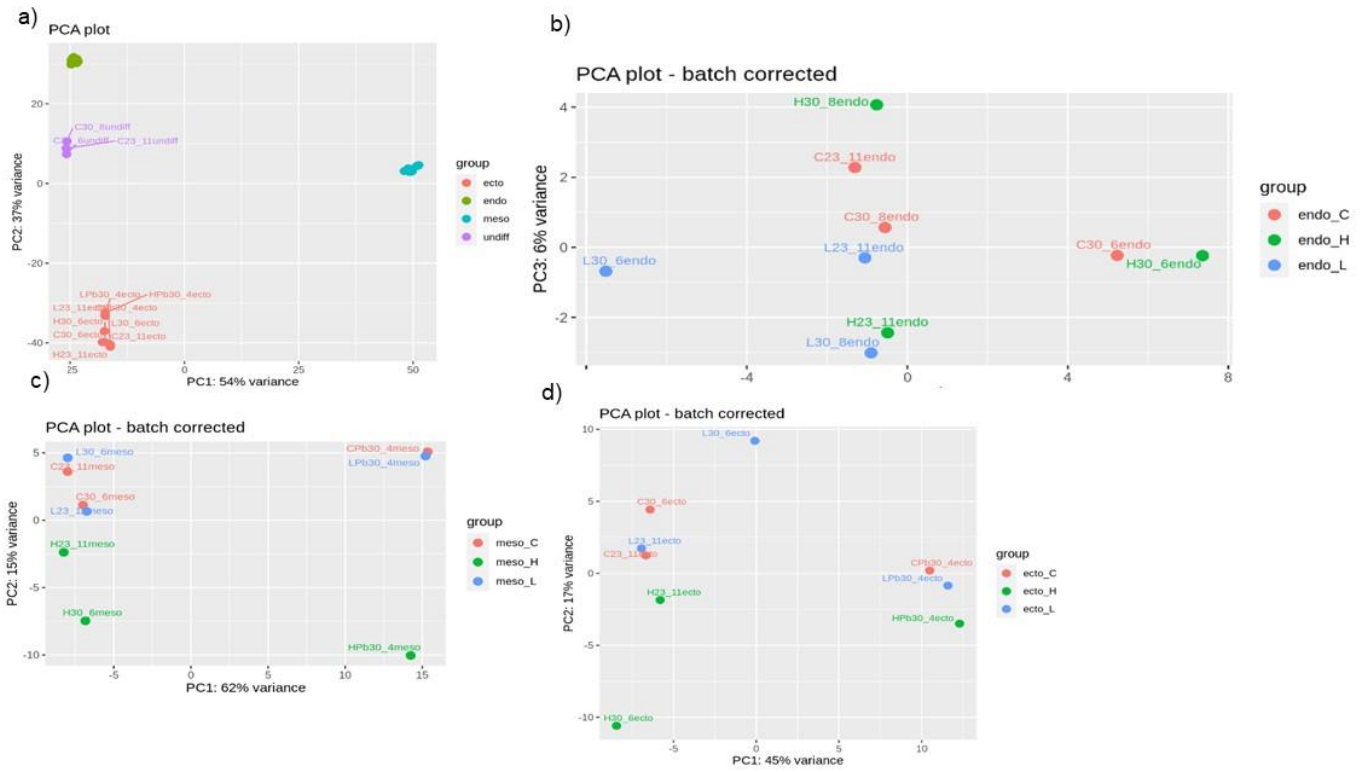


*Figure 13*: PCA analysis of gene expression profiles in undifferntiated hESC and hESCs induced to differentiate into ectoderm, mesoderm, and endoderm during 7 (ectoderm) or 5 (mesoderm and endoderm) days of exposure to 6.2 or 118 µg/L of $PbCl_2$ or vehicle. b) PCA of gene expression profiles of hESCs after induction of differentiation to endoderm, c) ectoderm, and d) mesoderm.


*Figure 14:* Data set comparison analysis showing canonical payways in hESCs that have been differentiated into the 3 major germ lineages during 4 or 6 days of exposure to $PbCl_2$ or vehicle. Z-scores and heatmap were computed using IPA. All entries had Z-score$\leq$-2 or $\geq$2.

# Transcriptomic/Genomic Endpoint

## Single Cell Transcriptome Sequencing of hESCs exposed to $PbCl_2$ for 6-days

Single Cell RNA sequencing analysis revealed 7 clusters of cells in undifferentiated hESCs, suggesting that hESCs were a diverse population (Figure 15). Clustering of hESCs was not significantly affected by 0.62, 6.2 and 118 µg/L $PbCl_2$ treatments (Figure 16), except that 118 µg/L $PbCl_2$ increased the proportion of cells in cluster 2 (Figure 17). Analysis of differential gene expression across all cells and treatments found numerous significant gene changes (Table 4a). However, when adjusted for a 20% false discovery rate, only a few genes remained significant (Table 4b). Genes significantly affected by treatment, irrespective of the cluster, included AC22140.1 and XACT (Table 4c). In cluster 1, only AC22140.1 was found to be significantly affected by treatment (Table 4d). Treatment significantly affected 4 genes in cluster 2: AC22140.1, SPRY4, ESYT2, and PIP4P2 (Table 4e). In cluster 2, the upregulation of 4 genes: AC007326.4, SERPINB9, EGR1, and USP9X were characteristic of cluster 2 (Figure 18-19). Moreover, the downregulation of DUSP6, HMGCS1, AK4, and THY1 was characteristic of cluster 2 (Figure 20-21).

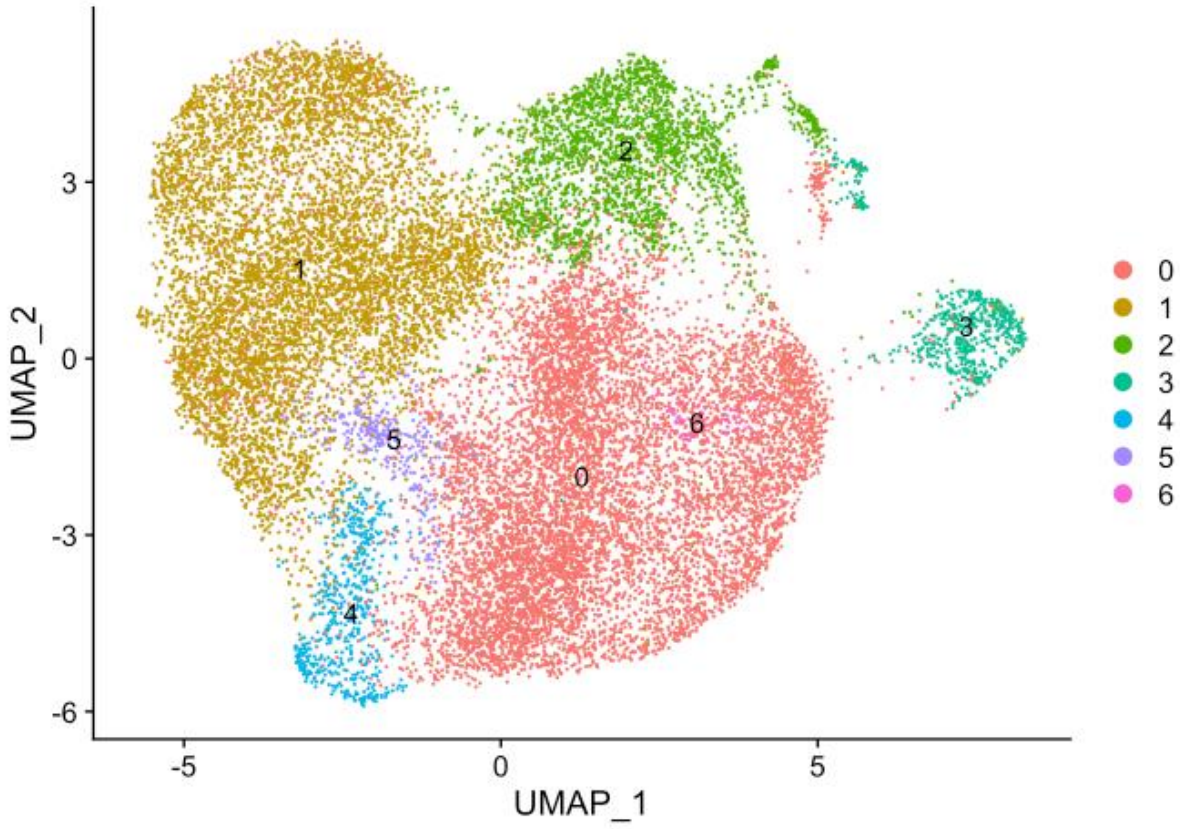


*Figure 15:* A Uniform Manifold Approximation and Projection (UMAP) analysis of the single cell transcriptome expression of hESCs exposed to $PbCl_2$ or type-1 water. Clusters are generated based on RNA expression profile. Clustering resolution was set at 0.2, to generate 7 clusters. Each point represents 1 cell.

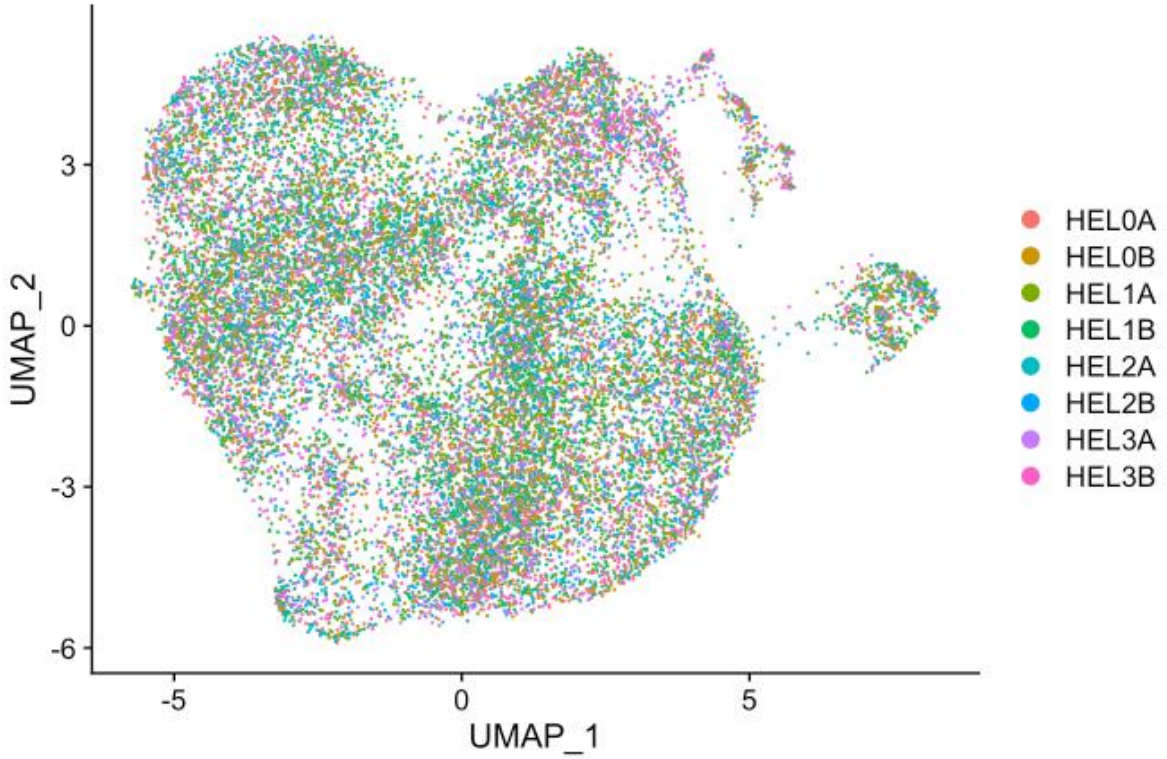


*Figure 16*: Replicate identification tagging of hESC from single cell transcriptomes on a UMAP analysis. HEL0, HEL1, HEL2, HEL3 represents solvent control, 0.62 µg/L, 6.2 µg/L, and 118 µg/L of $Pb^{2+}$ administered as $PbCl_2$, respectivly. "A" and "B" indicate matching replicates.

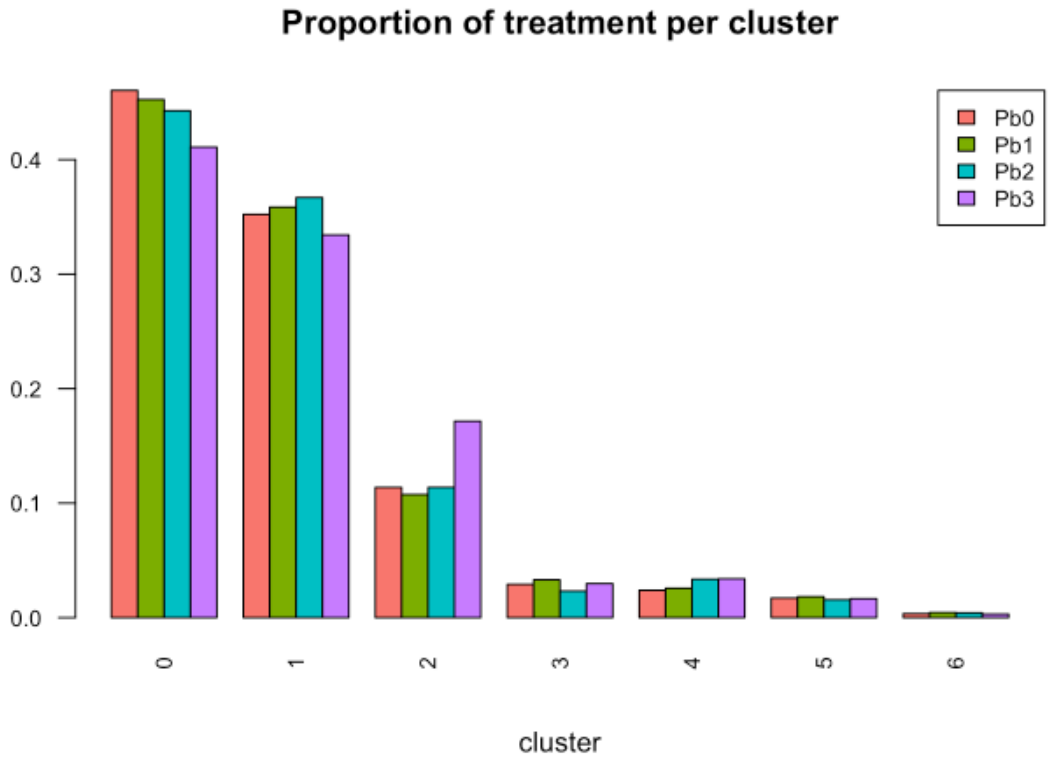


*Figure 17*: The effects of PbCl2 on the proportion of cells in each treatment tagged and assigned to each cluster.

*Table 7*: a) The number of differentially expressed genes across all clusters and doses with a significant p-value. P-values were not corrected for a large number of multiple comparisons. b) The number of differentially expressed genes across all clusters and doses with a significant p-value after correction with a 20% false discovery rate adjustment for multiple comparisons. Pb0, Pb1, Pb2, Pb3 signify doses 0.62 µg/L, 6.2 µg/L, and 118 µg/L of $Pb^{2+}$ respectively. c) The identification of the differentially expressed genes in all cells and their relative $\log_2$ fold change between the 118 µg/L treatment group and control. d) The identification of the differentially expressed genes in cluster 1 and their relative $\log_2$ fold change between the 118 µg/L treatment and control groups. e) The identification of the differentially expressed genes in cluster 2 and their relative $\log_2$ fold change between the 118

µg/L treatment and control groups. RE 118 µg/L and RE Control indicate relative expression of the 118 µg/L and solvent control respectively.

a) **Differentially expressed genes by cluster and dose; unadjusted p-value**

| | All cells | Cluster 0 | Cluster 1 | Cluster 2 | Cluster 3 | Cluster 4 | Cluster 5 | Cluster 6 |
|---|---|---|---|---|---|---|---|---|
| Pb1 vs Pb0 | 0 | 0 | 0 | 1 | 41 | 495 | 222 | 3,193 |
| Pb2 vs Pb0 | 0 | 0 | 0 | 1 | 240 | 705 | 602 | 3,909 |
| Pb3 vs Pb0 | 2 | 0 | 1 | 16 | 112 | 601 | 389 | 3,978 |

b) **Differentially expressed genes by cluster and dose**

| | All cells | Cluster 0 | Cluster 1 | Cluster 2 | Cluster 3 | Cluster 4 | Cluster 5 | Cluster 6 |
|---|---|---|---|---|---|---|---|---|
| Pb1 vs Pb0 | 0 | 0 | 0 | 0 | 0 | 0 | 0 | 0 |
| Pb2 vs Pb0 | 0 | 0 | 0 | 0 | 0 | 0 | 0 | 0 |
| Pb3 vs Pb0 | 2 | 0 | 1 | 4 | 0 | 0 | 0 | 0 |

c) **Differentially expressed genes in all cells; 118 µg/L vs Control**

| | P-value | $Log_2$ Fold-Change | RE 118 µg/L | RE Control | p_val_adj |
|---|---|---|---|---|---|
| AC022140.1 | 0 | -0.3061054 | 0.881 | 0.918 | 0.00e+00 |
| XACT | 0 | 0.2775596 | 0.417 | 0.360 | 2.96e-05 |

d) **Differentially expressed genes in cluster 1; 118 µg/L vs Control**

| | P-value | $Log_2$ Fold-Change | RE 118 µg/L | RE Control | p_val_adj |
|---|---|---|---|---|---|
| AC022140.1 | 0 | -0.3053566 | 0.927 | 0.953 | 0 |

e) **Differentially expressed genes in cluster 2; 118 µg/L vs Control**

| | P-value | $Log_2$ Fold-Change | RE 118 µg/L | RE Control | p_val_adj |
|---|---|---|---|---|---|
| AC022140.1 | 0.0e+00 | -0.4821046 | 0.779 | 0.874 | 0.0000008 |
| SPRY4 | 0.0e+00 | -0.4248280 | 0.539 | 0.718 | 0.0000014 |
| ESYT2 | 1.9e-06 | -0.3602022 | 0.504 | 0.616 | 0.0519602 |
| PIP4P2 | 3.5e-06 | -0.2693611 | 0.276 | 0.394 | 0.0979593 |

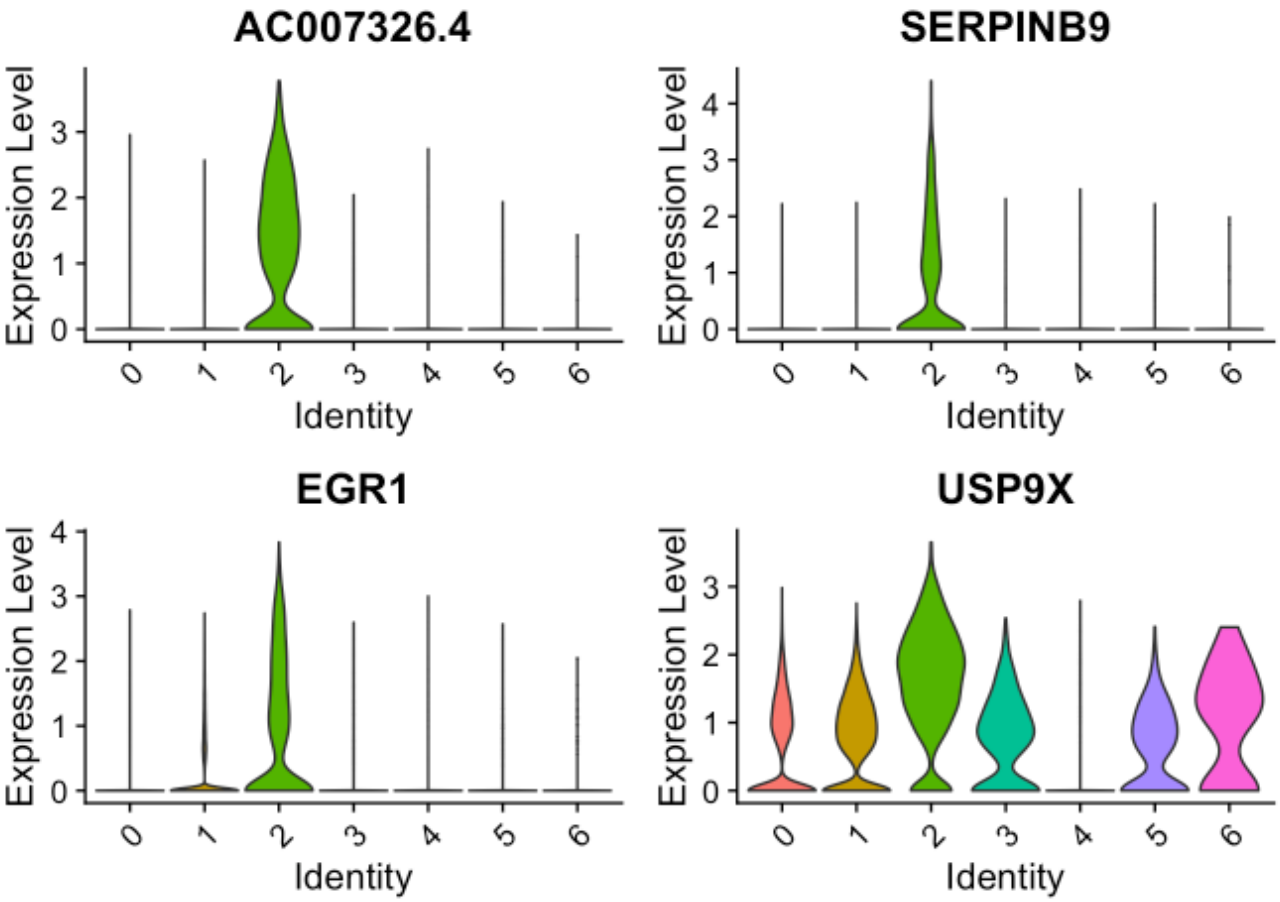


*Figure 18*: The expression distribution across all clusters of the 4 most differentially expressed and upregulated genes in cluster 2.

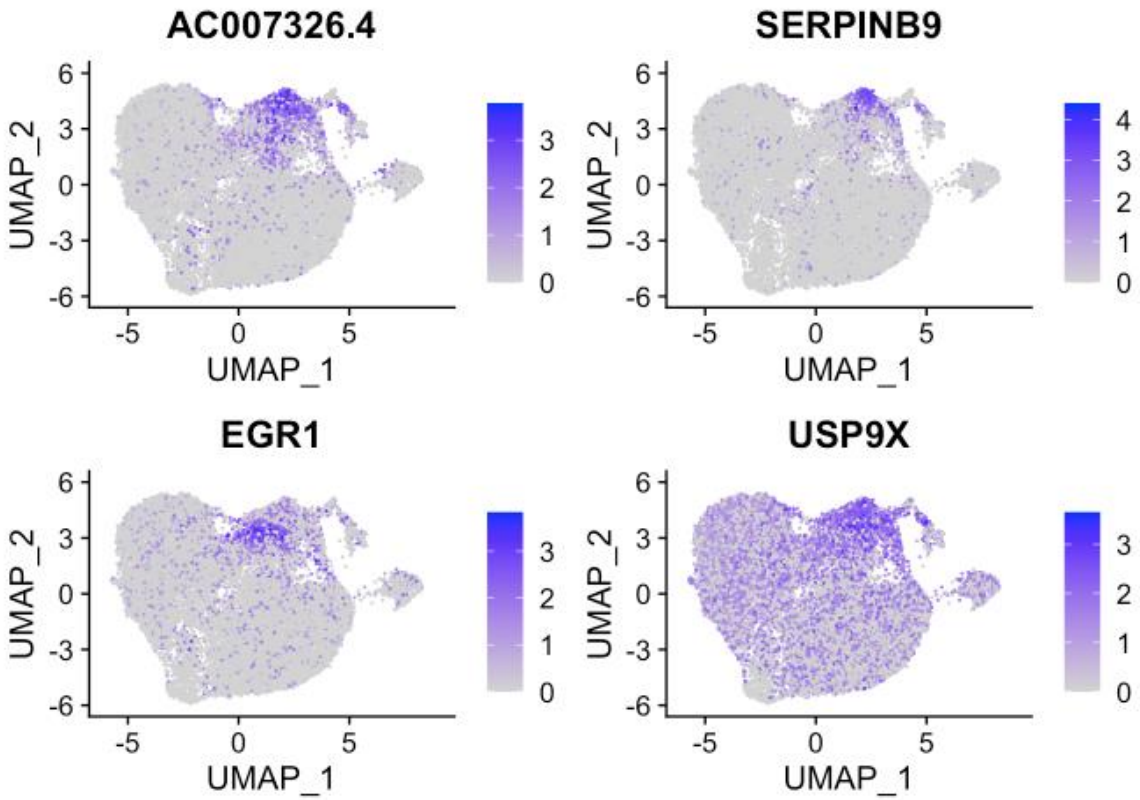


*Figure 19*: Representation of cells with increased expression of 4 genes that are most differentially expressed in cluster 2 on the UMAP.

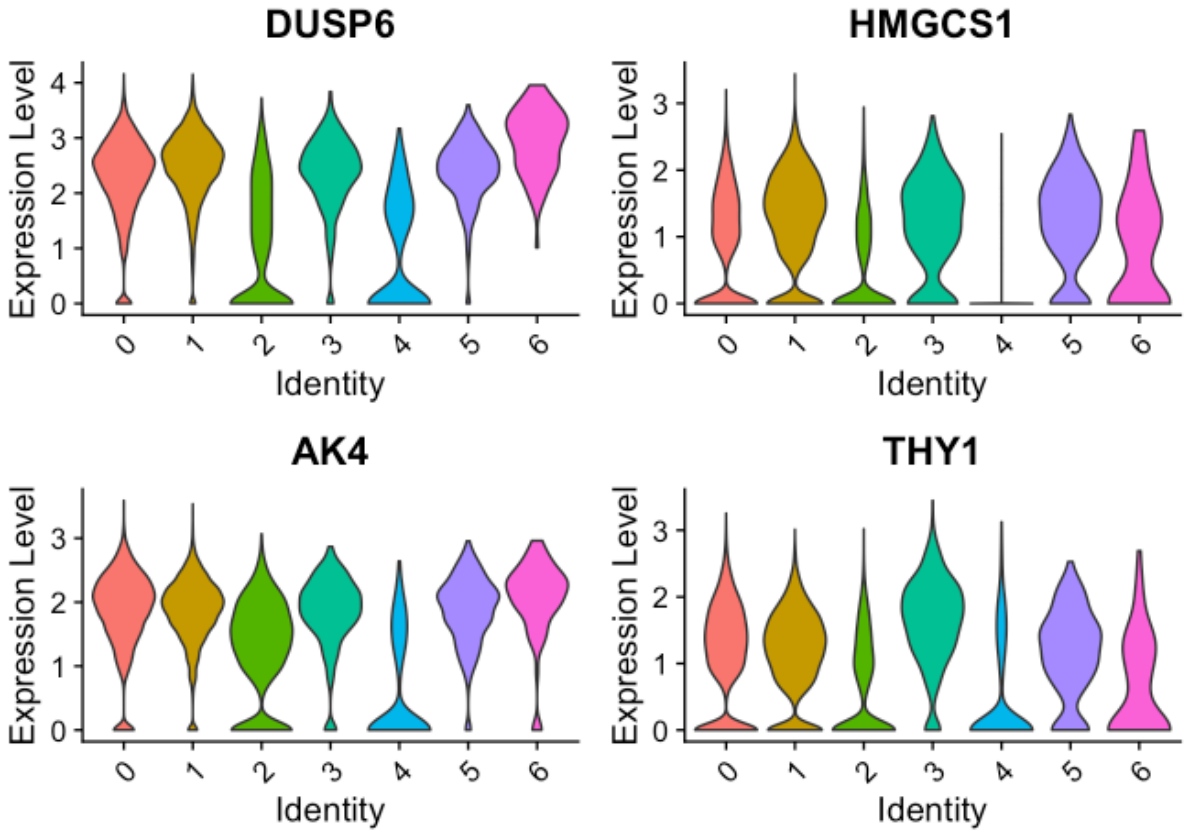


*Figure 20*: The expression distribution across all clusters of the 4 most differentially expressed and downregulated genes in cluster 2.

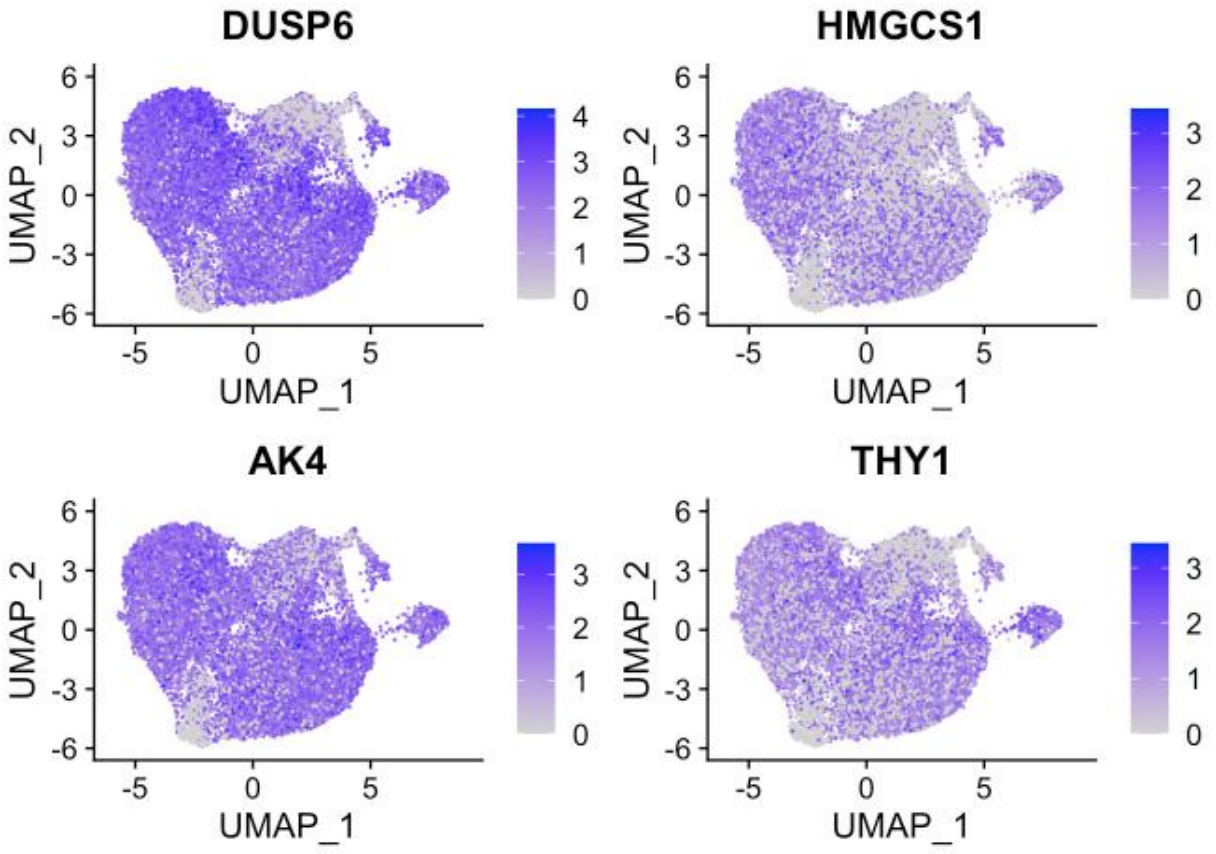


*Figure 21*: Representation of cells with decreased expression of 4 genes that were most differentially expressed in cluster 2 on the UMAP.

hESCs in different clusters had different functionalities enriched or suppressed compared with cells in other clusters; with cluster 4 being most distinct (Figure 22). Cluster 4 cells reported deactivation of self-renewal, as well as having the highest mitochondrial to nuclear transcript ratio (not shown). Cluster 4 cells showed gene expression profiles consistent with increased DNA damage, senescence, apoptosis/necrosis, and cell death, and decreased cell viability, movement, and proliferation, colony formation, DNA replication, and protein metabolism and catabolism.


*Figure 22*: Heat map generated based on Z-scores for relevent disease and cellular functions obtained from data set comparison analysis using IPA. A positive Z-score indicated predicted activation, and a negative Z-score indicates a predicted inhibition. Only entries with Z-score ≤-2 or ≥2 were included.

## DNA Methylation Status After 6 Days of Exposure to BPA, PFOS, or $PbCl_2$

Only BPA showed significant dose-response relationships in global 5-mc DNA methylation after 6 days of exposure. The lowest dose group, 0.25 µg/L BPA had a nearly 2-fold increase in methylation compared to solvent control. Meanwhile, the high dose groups, 250 and 2500 µg/L BPA, did not have any significant effects on global DNA methylation status (Figure 23a).

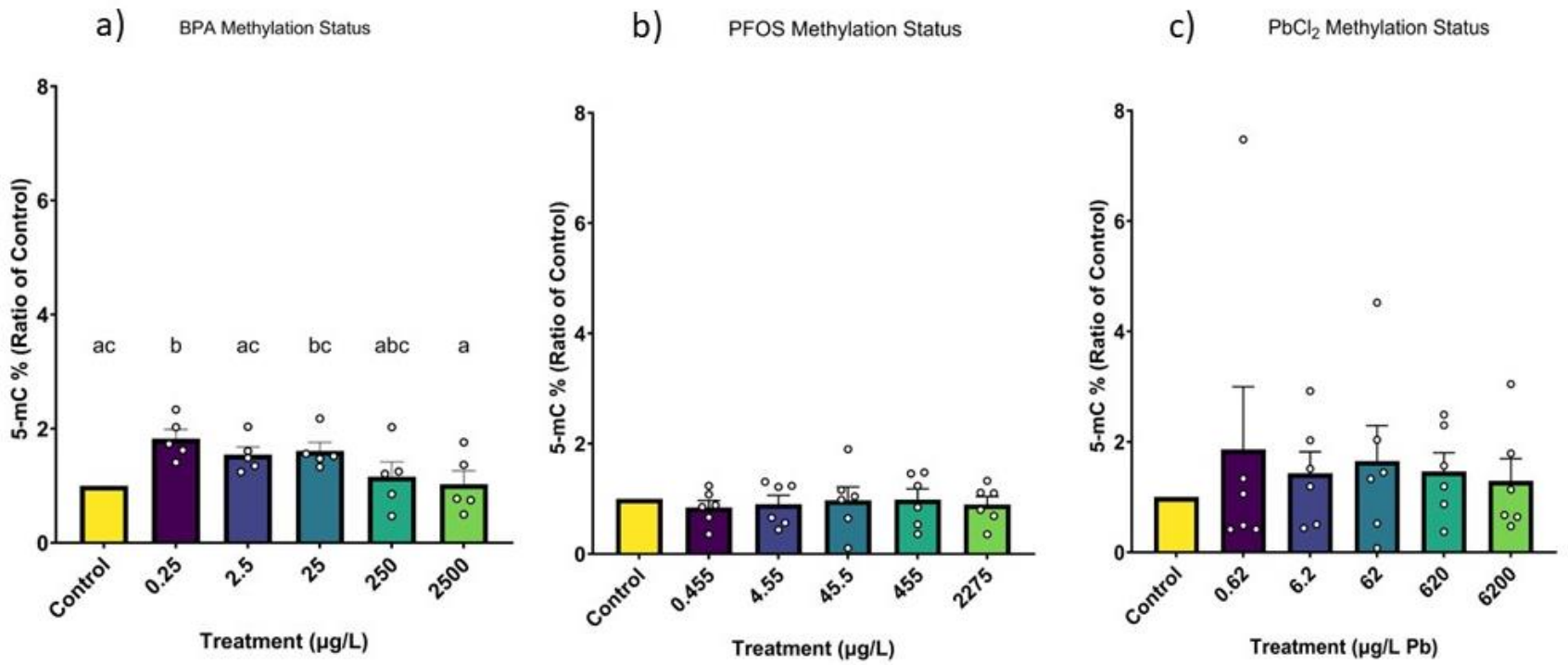


*Figure 23:* a) Effects of BPA on DNA methylation status in hESCs, n=5. b) Effects of PFOS on DNA methylation status in hESCs, n=6. c) Effects of $PbCl_2$ on DNA methylation status in hESCs, n=6. The percentage of 5'-methylated genomic DNA was measured in hESCs exposed to contaminants or type-1 water for 6 days. Values are shown as ratios of the control group of their respective batch. Error bars represent standard error. Letters with no overlap indicate comparisons with significant differences (p-value <0.05) when computed in an ANOVA on ranks.

# Discussion

## Inhibition of Proliferation Endpoint

The MDHA of hESC cultures was used to measure both cell population viability and proliferation, assuming that the protein expression and enzyme function of MDHA was not affected by treatment. Such effects of contaminant exposure may be evaluated by normalization of culture MDHA values against population size.

In this study, 2500 µg/L BPA significantly decreased population MDHA rate accompanied by a trend of decrease in live cell population, with no increase in cumulated cell death. This suggests that hESCs exposed to this dose of BPA suppressed cell proliferation in hESCs after 6 days of exposure. However, this suppression was likely underestimated by the population MDHA assay since the MDHA per cell was increased.

The suppression of population proliferation elicited by BPA has previously been observed in other types of cells, such as neural stem cells in rat brains (Tiwari et al. 2015) and human fetal lung fibroblasts (Mahemuti et al. 2018) at micromolar concentrations. This effect of BPA could be attributed to its estrogenic mode of action, either by competing with estrogen receptor binding or increasing endogenous production of estrogen (Lewis et al. 2000; Mahemuti et al. 2018; Takai et al. 2000). Estrogen is a known modulator of metabolism and has been shown to decrease metabolism rate and fetal birth weight and weight gain (Biegel et al. 1998; Honma et al. 2002).

PFOS at 2275 µg/L doses significantly decreased population MDHA rate after 6 days of exposure. This paralleled with decrease in total cell population size and a trend of decrease in live cell population, with no increase in cumulated population cell death or decrease in MDHA per cell. This suggests that 2275 µg/L PFOS decreased cell proliferation in hESCs after 6 days of exposure. PFOS at 455 µg/L significantly decreased MDHA rate with no

changes in total and live cell population size, nor cumulated cell death, suggesting that other factors may be involved in this effect of PFOS. In the literature, developmental toxicity of PFOS is only observed at late gestational stage exposure (Rayetta C. Grasty et al. 2003). Moreover, PFOS has preferred bioconcentration in the heart, lungs, and liver tissues. (Zeng et al. 2015). This study shows novel evidence of early-stage developmental toxicity attributed to PFOS exposure.

A study by Dong et al. also observed decreased MDHA in C17.2 neural stem cells exposed to 25-200 nM PFOS for 48 h (Dong et al. 2016). Additionally, a study by Pierozan and Karlsson found that PFOS increased population MDHA at lower concentrations (1 and 10 µM), but decreased it at higher concentrations (250-1000 µM), in MCF-10A cells after 72 h of exposure (Pierozan and Karlsson 2018). However, it was not clear if the decreased population MDHA was due to increased cell death or decreased proliferation in these two studies.

$PbCl_2$ diphasic effects on proliferation rate have yet to be examined in published literature. $PbCl_2$ exposure at 6.2 µg /L $Pb^{2+}$ significantly increased population MDHA rate accompanied by a trend of increase in total population size, without affecting cumulative population cell death and live cell population, or MDHA per cell after 6 days of exposure. This suggested that this dose of $PbCl_2$ increased cell proliferation. $PbCl_2$ at 620 µg /L $Pb^{2+}$ significantly decreased population MDHA rate, which paralleled with significant decrease in total population size and a trend of decrease in live cell population and cumulated cell death, as well as a trend of increase in MDHA per cell. This suggests that this dose of $PbCl_2$ strongly inhibited cell proliferation, which was underestimated by population MDHA assay.

Previous studies have investigated the inhibition of Pb on the proliferation rate of stem cells. However, these studies only detect monotonic decreases in proliferation rate at high doses. Human amniotic fluid stem cells were exposed to 50 µM Pb displayed a dose

dependent decrease in MDHA (C. Gundacker et al. 2012). Moreover, neurospheres generated from the neural stem cells of rat brains exposed to Pb at 0.01-10 µM has significantly decreased cellular proliferation rates, despite having no effect on neurosphere viability (F. Huang and Schneider 2004).

The observed effect of low-dose $PbCl_2$ exposure increasing proliferation rate may be attributed to survivorship bias. hESCs proliferate rapidly relative to other types of cells (Ruiz et al. 2011). This high proliferation rate, coupled with a low-intensity stressor and a relatively long dosing period, can cause weaker cells to die off disproportionately, causing the overall population to be enriched with more rapidly proliferating cells (Pasqualetti et al. 2023).

Alternatively, it is possible that $PbCl_2$ at 6.2 µg /L $Pb^{2+}$ stimulated adaptive response resulting in increased cell proliferation. This has previously been observed in lymphocyte, liver cells, and proximal tubular epithelium cell proliferation in rats. These studies all showed significantly higher proliferation rates in response to low level Pb exposure (Choie and Richter 1972; Columbano and Ledda 1982; Razani-Boroujerdi, Edwards, and Sopori 1999).

The results suggest that hESCs, and the WST-1 and total cell population measurements assays can reflect the known developmental effects of BPA, PFOS, and Pb on cell proliferation and metabolic rate as seen *in vivo*. Additionally, hESCs can elicit effects on proliferation at similar, or even lower, doses than those used *in vivo* or other *in vitro* models. The results also suggested that proliferation is more susceptible to chemicals' impact than cell death in hESCs. Additionally, based on these results, BPA was least, and $PbCl_2$ most, inhibitory to cell proliferation among the three contaminants. This is reflective of their known cytotoxicity ranking, suggesting that these assays can be used to differentiate cytotoxicity of chemicals in hESCs when there is no specific inhibition of chemicals on MDHA.

hESC confluency deviated significantly from the population size data previously collected. Additionally, the large degree of variability among replicates is very high. It's likely that cell surface area was changing in response to environmental signals. It has been previously documented that adherent cells can modulate their surface area in response to various stimuli (Höglsperger et al. 2023). Moreover, previous studies have shown that stem cells can change shape and surface area depending on cell state, for example, priming or differentiation (Bergert et al. 2021; J. H. Li, Trivedi, and Diz-Muñoz 2023) Therefore, confluency is not a well-suited candidate for the evaluation of proliferation in our hESC-based developmental toxicity screening model.

Effects of exposure to BPA and PFOS on the cell cycle of hESCs show a shift from G2/M to S-phase at low doses and a potential decrease in G0/G1 at high doses. This possible impediment to the cell cycle in the S-phase could be attributed to a number of possible mechanisms. For example, increased proliferation or DNA damage.

There is a lack of information concerning the effects of BPA on cell cycle in hESCs. In mouse ESCs, BPA decreased population MDHA at 5-100 μM with no influence on cell cycle (X. Chen et al. 2013). Additionally, enrichment of S-phase in cell cycle distribution has previously been attributed to an increase in cellular proliferation rate (Schnäbele et al. 2009). BPA has been shown to increase the proliferation of estrogen-receptor-positive MCF-7 human breast cancer cells and triggered transition of cells from G1 to S phase (X. Li et al. 2014). Moreover, BPA reversed the suppression of tamoxifen, an estrogen receptor modulator, on cell proliferation in MCF-7 cells which was associated with increased S and G2/M phase cells and ERα and ERRγ gene expression (B. Huang et al. 2019). Furthermore, BPA affected Phytoemagglutinin stimulated peripheral blood mononuclear cells (PBMC) proliferation causing an S-phase cell cycle accumulation at nanomolar concentrations, while BPA was almost ineffective in resting PBMC in rats (Di Pietro et al. 2020). In this study, a

trend of increase in cell proliferation was also observed with 0.25-250 µg/L BPA treatment coupled with a trend of increase in S phase cells, although not to a significant level. These results further imply that cell proliferation is a sensitive target of BPA. These findings align with the known estrogenic effects of BPA, which is associated with an increased proliferation rate at low doses (Ramakrishnan and Wayne 2008; Takai et al. 2000).

The effects of PFOS on cell cycle in hESCs have not been reported. In this study, PFOS at 0.455-450 µg/L caused an enrichment of S-phase hESCs in low-dose PFOS-treated cells. This was only coupled with increased proliferation measured by total population size, for the 45.5 µg/L dose group. Similarly, PFOS at 10 µM (~5000 µg/L) increased G0/G1-to-S phase transition of the cell cycle , which correlated with increased proliferation in human breast epithelial cells (Pierozan and Karlsson 2018). In contrast, PFOS at 10- and 200 µM (~100 mg/L) increased the expression of G1/S and S cyclins with no influence on cell viability and proliferation measured by MDHA assay in A549 lung carcinoma cell line (Jabeen et al. 2020). These suggested that cell cycle was a more sensitive endpoint than MDHA and total population counts in hESCs and cancer cell lines. In addition, the hESCs used in our study was a very diverse population as shown by our single cell RNA sequencing analysis, which made it difficult to detect small changes in population parameters such as MDHA and total population size.

Conversely, PFOS has been shown to elicit toxicity by the initiation of oxidative stress (T. Chen et al. 2012) and DNA damage due to reactive oxygen species (ROS) generation (Guo et al. 2016; Xu et al. 2013; Zheng et al. 2016). These mechanisms have previously been related to G1/G0 and S-phase arrest in HepG2 cells (Lee, Kim, and Nam 2017).

The effects of $Pb^{2+}$ on cell cycle in hESCs have not been reported. In mESCs, Pb acetate at 0.5-2.5 µM (~103-518 µg/L Pb) showed no effects on cell cycle (Monear and

Xhabija 2020). In human leukemia (HL-60) cells, $Pb(NO_3)_2$ at 10-30 µg/L increased G0/G1 phase cells accompanied by increased DNA damage and apoptosis (Yedjou, Tchounwou, and Tchounwou 2015). In this study, $PbCl_2$ exposure at 62 and 620 µg $Pb^{2+}$/L for 6-days caused hESCs to experience a significant enrichment in the proportion of S-phase cells. A trend of increase in S phase cells was also observed in 0.62 and 6.2 µg $Pb^{2+}$/L dose groups. These changes paralleled with a significant or a trend of increase in cell proliferation for 0.62, 6.2, and 62 µg /L $Pb^{2+}$ dose groups, suggesting that the increase in DNA replication in S-phase contributed to the increased proliferation in these groups. It was surprising however that the increased S-phase cells in 620 µg /L $Pb^{2+}$ was accompanied with a significant decrease in proliferation. This suggests that 620 µg /L $Pb^{2+}$ increased DNA replication and meanwhile suppressed downstream events of cell cycle such as segregation of chromosomes that could be halted due to impaired microtubule-kinetochore interaction (Laflamme et al. 2019).

These results show that our hESC-based developmental toxicity screening model is suitable for screening and differentiating developmental toxicities and can accurately describe the proliferation endpoint toxic effects of chemicals with different modes of action.

## Inhibition of Differentiation Endpoint

These results show that differentiation was successful for all 3 lineages at all doses. However, the transcriptome of each sample has vastly differing gene expression profiles. These profiles are driven by passage generation rather than dosage. Some marker genes show dose-dependent relationships, especially in ectoderm lineage cells. This may provide insights into the mechanism of neurodevelopment inhibition by Pb, as ectoderm is the precursor to neural tissue (H. Li et al. 2009).

There is a possible effect of dose on Euclidean distance in PCAs. We observed moderate clustering based on dose in ectoderm and mesoderm. However, there was still a large variation within those clusters. That could suggest global DNA damage due to $PbCl_2$

exposure, as opposed to a specific expression profile. Pb exposure has been shown to elicit DNA damage due to ROS generation (Kelainy, Ibrahim Laila, and Ibrahim 2019; X. Yang et al. 2014).

Moreover, changes in global DNA methylation could also lead to the global shifts in gene expression profiles we observed. Pb exposure is known to have effects on genomic methylation status (Senut et al. 2014). Incidentally, cluster 2 of the single-cell transcriptome sequencing data, the cluster most associated with Pb exposure, showed an upregulation of USP9X, a marker for DNA damage repair (O'Dea and Santocanale 2020).

Of the lineage markers, ectoderm seemed to have the greatest number of significantly different marker genes compared to controls. Most of these genes are upregulated and would suggest an induction of differentiation. Previous studies have measured the effects of Pb on stem cell-ectoderm differentiation and found downregulation of ectoderm markers, which would suggest an inhibition of ectoderm differentiation (Abdullah et al. 2014). Ectoderm is the precursor tissue to neuronal precursors. This effect on the differentiation of ectoderm to be related to the known neurodevelopmental toxicity of Pb.

Additionally, several genes were found to be differentially expressed in different lineages in response to Pb exposure. These include several metallothionines, which are common excretion/response proteins to heavy metal exposure. This shows that hESCs can respond to Pb exposure similarly to *in vivo* models.

This assay showed that Pb had upregulating effects on expression of ectoderm lineage markers, potentially affecting ectoderm differentiation. This is similar to the known developmental toxicity of lead, which inhibits the differentiation into ectoderm and neurospheres (Abdullah et al. 2014; Mansel et al. 2019). The study by Mansel et al. used 1 µM (207.2 µg/L) as their lowest dose, where they observed significant inhibition. Here, we

used 118 µg/L as out highest dose. This could relate to why our results show opposite trends to Mansel et al. and Abdullah et al..

Pb had significant effects on a number of lineage markers in all 3 lineages. This shows that hESCs are able to reflect toxic effects on differentiation, which is one of the major endpoints of the EST.

## Transcrptomic/Genomic Endpoint

The single cell transcriptome sequencing analysis revealed 7 clusters of hESCs with different gene expression profiles, suggesting that the hESCs used in this study were a mix of diverse populations. This individual heterogeneity of hESC populations is consistent with its pluripotent nature and could be an advantage for adaptation and survival in response to environmental and nutritional stresses (S. Yang, Cho, and Jang 2021). Such diversity could also be induced by spatial and temporal asymmetry in cell adhesion and processing, which imposed a challenge for detecting significant effects of chemicals. This might have partly contributed to the minimal effects of $PbCl_2$ on global gene expression in hESCs observed in this study, suggesting that taking measures to control heterogeneity in experiments is necessary (Hayashi, Ohnuma, and Furue 2019).

The single-cell transcriptomic sequencing data showed significant upregulation of XACT in hESCs exposed to 118 µg /L $Pb^{2+}$. XACT has been investigated as a contributor to X-chromosome inactivation (LaSalle 2022; Vallot et al. 2013). XACT competes with XIST to control X-chromosome activity in both early human pre-implantation embryos and naïve hESCs (Vallot et al. 2017). XACT is weakly conserved across mammals and absent from the mouse (Vallot et al. 2013), suggesting the importance of using hESCs instead of rodent models for studying the effects of chemicals. Although this gene was only upregulated by 1.2-fold overall in hESCs exposed to 118 µg/L $Pb^{2+}$, it is the most upregulated gene (by 4-fold) in cluster 4 compared with other clusters. A trend of dose-dependent increase in

proportion of cluster 4 cells up to 142% for the 118 µg /L $Pb^{2+}$ dose group were observed in $PbCl_2$ treated hESCs, although they did not reach significant levels (p=0.130). This cluster of cells also had significantly decreased expression of genes including TP53, DNMTs, SP1, E2F, HDACs, SAPs, RBBPs, and SIN3A in the DNA methylation and transcriptional repressing signaling pathway, which would lead to inhibition of DNA condensation, and subsequent suppression of X-chromosome inactivation (XCI) (Appendix 11). This is consistent with its known function in antagonizing XCI in hESCs. A total of at least 140 X-chromosome genes were differentially expressed, nearly all downregulated. The alterations in the X-chromosome genes predicted decreased cell viability, cell survival, biosynthesis of nucleotides, synthesis of ATP, cognition, and body size. Mutations in many of these genes have been related to various hereditary diseases, neurological problems, and developmental disorders (IPA based knowledge). This suggested that exposure to higher dose levels of Pb may increase the risk of these diseases. The expression and coating by XACT was shown to be the early events in X-chromosome inactivation erosion in hESCs, suggesting a role for XACT in the epigenetic instability of hESCs (Vallot et al. 2015). The increased XACT expression in hESCs exposed to $PbCl_2$ may increase their susceptibility to epigenetic modulations, although more experiments are required to confirm this.

In a study by Motosugi et al., deletion of XACT resulted in the upregulation of neuron-related genes, facilitating neural differentiation in both male and eroded female hPSCs (Motosugi et al. 2021). Thus, this finding could suggest a novel mechanism of Pb neurotoxicity observed in humans. Although it remains to be investigated if the upregulation of XACT gene by $PbCl_2$ in hESCs will lead to a suppression of neuronal differentiation.

Cluster 2 displayed an enrichment of high dose Pb exposed hESCs. IPA analysis indicated that these cells had increased proportion on S-phase cells and increased cell proliferation. Additionally, cluster 4 also displayed an enrichment of high Pb dosed cells,

approximately 140% of the control group population size. However, this cluster showed an inverse biological response to cluster 2, with respect to cell proliferation. This effect shows the strength of single cell transcriptome sequencing techniques. Since cluster 2 has a population size approximately 4-fold greater than cluster 2, a whole population sequencing analysis would have reported an average increase in proliferation. This would have resulted in the loss of the population heterogeneity information that we show here.

This population heterogeneity in hESCs can possibly be attributed to the spatial dynamics and colony formation habits of hESCs. For example, cells located in the center of a colony may be exposed to a lower level of $PbCl_2$ than those located in outer layers of the colony. This is because the outer cells have more exposed surface area and are typically less densely situated. It is also possible that individual cells in a hESC population had different sensitivities to $PbCl_2$, resulting in different biological consequences. These could explain why there was a lack of significant effects of $PbCl_2$ in hESCs at the dose levels used.

Furthermore, the characteristic gene markers selected for cluster 2, the cluster most associated with high Pb exposed cells, had upregulation of SERPINB9 and EGR1, genes associated with tumor formation (Ibáñez-Molero et al. 2022; Sun et al. 2022). Additionally, cluster 2 had downregulation of DUSP6, which is linked to tumor suppression and tumor cell apoptosis (Ma et al. 2013). These gene expression patterns may help to explain the novel diphasic proliferation effects observed in the WST-1 assay. Characteristics of cluster 2 also include upregulation of USP9X. This gene plays a role in DNA damage repair (O'Dea and Santocanale 2020). This correlates well with the known DNA damage effects of Pb exposure.

Concurrently, these data show hESCs within the same population are not homogenous in mRNA expression. This indicates that despite sharing treatment conditions and passage generation, individual cells may be undergoing drastically different processes.

Analysis of large data sets with numerous multiple comparisons can result in high Type I error and limits its statistical power. However, this assay provides valuable insights into potential mechanisms of toxicity that fulfill the recommended improvements to the ECVAM mEST proposed by Seiler et al. It is noteworthy that other transcriptomics studies using embryonic stem cells of various species often also report a small proportion of gene expression changes. This assay provides invaluable mechanistic insight to our developmental toxicity screening protocol.

The genomic methylation effects of BPA observed here in hESCs is similar to results in non-hESC *in vitro* studies. Briefly, SH-SY5Y cells were exposed to 10 µM of BPA (~2283 µg/L BPA) for 96 hours. They observed a 1.3-fold increase in global 5-mc methylation status (Senyildiz et al. 2017). Our results show a greater effect size, at nearly $1/10000^{th}$ of the dose. This information on epigenetics can contribute to the understanding of mechanisms of toxicity in our developmental toxicity screening protocol.

# Conclusion

Our results suggest that among the three chemicals, BPA is the least cytotoxic, followed by PFOS, while $PbCl_2$ is the most cytotoxic to hESCs. BPA increased metabolic enzyme activity per cell, had no effects on cell confluency and cell death, decreased the proportion of cells in the G2/M phase and dramatically decreased DNA methylation in hESCs. PFOS had no effect on metabolic enzyme activity per cell, cell death, and DNA methylation and decreased cell proliferation and cell confluency at higher doses while also increasing the proportion of S-phase cells. $PbCl_2$ had no effects on metabolic enzyme activity per cell, cell confluency, cell death, and DNA methylation but increased cell proliferation at low doses and decreased cell proliferation at high doses while also increasing the proportion of the S-phase cells.

These results suggest that hESCs could differentiate the three chemicals in their toxicity levels and specificities and thus can be used as an in vitro model for screening chemicals for early developmental toxicity. Our results also suggest that less toxic chemicals such as BPA can affect early embryo development at very low concentrations (~1 nM+background) by affecting epigenetic endpoints such as DNA methylation, although such effects may not be seen with higher concentrations. Moreover, hESCs could elicit toxicity, often at greater than ±50% from control. This is the standard used in the murine EST to define a compound as developmentally toxic. Additionally, hESCs could elicit toxicity at dosages much lower than in *in vivo* testing. This shows that hESCs have a greater sensitivity to toxicity. The doses that we report as the lowest observed adverse effect level (LOAEL) in hESCs vs the LOAEL reported *in vivo* can be seen in table 8.

*Table 8:* The LOAEL for developmental toxicity endpoints reported in hESCs in this study versus *in vivo* studies in published literature.

| | *hESCs* | *In Vivo* |
|---|---|---|
| *BPA* | 0.25 µg/L | 50 µg/kg/day (Richter et al. 2007) |
| *PFOS* | 45.5 µg/L | 0.12 mg/kg/day (Narizzano et al. 2022) |
| *$PbCl_2$* | 0.62 µg/L | 9.5 mg/kg/day (van Ravenzwaay et al. 2017) |

*Table 9*: Cytotoxicity endpoint comparison for BPA, PFOS, $PbCl_2$ in hESCs. Values in brackets show the lowest concentration of a significant effect for each respective arrow.

| *Endpoints* | *BPA* *(0.25-2500 µg/L)* | *PFOS* *(0.455-2275 µg/L)* | *PbCl2* *(0.62-6200 µg/L)* |
|---|---|---|---|
| *Proliferation/well* | ↓ (2500 µg/L) | ↓ (455 µg/L) | ↑+↓ (6.2+620 µg/L) |
| *Metabolic activity/cell* | ↑ (2500 µg/L) | ↔ | ↔ |
| *Cell proliferation* | ↔ | ↑+↓ (45.5+2275 µg/L) | ↑↑+↓↓ (0.62+620 µg/L) |
| *Cell viability* | ↔ | ↔ | ↔ |
| *Cell death* | ↔ | ↔ | ↔ |
| *Confluency* | ↔ | ↓↓ (45.5 µg/L) | ↔ |
| *Cell Cycle* | G2/M↓ (25 µg/L) | S↑ (0.455 µg/L) | S↑ (62 µg/L) |
| *DNA methylation* | ↓↓ | ↔ | ↔ |

Our single-cell transcriptome analysis suggests that hESCs are a diverse population of cells with different gene expression profiles and different patterns of regulatory networks. Such diversity in hESCs would favor their survival and adaptation to environmental and nutritional changes. This is also reflected by the significant batch differences in gene expression profiles and a lack of detected $PbCl_2$ treatment effects in hESCs. Non-lethal dosed (118 µg/L $PbCl_2$) hESCs were enriched in cluster 2, with increased expression of pluripotent regulator genes and activated stress response pathways. This suggests that this dose of $PbCl_2$ created a selection/survivor bias for a more resistant population in hESCs. The gene expression profiles in differentiated cells differed from those in undifferentiated hESCs regardless of $PbCl_2$ treatment, suggesting the differentiation processes were successful. However, the mean maternal blood concentration (6.2 µg/L Pb) and a nearly 20-fold increase (118 µg/L) caused several changes in gene expression during induction of differentiation from hESC to endoderm, ectoderm, and mesoderm. Differentiation of hESC to

Ectoderm seemed to be more sensitive than endoderm and mesoderm to $PbCl_2$-induced gene changes, which aligns with the known neurodevelopmental toxicity of $PbCl_2$. At a higher dose, $PbCl_2$ had similar, if not greater, extent of effects on gene expression during differentiation of hESC to mesoderm as to ectoderm. Although $PbCl_2$ did not significantly affect the expression of germ layer marker genes, some changes were specific to the germ layer and were similarly affected by both low and high $PbCl_2$ doses. These genes may be used as biomarkers of $PbCl_2$ exposure in hESCs, although their functions and associated biological consequences remain to be examined. Our results suggest that the exposure to environmentally relevant concentrations of $PbCl_2$ during pre, peri-, and post-implantation embryo (blastocyst stage) development can affect hESCs population composition and alter gene expression during germ layer differentiation, which may lead to altered pregnancy outcomes.

Overall, our data supported our hypotheses, suggesting hESCs is a useful in vitro model for screening chemicals for their toxicity in early embryo development at pre-, peri-, and post-implantation stages in embryo development.

hESCs in this model provide several advantages to developmental toxicity testing compared to *in vivo* experiments. Conversely, this model has limitations that must be understood before implementation in a regulatory context. Firstly, hESCs are unable to replicate any fetal-maternal interactions. This type of *in vitro* model does not consider the role of the placental barrier, which can modulate toxicant exposure. Additionally, there is no accounting for potential maternal metabolism, which can increase or decrease the toxicity of toxicants (Dimopoulou et al. 2018; Luz and Tokar 2018; Wobus and Löser 2011). Further limitations of this model include the 2-dimensional (2D) nature of the hESC cultures. It has been shown numerous times that 2D adherent cultures are not fully representative of embryo-toxicant interactions. This is due to the lack of complex structure and the modulation of the

extracellular membrane proteins caused by 2D adherent cultures. Whereas 3-dimensional models can better reflect the embryo-toxicant interactions (Handral et al. 2016; Pampaloni, Reynaud, and Stelzer 2007; Sengupta et al. 2014). Finally, hESCs have been shown to be highly sensitive to solvent effects. Common toxicant solvents, such as ethanol and DMSO, at low concentrations have been shown to have significant effects on pluripotency and differentiation of hESCs (Luz and Tokar 2018).

Several diverse assays were applied in this methodology to assess their efficacy as tools in a screening model for developmental toxicity using hESCs. Some assays performed better at identifying their designated toxic endpoint than others.

For the inhibition of proliferation endpoint, the WST-1, population counting, and cell confluency assays were used. The WST-1 assay performed well, being easy and cost effective to perform. Additionally, the results of this assay were consistent with the published toxic effects BPA and PFOS. Moreover, the novel effects observed in Pb are plausible and occur at concentrations that have little to no data in the literature. The cell population assay was an effective companion assay to the WST-1 as it allowed us to differentiate between proliferation effects and mortality. It also allowed us to normalize metabolic effects by population size, providing additional insights into potential mechanisms. The cell confluence assay requires expensive and cumbersome equipment. Furthermore, the results it provided were inconsistent with both literature results and the population count data. As previously stated, the confluency assay may not be an effective measure of cell proliferation. Cell cycle phase distribution was able to somewhat point at the known proliferation effects of our reference contaminants. However, cell cycle phase shifts can be attributed to several different endpoints. Therefore, the cell cycle distributions alone may not be strong evidence of effects on proliferation.

For the inhibition of differentiation endpoint, the trilineage differentiation kit was highly effective at inducing differentiation. However, the doses tested showed only a low degree of significantly affected genes. Additionally, few effects on differentiation markers were observed, and those that were observed were inconsistent with published literature. Whole transcriptome sequencing revealed several genes of interest that are related to metal toxicity, while also providing lineage markers and pluripotency genes. This makes it an effective tool for detecting effects on differentiation where they are present.

For the transcriptomic and genomic endpoint, the single cell transcriptome sequencing is a powerful tool that highlights the large degree of variation in hESCs. Moreover, this large variation in gene expression by hESCs is a benefit to capturing the real-world variability of human fetal development. Single cell transcriptome sequencing has the unique ability to capture this cell to cell variation; and prevents larger majority populations from drowning out potential smaller effect sizes. This assay also provided a large swath of data that showed evidence of a potential novel mechanism of Pb developmental neurotoxicity via the XACT gene.

Future studies related to hESC use in regulatory toxicology would strive to improve this model and expand its capabilities. That includes improved methods of effective dose seeking. In this study, doses that were seen as toxic in the WST-1 assay were used to select doses for transcriptome and differentiation sequencing. However, effects seen at those doses proved to be weak. Furthermore, investigations into the spatial dynamics of 2D adherent cells in relation to toxicant exposure are warranted. Here we saw significant genetic heterogeneity that could be related to the colony formation properties of hESCs. Finally, a large-scale validation study should be undertaken. This would involve many different labs and contaminants to test the efficacy of our proposed model to detect handling effects and ensure its efficacy for a wide range of early developmental toxicants.

# References


Abbott, Barbara D. et al. 2009. “Developmental Toxicity of Perfluorooctane Sulfonate (PFOS) Is Not Dependent on Expression of Peroxisome Proliferator Activated Receptor-Alpha (PPARα) in the Mouse.” *Reproductive Toxicology* 27(3–4): 258–65.

Abdullah, Mariam et al. 2014. “Diverse Effects of Lead Nitrate on the Proliferation, Differentiation, and Gene Expression of Stem Cells Isolated from a Dental Origin.” *The Scientific World Journal* 2014.

Adeleye, Yeyejide et al. 2015. “Implementing Toxicity Testing in the 21st Century (TT21C): Making Safety Decisions Using Toxicity Pathways, and Progress in a Prototype Risk Assessment.” *Toxicology* 332: 102–11. http://dx.doi.org/10.1016/j.tox.2014.02.007.

Aglan, Hoda Samir et al. 2021. “Developmental Toxicity of Lead in Rats after Gestational Exposure and the Protective Role of Taurine.” *Journal of Biochemical and Molecular Toxicology* 35(8).

Akhtar, Aysha. 2012. Animals and Public Health *The Costs of Animal Experiments*.

Allison, Jerry D, and Terry L Allison. 2005. “PARTITION COEFFICIENTS FOR METALS IN SURFACE WATER , SOIL , AND WASTE By.” (July).

Andreatta, Massimo, and Santiago J. Carmona. 2021. “UCell: Robust and Scalable Single-Cell Gene Signature Scoring.” *Computational and Structural Biotechnology Journal* 19: 3796–98. https://doi.org/10.1016/j.csbj.2021.06.043.

Arbuckle, Tye E. et al. 2014. “Phthalate and Bisphenol A Exposure among Pregnant Women in Canada - Results from the MIREC Study.” *Environment International* 68: 55–65. http://dx.doi.org/10.1016/j.envint.2014.02.010.

———. 2016. “Maternal and Fetal Exposure to Cadmium, Lead, Manganese and Mercury: The MIREC Study.” *Chemosphere* 163: 270–82. http://dx.doi.org/10.1016/j.chemosphere.2016.08.023.

Ashburner, Michael et al. 2000. “Gene Ontology: Tool for the Unification of Biology.” *Nature Genetics* 25(1): 25–29.

Aungst, Bruce J., James A. Dolce, and Ho Leung Fung. 1981. “The Effect of Dose on the Disposition of Lead in Rats after Intravenous and Oral Administration.” *Toxicology and Applied Pharmacology* 61(1): 48–57.

Bartholomeusz, R. K., N. W. Bruce, and A. M. Lynch. 1999. “Embryo Survival, and Fetal and Placental Growth Following Elevation of Maternal Estradiol Blood Concentrations in the Rat.” *Biology of Reproduction* 61(1): 46–50.

Bergert, Martin et al. 2021. “Cell Surface Mechanics Gate Embryonic Stem Cell Differentiation.” *Cell Stem Cell* 28(2): 209-216.e4.

Berthiaume, Jessica, and Kendall B. Wallace. 2002. “Perfluorooctanoate, Perflourooctanesulfonate, and N-Ethyl Perfluorooctanesulfonamido Ethanol; Peroxisome Proliferation and Mitochondrial Biogenesis.” *Toxicology Letters* 129(1–2): 23–32.

Betharia, Swati, and Timothy J. Maher. 2012. “Neurobehavioral Effects of Lead and Manganese Individually and in Combination in Developmentally Exposed Rats.” *NeuroToxicology* 33(5): 1117–27. http://dx.doi.org/10.1016/j.neuro.2012.06.002.

Bhattacharya, Sudin et al. 2011. “Toxicity Testing in the 21st Century: Defining New Risk Assessment Approaches Based on Perturbation of Intracellular Toxicity Pathways.” *PLoS ONE* 6(6).

Biegel, Lisa B. et al. 1998. “90-Day Feeding and One-Generation Reproduction Study in Crl:CD BR Rats with 17β-Estradiol.” *Toxicological Sciences* 44(2): 116–42.

Bonefeld-Jørgensen, Eva C., Manhai Long, Marlene V. Hofmeister, and Anne Marie Vinggaard. 2007. “Endocrine-Disrupting Potential of Bisphenol A, Bisphenol A Dimethacrylate, 4-n-Nonylphenol, and 4-n-Octylphenol in Vitro: New Data and a Brief Review.” *Environmental Health Perspectives* 115(SUPPL1): 69–76.

Borrirukwisitsak, Siriporn, Helen E. Keenan, and Caroline Gauchotte-Lindsay. 2012. “Effects of Salinity, PH and Temperature on the Octanol-Water Partition Coefficient of Bisphenol A.” *International Journal of Environmental Science and Development* (August 2015): 460–64.

Bracken, Michael B. 2009. “Why Animal Studies Are Often Poor Predictors of Human Reactions to Exposure.” *Journal of the Royal Society of Medicine* 102(3): 120–22.

Buick, Julie K. et al. 2021. “A Modern Genotoxicity Testing Paradigm: Integration of the High-Throughput CometChip® and the TGx-DDI Transcriptomic Biomarker in Human HepaRG™ Cell Cultures.” *Frontiers in Public Health* 9(August): 1–19.

Calderon-Gierszal, Esther L., and Gail S. Prins. 2015. “Directed Differentiation of Human Embryonic Stem Cells into Prostate Organoids in Vitro and Its Perturbation by Low-Dose Bisphenol a Exposure.” *PLoS ONE* 10(7): 1–20.

Carbon, Seth et al. 2009. “AmiGO: Online Access to Ontology and Annotation Data.” *Bioinformatics* 25(2): 288–89.

Case, M. T., R. G. York, and M. S. Christian. 2001. “Rat and Rabbit Oral Developmental Toxicology Studies with Two Perfluorinated Compounds.” *International Journal of Toxicology* 20(2): 101–9.

Chapin, Robert et al. 2008. “State of the Art in Developmental Toxicity Screening Methods and a Way Forward: A Meeting Report Addressing Embryonic Stem Cells, Whole Embryo Culture, and Zebrafish.” *Birth Defects Research Part B - Developmental and Reproductive Toxicology* 83(4): 446–56.

Chen, Jiangfei et al. 2014. “Early Life PFOS Exposure Impairs Zebrafish Organogenesis.” *Aquat Toxicol*: 124–32.

Chen, Shifu, Yanqing Zhou, Yaru Chen, and Jia Gu. 2018. “Fastp: An Ultra-Fast All-in-One FASTQ Preprocessor.” *Bioinformatics* 34(17): i884–90.

Chen, Tian et al. 2012. “Prenatal PFOS Exposure Induces Oxidative Stress and Apoptosis in the Lung of Rat Off-Spring.” *Reproductive Toxicology* 33(4): 538–45.

Chen, Xiaojiao et al. 2013. “Effect of Bisphenol A on Pluripotency of Mouse Embryonic Stem Cells and Differentiation Capacity in Mouse Embryoid Bodies.” *Toxicology in Vitro* 27(8): 2249–55.

Choi, Geun Hyoung et al. 2017. “Perfluorooctanoic Acid (PFOA) and Perfluorooctanesulfonic Acid (PFOS) Concentrations in the South Korean Agricultural Environment: A National Survey.” *Journal of Integrative Agriculture* 16(8): 1841–51. http://dx.doi.org/10.1016/S2095-3119(16)61585-X.

Choie, D. D., and G. W. Richter. 1972. “Cell Proliferation in Rat Kidney Induced by Lead Acetate and Effects of Uninephrectomy on the Proliferation.” *American Journal of Pathology* 66(2): 265–75.

Chou, Wei Chun et al. 2011. “Biomonitoring of Bisphenol A Concentrations in Maternal and Umbilical Cord Blood in Regard to Birth Outcomes and Adipokine Expression: A Birth Cohort Study in Taiwan.” *Environmental Health: A Global Access Science Source* 10(1): 1–10.

Choudhuri, Supratim et al. 2018. “From Classical Toxicology to Tox21: Some Critical Conceptual and Technological Advances in the Molecular Understanding of the Toxic Response Beginning from the Last Quarter of the 20th Century.” *Toxicological Sciences* 161(1): 5–22.

Columbano, A, and G M Ledda. 1982. “Liver Cell Proliferation Induced of Lead Nitrate.” *Am J Pathol* 110(1): 83–88.

DeLuca, Nicole M. et al. 2022. “Human Exposure Pathways to Poly- and Perfluoroalkyl Substances (PFAS) from Indoor Media: A Systematic Review.” *Environment International* 162(December 2020): 1–7.

Dimopoulou, Myrto et al. 2018. “A Comparison of the Embryonic Stem Cell Test and Whole Embryo Culture Assay Combined with the BeWo Placental Passage Model for Predicting the Embryotoxicity of Azoles.” *Toxicology Letters* 286(December 2017): 10–21.

https://doi.org/10.1016/j.toxlet.2018.01.009.

Dong, Xuan et al. 2016. “Perfluorooctane Sulfonate (PFOS) Impairs the Proliferation of C17.2 Neural Stem Cells via the Downregulation of GSK-3β/β-Catenin Signaling.” *Journal of Applied Toxicology* 36(12): 1591–98.

Englund, Mikael C.O., Peter Sartipy, and Johan Hyllner. 2011. “Human Embryonic Stem Cells.” *Regenerative Medicine: From Protocol to Patient* 10: 169–86.

Ewels, Philip A. et al. 2020. “The Nf-Core Framework for Community-Curated Bioinformatics Pipelines.” *Nature Biotechnology* 38(3): 276–78.

Fillion, Myriam et al. 2014. “Identification of Environmental Sources of Lead Exposure in Nunavut (Canada) Using Stable Isotope Analyses.” *Environment International* 71: 63–73. http://dx.doi.org/10.1016/j.envint.2014.06.004.

Fisher, Mandy et al. 2016. “Concentrations of Persistent Organic Pollutants in Maternal and Cord Blood from the Maternal-Infant Research on Environmental Chemicals (MIREC) Cohort Study.” *Environmental Health: A Global Access Science Source* 15(1): 1–14. http://dx.doi.org/10.1186/s12940-016-0143-y.

Gewurtz, Sarah B. et al. 2021. “Bisphenol A in the Canadian Environment: A Multimedia Analysis.” *Science of the Total Environment* 755: 142472. https://doi.org/10.1016/j.scitotenv.2020.142472.

Giritharan, Gnanaratnam, Dusko Ilic, Matthew Gormley, and Ana Krtolica. 2011. “Human Embryonic Stem Cells Derived from Embryos at Different Stages of Development Share Similar Transcription Profiles.” *PLoS ONE* 6(10).

Golub, Mari S. et al. 2010. “Bisphenol A: Developmental Toxicity from Early Prenatal Exposure.” *Birth Defects Research Part B - Developmental and Reproductive Toxicology* 89(6): 441–66.

Grandjean, Philippe, and Philip J. Landrigan. 2014. “Neurobehavioural Effects of Developmental Toxicity.” *The Lancet Neurology* 13(3): 330–38.

Grasty, R. C. et al. 2005. “Effects of Prenatal Perfluorooctane Sulfonate (PFOS) Exposure on Lung Maturation in the Perinatal Rat.” *Birth Defects Research Part B - Developmental and Reproductive Toxicology* 74(5): 405–16.

Grasty, Rayetta C., Brian E. Grey, Christopher S. Lau, and John M. Rogers. 2003. “Prenatal Window of Susceptibility to Perfluorooctane Sulfonate-Induced Neonatal Mortality in the Sprague-Dawley Rat.” *Birth Defects Research Part B - Developmental and Reproductive Toxicology* 68(6): 465–71.

Gundacker, C. et al. 2012. “Proliferation Potential of Human Amniotic Fluid Stem Cells Differently Responds to Mercury and Lead Exposure.” *Amino Acids* 43(2): 937–49.

Gundacker, Claudia, Klaudia Graf-Rohrmeister, et al. 2021. “Gene Variants Determine Placental Transfer of Perfluoroalkyl Substances (PFAS), Mercury (Hg) and Lead (Pb), and Birth Outcome: Findings From the UmMuKi Bratislava-Vienna Study.” *Frontiers in Genetics* 12(June): 1–17.

Gundacker, Claudia, Martin Forsthuber, et al. 2021. “Lead (Pb) and Neurodevelopment: A Review on Exposure and Biomarkers of Effect (BDNF, HDL) and Susceptibility.” *International Journal of Hygiene and Environmental Health* 238.

Guo, Xiaoying et al. 2016. “Perfluorooctane Sulfonate Exposure Causes Gonadal Developmental Toxicity in Caenorhabditis Elegans through ROS-Induced DNA Damage.” *Chemosphere* 155: 115–26.

Hafemeister, Christoph, and Rahul Satija. 2019. “Normalization and Variance Stabilization of Single-Cell RNA-Seq Data Using Regularized Negative Binomial Regression.” *Genome Biology* 20(296).

Hahladakis, John N., Eleni Iacovidou, and Spyridoula Gerassimidou. 2023. “An Overview of the Occurrence, Fate, and Human Risks of the Bisphenol-A Present in Plastic Materials,

Components, and Products." *Integrated Environmental Assessment and Management* 19(1): 45–62.

Handral, Harish K. et al. 2016. "Pluripotent Stem Cells: An in Vitro Model for Nanotoxicity Assessments." *Journal of Applied Toxicology* 36(10): 1250–58.

Hao, Yuhan et al. 2021. "Integrated Analysis of Multimodal Single-Cell Data." *Cell* 184(13): 3573-3587.e29. https://doi.org/10.1016/j.cell.2021.04.048.

Haughom, Bente, and Øystein Spydevold. 1992. "The Mechanism Underlying the Hypolipemic Effect of Perfluorooctanoic Acid (PFOA), Perfluorooctane Sulphonic Acid (PFOSA) and Clofibric Acid." *Biochimica et Biophysica Acta (BBA)/Lipids and Lipid Metabolism* 1128(1): 65–72.

Hayashi, Yohei, Kiyoshi Ohnuma, and Miho K. Furue. 2019. "Pluripotent Stem Cell Heterogeneity." In *Stem Cells Heterogeneity - Novel Concepts*, , 71–94.

He, Ying. 2023. "Per- and Polyfluoroalkyl Substances (PFAS) in China' s Groundwater Resources: Concentration, Composition, and Human Health Risk." *E3S Web of Conferences* 406.

Höglsperger, Fabian et al. 2023. "Rapid and Reversible Optical Switching of Cell Membrane Area by an Amphiphilic Azobenzene." *Nature Communications* 14(1): 1–12.

Honma, Shizuka et al. 2002. "Low Dose Effect of in Utero Exposure to Bisphenol A and Diethylstilbestrol on Female Mouse Reproduction." *Reproductive Toxicology* 16(2): 117–22.

Huang, Bin et al. 2019. "The Modulatory Role of Low Concentrations of Bisphenol A on Tamoxifen-Induced Proliferation and Apoptosis in Breast Cancer Cells." *Environmental Science and Pollution Research* 26(3): 2353–62.

Huang, Funan, and J. S. Schneider. 2004. "Effects of Lead Exposure on Proliferation and Differentiation of Neural Stem Cells Derived from Different Regions of Embryonic Rat Brain." *NeuroToxicology* 25(6): 1001–12.

Ibáñez-Molero, Sofía et al. 2022. “SERPINB9 Is Commonly Amplified and High Expression in Cancer Cells Correlates with Poor Immune Checkpoint Blockade Response.” *OncoImmunology* 11(1). https://doi.org/10.1080/2162402X.2022.2139074.

Ilic, Dusko, and Caroline Ogilvie. 2017. “Concise Review: Human Embryonic Stem Cells—What Have We Done? What Are We Doing? Where Are We Going?” *Stem Cells* 35(1): 17–25.

Jarvis, Amanda L. et al. 2021. “Perfluorooctane Sulfonate in US Ambient Surface Waters: A Review of Occurrence in Aquatic Environments and Comparison to Global Concentrations.” *Environmental Toxicology and Chemistry* 40(9): 2425–42.

Jennings, Paul. 2015. “‘The Future of in Vitro Toxicology.’” *Toxicology in Vitro* 29(6): 1217–21.

Juric, Amanda K. et al. 2018. “Risk Assessment of Dietary Lead Exposure among First Nations People Living On-Reserve in Ontario, Canada Using a Total Diet Study and a Probabilistic Approach.” *Journal of Hazardous Materials* 344: 55–63. http://dx.doi.org/10.1016/j.jhazmat.2017.09.035.

Kasten-Jolly, Jane, Nina Pabello, Valerie J. Bolivar, and David A. Lawrence. 2012. “Developmental Lead Effects on Behavior and Brain Gene Expression in Male and Female BALB/CAnNTac Mice.” *NeuroToxicology* 33(5): 1005–20. http://dx.doi.org/10.1016/j.neuro.2012.04.017.

Kazemi, Sohrab, Nader Bahramifar, Ali Akbar Moghadamnia, and Seyed Gholam Ali Jorsarae. 2016. “Detection of Bisphenol A and Nonylphenol in Rat`s Blood Serum, Tissue and Impact on Reproductive System.” *Electronic physician* 8(8): 2772–80.

Kelainy, Eman G., Ibrahim M. Ibrahim Laila, and Shaimaa R. Ibrahim. 2019. “The Effect of Ferulic Acid against Lead-Induced Oxidative Stress and DNA Damage in Kidney and Testes of Rats.” *Environmental Science and Pollution Research* 26(31): 31675–84.

Kim, Daehwan et al. 2019. “Graph-Based Genome Alignment and Genotyping with HISAT2 and HISAT-Genotype.” *Nature Biotechnology* 37(8): 907–15.

Kim, Hoon et al. 2013. “Modulation of β-Catenin Function Maintains Mouse Epiblast Stem Cell and Human Embryonic Stem Cell Self-Renewal.” *Nature Communications* 4.

Kim, Jong Choon et al. 2001. “Evaluation of Developmental Toxicity in Rats Exposed to the Environmental Estrogen Bisphenol A during Pregnancy.” *Life Sciences* 69(22): 2611–25.

Krewski, Daniel et al. 2010. “Toxicity Testing in the 21st Century: A Vision and a Strategy.” *Journal of Toxicology and Environmental Health - Part B: Critical Reviews* 13(2–4): 51–138.

Kristiansson, Erik, Jessica Coria, Lina Gunnarsson, and Mikael Gustavsson. 2021. “Does the Scientific Knowledge Reflect the Chemical Diversity of Environmental Pollution? – A Twenty-Year Perspective.” *Environmental Science and Policy* 126(September): 90–98. https://doi.org/10.1016/j.envsci.2021.09.007.

Kubo, Kazuhiko et al. 2003. “Low Dose Effects of Bisphenol A on Sexual Differentiation of the Brain and Behavior in Rats.” *Neuroscience Research* 45(3): 345–56.

Kubo, Kazuhiko, Okio Arai, Rika Ogata, and Minoru Omura. 2001. “Exposure to Bisphenol A during the Fetal and Suckling Periods Disrupts Sexual Differentiation of the Locus Coeruleus and of Behavior in the Rat.” *Neuroscience Letters* 304: 73–76. papers3://publication/uuid/D96922AB-5C53-4FA4-9EE5-268FEBB41609.

Laflamme, Guillaume et al. 2019. “Interphase Microtubules Safeguard Mitotic Progression by Suppressing an Aurora B-Dependent Arrest Induced by DNA Replication Stress.” *Cell Reports* 26(11): 2875-2889.e3. https://doi.org/10.1016/j.celrep.2019.02.051.

Lalonde, Benoit, and Christine Garron. 2020. “Spatial and Temporal Distribution of BPA in the Canadian Freshwater Environment.” *Archives of Environmental Contamination and Toxicology* 78(4): 568–78. https://doi.org/10.1007/s00244-020-00721-2.

LaSalle, Janine M. 2022. “X Chromosome Inactivation Timing Is Not EXACT: Implications for Autism Spectrum Disorders.” *Frontiers in Genetics* 13(March): 1–10.

Lau, Christopher et al. 2003. “Exposure to Perfluorooctane Sulfonate during Pregnancy in Rat and Mouse. II: Postnatal Evaluation.” *Toxicological Sciences* 74(2): 382–92.

Lau, Christopher, John L. Butenhoff, and John M. Rogers. 2004. “The Developmental Toxicity of Perfluoroalkyl Acids and Their Derivatives.” *Toxicology and Applied Pharmacology* 198(2): 231–41.

Lee, Jung Im, In-Hye Kim, and Taek-Jeong Nam. 2017. “Crude Extract and Solvent Fractions of Calystegia Soldanella Induce G1 and S Phase Arrest of the Cell Cycle in HepG2 Cells.” *International Journal of Oncology* 50: 414–20.

Lemmen, Josephine G., Roel J. Arends, Paul T. van der Saag, and Bart van der Burg. 2004. “In Vivo Imaging of Activated Estrogen Receptors in Utero by Estrogens and Bisphenol A.” *Environmental Health Perspectives* 112(15): 1544–49.

Lewis, Jill B. et al. 2000. “4-Hydroxytamoxifen-Induced Cytotoxicity and Bisphenol A: Competition for Estrogen Receptors in Human Breast Cancer Cell Lines.” *In Vitro Cellular and Developmental Biology - Animal* 36(5): 320–26.

Li, Bai, Xiaolei Jin, and Hing Man Chan. 2023. “Effects of Low Doses of Methylmercury (MeHg) Exposure on Definitive Endoderm Cell Differentiation in Human Embryonic Stme Cells.” *Archives of Toxicology*.

Li, Bai, Yi hang Kevin Pan, Xiaolei Jin, and Hing Man Chan. 2023. “Using Cultured Human Embryonic Stem Cells to Study the Effefcts of an Environmental Chemical Mixture on Early-Stage Embryo Development.” *Cell Biology and Toxicology*.

Li, Bai, Cunye Qiao, Xiaolei Jin, and Hing Man Chan. 2021. “Characterizing the Low-Dose Effects of Methylmercury on the Early Stages of Embryo Development Using Cultured Human Embryonic Stem Cells.” *Environmental health perspectives* 129(7): 77007.

Li, Huawei et al. 2009. “Differentiation of Neurons from Neural Precursors Generated in Floating

Spheres from Embryonic Stem Cells." *BMC Neuroscience* 10: 122.

Li, Jia Hui, Vikas Trivedi, and Alba Diz-Muñoz. 2023. "Understanding the Interplay of Membrane Trafficking, Cell Surface Mechanics, and Stem Cell Differentiation." *Seminars in Cell and Developmental Biology* 133(May 2022): 123–34.

Li, Xiaoting et al. 2014. "Curcumin Modulates MiR-19/PTEN/AKT/P53 Axis to Suppress Bisphenol A-Induced MCF-7 Breast Cancer Cell Proliferation." *Phytotherapy Research* 28(10): 1553–60.

Liu, Hui et al. 2017. "Embryotoxicity Estimation of Commonly Used Compounds with Embryonic Stem Cell Test." *Molecular Medicine Reports* 16(1): 263–71.

Liu, Shuyu, Nuoya Yin, and Francesco Faiola. 2017. "Prospects and Frontiers of Stem Cell Toxicology." *Stem Cells and Development* 26(21): 1528–39.

Loueniva, H Korpela, and E Yrjänheikki Kauppila. 1986. "Lead and Cadmium Concentrations in Maternal and Umbilical Cord Blood, Amniotic Fluid, Placenta, and Amniotic Membranes." *Am J Obstet Gynecol* 155(5): 1086–89.

Louis, Germaine M.Buck et al. 2011. "Designing Prospective Cohort Studies for Assessing Reproductive and Developmental Toxicity during Sensitive Windows of Human Reproduction and Development-the LIFE Study." *Paediatric and Perinatal Epidemiology* 25(5): 413–24.

Luebker, Deanna J., Raymond G. York, et al. 2005. "Neonatal Mortality from in Utero Exposure to Perfluorooctanesulfonate (PFOS) in Sprague-Dawley Rats: Dose-Response, and Biochemical and Pharamacokinetic Parameters." *Toxicology* 215(1–2): 149–69.

Luebker, Deanna J., Marvin T. Case, et al. 2005. "Two-Generation Reproduction and Cross-Foster Studies of Perfluorooctanesulfonate (PFOS) in Rats." *Toxicology* 215(1–2): 126–48.

Luz, Anthony L., and Erik J. Tokar. 2018. "Pluripotent Stem Cells in Developmental Toxicity Testing: A Review of Methodological Advances." *Toxicological Sciences* 165(1): 31–39.

Lv, Ziquan et al. 2013. “Glucose and Lipid Homeostasis in Adult Rat Is Impaired by Early-Life Exposure to Perfluorooctane Sulfonate.” *Environmental Toxicology* 28(9): 532–42.

Ma, Jianjuan, Xiying Yu, Liping Guo, and Shih Hsin Lu. 2013. “DUSP6, a Tumor Suppressor, Is Involved in Differentiation and Apoptosis in Esophageal Squamous Cell Carcinoma.” *Oncology Letters* 6(6): 1624–30.

Mahemuti, Laziyan et al. 2018. “Bisphenol A Induces DSB-ATM-P53 Signaling Leading to Cell Cycle Arrest, Senescence, Autophagy, Stress Response, and Estrogen Release in Human Fetal Lung Fibroblasts.” *Archives of Toxicology* 92(4): 1453–69. http://dx.doi.org/10.1007/s00204-017-2150-3.

Mansel, Clayton et al. 2019. “Lead Exposure Reduces Survival, Neuronal Determination, and Differentiation of P19 Stem Cells.” *Neurotoxicology and Teratology* 72(September 2018): 58–70. https://doi.org/10.1016/j.ntt.2019.01.005.

Matsuura, Satomu et al. 2004. “Effects of Estradiol Administration on Feto-Placental Growth in Rat.” *Early Human Development* 77(1–2): 47–56.

McClain, R. M., and B. A. Becker. 1975. “Teratogenicity, Fetal Toxicity, and Placental Transfer of Lead Nitrate in Rats.” *Toxicology and Applied Pharmacology* 31(1): 72–82.

Monear, Nicodemus C., and Besa Xhabija. 2020. “The Effect of Lead during the Flint Water Crisis on Mouse Embryonic Stem Cells Self-Renewal and Differentiation Markers.” *Toxicology in Vitro* 63(October 2019): 104719. https://doi.org/10.1016/j.tiv.2019.104719.

Montrose, L., C. Faulk, J. Francis, and D. C. Dolinoy. 2017. “Perinatal Lead (Pb) Exposure Results in Sex and Tissue-Dependent Adult DNA Methylation Alterations in Murine IAP Transposons.” *Environmental and Molecular Mutagenesis* 58(8): 540–50.

Montrose, Luke et al. 2020. “Neonatal Lead (PB) Exposure and DNA Methylation Profiles in Dried Bloodspots.” *International Journal of Environmental Research and Public Health* 17(18): 1–17.

Morrissey, Richard E. et al. 1987. “The Developmental Toxicity of Bisphenol a in Rats and Mice.” *Toxicological Sciences* 8(4): 571–82.

Motosugi, Nami et al. 2021. “Deletion of LncRNA XACT Does Not Change Expression Dosage of X-Linked Genes, but Affects Differentiation Potential in HPSCs.” *Cell Reports* 35(10): 109222. https://doi.org/10.1016/j.celrep.2021.109222.

Naciff, Jorge M. et al. 2003. “Gene Expression Profile Induced by 17α-Ethynyl Estradiol in the Prepubertal Female Reproductive System of the Rat.” *Toxicological Sciences* 72(2): 314–30.

———. 2005. “Gene Expression Changes Induced in the Testis by Transplacental Exposure to High and Low Doses of 17α-Ethynyl Estradiol, Genistein, or Bisphenol A.” *Toxicological Sciences* 86(2): 396–416.

Narizzano, Allison M. et al. 2022. “Reproductive and Developmental Toxicity of Perfluorooctane Sulfonate (PFOS) in the White-Footed Mouse (Peromyscus Leucopus).” *Reproductive Toxicology* 113(August): 120–27. https://doi.org/10.1016/j.reprotox.2022.08.011.

Nishikawa, Miyu et al. 2010. “Placental Transfer of Conjugated Bisphenol A and Subsequent Reactivation in the Rat Fetus.” *Environmental Health Perspectives* 118(9): 1196–1203.

Nishizawa, Hanako et al. 2005a. “Effects of In Utero Exposure to Bisphenol A on Expression of RARα and RXRα MRNAs in Murine Embryos.” *Journal of Reproduction and Development* 51(3): 315–24.

———. 2005b. “Effects of in Utero Exposure to Bisphenol A on MRNA Expression of Arylhydrocarbon and Retinoid Receptors in Murine Embryos.” *Journal of Reproduction and Development* 51(3): 315–24.

Nishizawa, Hanako, Satoshi Imanishi, and Noboru Manabe. 2005. “Effects of Exposure In Utero to Bisphenol A on the Expression of Aryl Hydrocarbon Receptor, Related Factors, and Xenobiotic Metabolizing Enzymes in Murine Embryos.” *Journal of Reproduction and Development* 51(5):

593–605.

O'Dea, Rachel, and Corrado Santocanale. 2020. "Non-Canonical Regulation of Homologous Recombination DNA Repair by the USP9X Deubiquitylase." *Journal of Cell Science* 133(3): 1–12.

Odorico, J, R Pedersen, and S.C Zhang. 2005. *Human Embryonic Stem Cells*.

Ostertag, Sonja K. et al. 2009. "Estimated Dietary Exposure to Fluorinated Compounds from Traditional Foods among Inuit in Nunavut, Canada." *Chemosphere* 75(9): 1165–72. http://dx.doi.org/10.1016/j.chemosphere.2009.02.053.

Pampaloni, Francesco, Emmanuel G. Reynaud, and Ernst H.K. Stelzer. 2007. "The Third Dimension Bridges the Gap between Cell Culture and Live Tissue." *Nature Reviews Molecular Cell Biology* 8(10): 839–45.

Paris, Françoise et al. 2002. "Phenylphenols, Biphenols, Bisphenol-A and 4-Tert-Octylphenol Exhibit α and β Estrogen Activities and Antiandrogen Activity in Reporter Cell Lines." *Molecular and Cellular Endocrinology* 193(1–2): 43–49.

Pasqualetti, Francesco et al. 2023. "The Impact of Survivorship Bias in Glioblastoma Research." *Critical Reviews in Oncology/Hematology* 188(June): 104065. https://doi.org/10.1016/j.critrevonc.2023.104065.

Patro, Rob et al. 2017. "Salmon Provides Fast and Bias-Aware Quantification of Transcript Expression." *Nature Methods* 14(4): 417–19.

Pierozan, Paula, and Oskar Karlsson. 2018. "PFOS Induces Proliferation, Cell-Cycle Progression, and Malignant Phenotype in Human Breast Epithelial Cells." *Archives of Toxicology* 92(2): 705–16.

Di Pietro, Paola et al. 2020. "Bisphenol A Induces DNA Damage in Cells Exerting Immune Surveillance Functions at Peripheral and Central Level." *Chemosphere* 254: 126819. https://doi.org/10.1016/j.chemosphere.2020.126819.

Plattard, N. et al. 2022. “Hepatic Metabolism of Chlorinated Derivatives of Bisphenol A (ClxBPA) and Interspecies Differences between Rats and Humans.” *Archives of Toxicology* 96(3): 783–92. https://doi.org/10.1007/s00204-021-03217-7.

R Core Team. 2018. *R: A Language and Environment for Statistical Computing*. Vienna, Austria: R Foundation for Statistical Computing. https://www.r-project.org/.

Raj, Deep, Adarsh Kumar, Tripti, and Subodh Kumar Maiti. 2022. “Health Risk Assessment of Children Exposed to the Soil Containing Potentially Toxic Elements: A Case Study from Coal Mining Areas.” *Metals* 12(11).

Ramakrishnan, Siddharth, and Nancy L. Wayne. 2008. “Impact of Bisphenol-A on Early Embryonic Development and Reproductive Maturation.” *Reproductive Toxicology* 25(2): 177–83.

van Ravenzwaay, B., X. Jiang, T. Luechtefeld, and T. Hartung. 2017. “The Threshold of Toxicological Concern for Prenatal Developmental Toxicity in Rats and Rabbits.” *Regulatory Toxicology and Pharmacology* 88: 157–72. http://dx.doi.org/10.1016/j.yrtph.2017.06.008.

Razani-Boroujerdi, S., B. Edwards, and M L. Sopori. 1999. “Lead Stimulates Lymphocyte Proliferation through Enhanced T Cell-B Cell Interaction.” *Journal of Pharmacology and experimental therapeutics* 288(2): 714–19.

Richter, Catherine A. et al. 2007. “In Vivo Effects of Bisphenol A in Laboratory Rodent Studies.” *Reproductive Toxicology* 24(2): 199–224.

Ruiz, Sergio et al. 2011. “A High Proliferation Rate Is Required for Cell Reprogramming and Maintenance of Human Embryonic Stem Cell Identity.” *Current Biology* 21(1): 45–52.

Russel, W., and R. Burch. 1959. *The Principles of Humane Experimental Technique*.

Rydell-Törmänen, Kristina, and Jill R. Johnson. 2019. “The Applicability of Mouse Models to the Study of Human Disease Kristina.” *Methods in Molecular Biology* 1940: 3–22.

Schnäbele, Kerstin et al. 2009. “Effects of Adipocyte-Secreted Factors on Cell Cycle Progression in HT29 Cells.” *European Journal of Nutrition* 48(3): 154–61.

Scholz, G. et al. 1999. “Prevalidation of the Embryonic Stem Cell Test (EST) - A New in Vitro Embryotoxicity Test.” *Toxicology in Vitro* 13(4–5): 675–81.

Seiler, Andrea et al. 2004. “Improvement of an in Vitro Stem Cell Assay for Developmental Toxicity: The Use of Molecular Endpoints in the Embryonic Stem Cell Test.” *Reproductive Toxicology* 18(2): 231–40.

Sengupta, Srikumar et al. 2014. “Aggregate Culture of Human Embryonic Stem Cell-Derived Hepatocytes in Suspension Are an Improved In Vitro Model for Drug Metabolism and Toxicity Testing.” *Toxicological Sciences* 140(1): 236–45.

Senut, Marie Claude et al. 2014. “Lead Exposure Disrupts Global DNA Methylation in Human Embryonic Stem Cells and Alters Their Neuronal Differentiation.” *Toxicological Sciences* 139(1): 142–61.

Senyildiz, Mine et al. 2017. “Effects of BPA on Global DNA Methylation and Global Histone 3 Lysine Modifications in SH-SY5Y Cells: An Epigenetic Mechanism Linking the Regulation of Chromatin Modifiying Genes.” *Toxicology in Vitro* 44(January): 313–21.

Shanks, Niall, Ray Greek, and Jean Greek. 2009. “Are Animal Models Predictive for Humans?” *Philosophy, Ethics, and Humanities in Medicine* 4(1): 1–20.

Shi, Taoran et al. 2019. “Status of Lead Accumulation in Agricultural Soils across China (1979–2016).” *Environment International* 129(May): 35–41. https://doi.org/10.1016/j.envint.2019.05.025.

Shi, Xiongjie et al. 2008. “Developmental Toxicity and Alteration of Gene Expression in Zebrafish Embryos Exposed to PFOS.” *Toxicology and Applied Pharmacology* 230(1): 23–32.

Smith, Caroline C., and Hugh S. Taylor. 2007. “Xenoestrogen Exposure Imprints Expression of Genes

(Hoxa10) Required for Normal Uterine Development." *The FASEB Journal* 21(1): 239–46.

Sobolewski, Marissa et al. 2018. "Developmental Lead Exposure and Prenatal Stress Result in Sex-Specific Reprograming of Adult Stress Physiology and Epigenetic Profiles in Brain." *Toxicological Sciences* 163(2): 478–89.

Sogorb, Miguel A. et al. 2014. "An Integrated Approach for Detecting Embryotoxicity and Developmental Toxicity of Environmental Contaminants Using in Vitro Alternative Methods." *Toxicology Letters* 230(2): 356–67. http://dx.doi.org/10.1016/j.toxlet.2014.01.037.

Soneson, Charlotte, Michael I. Love, and Mark D. Robinson. 2016. "Differential Analyses for RNA-Seq: Transcript-Level Estimates Improve Gene-Level Inferences." *F1000Research* 4: 1–23.

Spielmann, Horst et al. 2004. "Validation of the Embryonic Stem Cell Test in the International ECVAM Validation Study on Three in Vitro Embryotoxicity Tests." *ATLA Alternatives to Laboratory Animals* 32(3): 245–74.

Sun, Ruifang et al. 2022. "FOCAD/MiR-491-5p, Downregulated by EGR1, Function as Tumor Suppressor by Inhibiting the Proliferation and Migration of Gastric Cancer Cells." *Progress in Biophysics and Molecular Biology* 176(July): 25–37. https://doi.org/10.1016/j.pbiomolbio.2022.06.003.

Susiarjo, Martha, Terry J. Hassold, Edward Freeman, and Patricia A. Hunt. 2007. "Bisphenol A Exposure in Utero Disrupts Early Oogenesis in the Mouse." *PLoS Genetics* 3(1): 0063–0070.

Takai, Yasushi et al. 2000. "Estrogen Receptor-Mediated Effects of a Xenoestrogen, Bisphenol A, on Preimplantation Mouse Embryos." *Biochemical and Biophysical Research Communications* 270(3): 918–21.

Thayer, Kristina A. et al. 2015. "Pharmacokinetics of Bisphenol A in Humans Following a Single Oral Administration." *Environmental International* 83(1): 107–15.

Thibodeaux, Julie R. et al. 2003. “Exposure to Perfluorooctane Sulfonate during Pregnancy in Rat and Mouse. I: Maternal and Prenatal Evaluations.” *Toxicological Sciences* 74(2): 369–81.

Thomson, James A et al. 1998. “Embryonic Stem Cell Lines Derived from Human Blastocysts Published by : American Association for the Advancement of Science Stable URL : Http://Www.Jstor.Org/Stable/2897366 Linked References Are Available on JSTOR for This Article : Embryonic Stem Cell Li.” *Science* 282(5391): 1145–47.

Tiwari, Shashi Kant et al. 2015. “Inhibitory Effects of Bisphenol-A on Neural Stem Cells Proliferation and Differentiation in the Rat Brain Are Dependent on Wnt/β-Catenin Pathway.” *Molecular Neurobiology* 52(3): 1735–57.

Tyl, R. W. et al. 2002. “Three-Generation Reproductive Toxicity Study of Dietary Bisphenol A in CD Sprague-Dawley Rats.” *Toxicological Sciences* 68(1): 121–46.

Uwayezu, Jean-Noel, Leo W. Y. Yeung, and Mattias Bäckström. 2022. “Sorption of Perfluorooctane Sulfonic Acid Including Its Isomers to Soils: Effects of PH, Natural Organic Matter and Na2SO4.” *Frontiers in Environmental Chemistry* 3(June): 1–11.

Vallot, Céline et al. 2013. “XACT, a Long Noncoding Transcript Coating the Active X Chromosome in Human Pluripotent Cells.” *Nature Genetics* 45(3): 239–41. http://dx.doi.org/10.1038/ng.2530.

———. 2017. “XACT Noncoding RNA Competes with XIST in the Control of X Chromosome Activity during Human Early Development.” *Cell Stem Cell* 20(1): 102–11.

Vinggaard, Anne Marie, Jay Niemelä, Eva Bay Wedebye, and Gunde Egeskov Jensen. 2008. “Screening of 397 Chemicals and Development of a Quantitative Structure-Activity Relationship Model for Androgen Receptor Antagonism.” *Chemical Research in Toxicology* 21(4): 813–23.

Wan, Yan jian et al. 2010. “Alterations in Tumor Biomarker GSTP Gene Methylation Patterns Induced by Prenatal Exposure to PFOS.” *Toxicology* 274(1–3): 57–64.

Wobus, Anna M., and Peter Löser. 2011. “Present State and Future Perspectives of Using Pluripotent Stem Cells in Toxicology Research.” *Archives of Toxicology* 85(2): 79–117.

Xu, Dongmei, Chandan Li, Yuezhong Wen, and Weiping Liu. 2013. “Antioxidant Defense System Responses and DNA Damage of Earthworms Exposed to Perfluorooctane Sulfonate (PFOS).” *Environmental Pollution* 174: 121–27. http://dx.doi.org/10.1016/j.envpol.2012.10.030.

Yang, Renjun et al. 2020. “F–53B and PFOS Treatments Skew Human Embryonic Stem Cell in Vitro Cardiac Differentiation towards Epicardial Cells by Partly Disrupting the WNT Signaling Pathway.” *Environmental Pollution* 261: 114153. https://doi.org/10.1016/j.envpol.2020.114153.

Yang, Seungbok, Yoonjae Cho, and Jiwon Jang. 2021. “Single Cell Heterogeneity in Human Pluripotent Stem Cells.” *BMB Reports* 54(10): 505–15.

Yang, Xinyi et al. 2014. “Role of the Mitochondrial Ca2+ Uniporter in Pb2+-Induced Oxidative Stress in Human Neuroblastoma Cells.” *Brain Research* 1575: 12–21. http://dx.doi.org/10.1016/j.brainres.2014.05.032.

Yaoi, Takeshi et al. 2008. “Genome-Wide Analysis of Epigenomic Alterations in Fetal Mouse Forebrain after Exposure to Low Doses of Bisphenol A.” *Biochemical and Biophysical Research Communications* 376(3): 563–67. http://dx.doi.org/10.1016/j.bbrc.2008.09.028.

Yedjou, Clement G., Hervey M. Tchounwou, and Paul B. Tchounwou. 2015. “DNA Damage, Cell Cycle Arrest, and Apoptosis Induction Caused by Lead in Human Leukemia Cells.” *International Journal of Environmental Research and Public Health* 13(1).

Yin, Nuoya et al. 2019. “Embryonic Stem Cell- and Transcriptomics-Based in Vitro Analyses Reveal That Bisphenols A, F and S Have Similar and Very Complex Potential Developmental Toxicities.” *Ecotoxicology and Environmental Safety* 176(February): 330–38. https://doi.org/10.1016/j.ecoenv.2019.03.115.

Yu, Danyang et al. 2021. “Identifying the Source of Heavy Metal Pollution and Apportionment in Agricultural Soils Impacted by Different Smelters in China by the Positive Matrix Factorization Model and the Pb Isotope Ratio Method.” *Sustainability (Switzerland)* 13(12).

Zanatta, Alysson et al. 2010. “The Role of the Hoxa10/HOXA10 Gene in the Etiology of Endometriosis and Its Related Infertility: A Review.” *Journal of Assisted Reproduction and Genetics* 27(12): 701–10.

Zeng, Huai-cai et al. 2015. “Prenatal Exposure to PFOS Caused Mitochondia-Mediated Apoptosis in Heart of Weaned Rat.” *Environmental Toxicology* 30(9): 1082–90.

Zhang, Bo et al. 2020. “Concentrations of Bisphenol A and Its Alternatives in Paired Maternal–Fetal Urine, Serum and Amniotic Fluid from an e-Waste Dismantling Area in China.” *Environment International* 136(January): 105407. https://doi.org/10.1016/j.envint.2019.105407.

Zheng, Xiao Qi, Ya Juan Shi, Yong Long Lu, and Xiang Bo Xu. 2016. “Growth Inhibition and DNA Damage in the Earthworm (Eisenia Fetida) Exposed to Perfluorooctane Sulphonate and Perfluorooctanoic Acid.” *Chemistry and Ecology* 32(2): 103–16.

Zhu, Anqi, Joseph G. Ibrahim, and Michael I. Love. 2019. “Heavy-Tailed Prior Distributions for Sequence Count Data: Removing the Noise and Preserving Large Differences.” *Bioinformatics* 35(12): 2084–92.

Zuluaga Rodríguez, Julián, Sara Elisa Gallego Ríos, and Claudia María Ramírez Botero. 2015. “CONTENT OF Hg, Cd, Pb AND As IN FISH SPECIES: A REVIEW.” *Vitae* 22(2): 148–59. http://dx.doi.org/10.17533/udea.vitae.v22n2a09.

# Contributions of Collaborators

Analysis of single cell transcriptomics and differentiated whole transcriptome was performed by Chris Porter, a bioinformatician at the Ottawa Hospital Research Institute. IPA analysis of the single cell transcriptome data was offered by Dr. Dawn Jin. Transcriptome sequencing of differentiation samples was performed by Novogene. Library preparation and single cell transcriptome tagging was performed by Natasha Kienapple. The stem cell maintenance protocol was created by Dr. Bai Li.

# Appendix

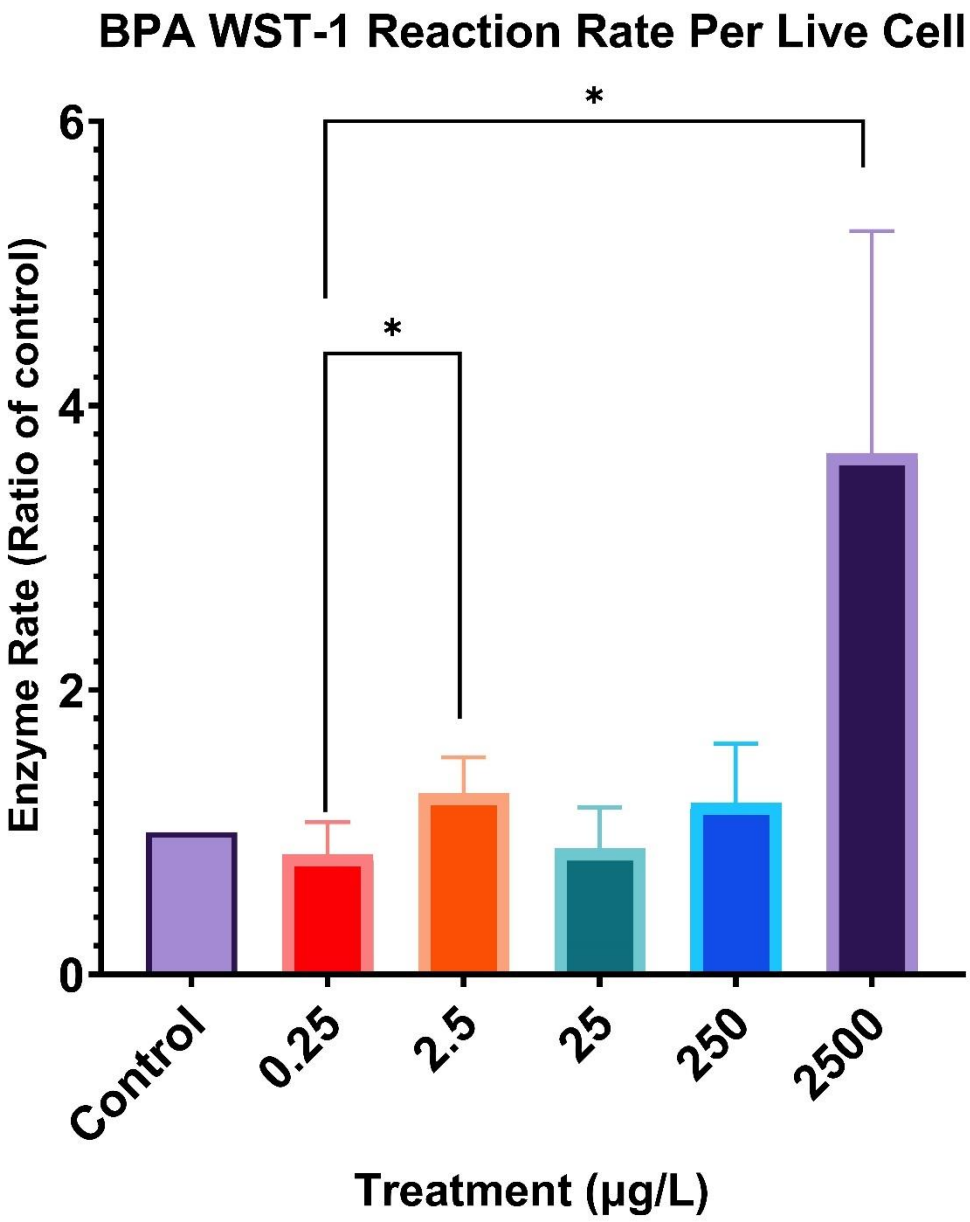


*Appendix 1:* Rates of mitochondrial dehydrogenase activity per live cell. Measurements were taken from hESCs exposed to BPA for 6-days. Measurements were recorded over 2-hours. Values are given as ratios compared to control of each batch. Error bars represent standard error. Asterisks represent groups with significant difference when computed in an ANOVA by ranks ($p$-value$<0.05$). $n=6$.

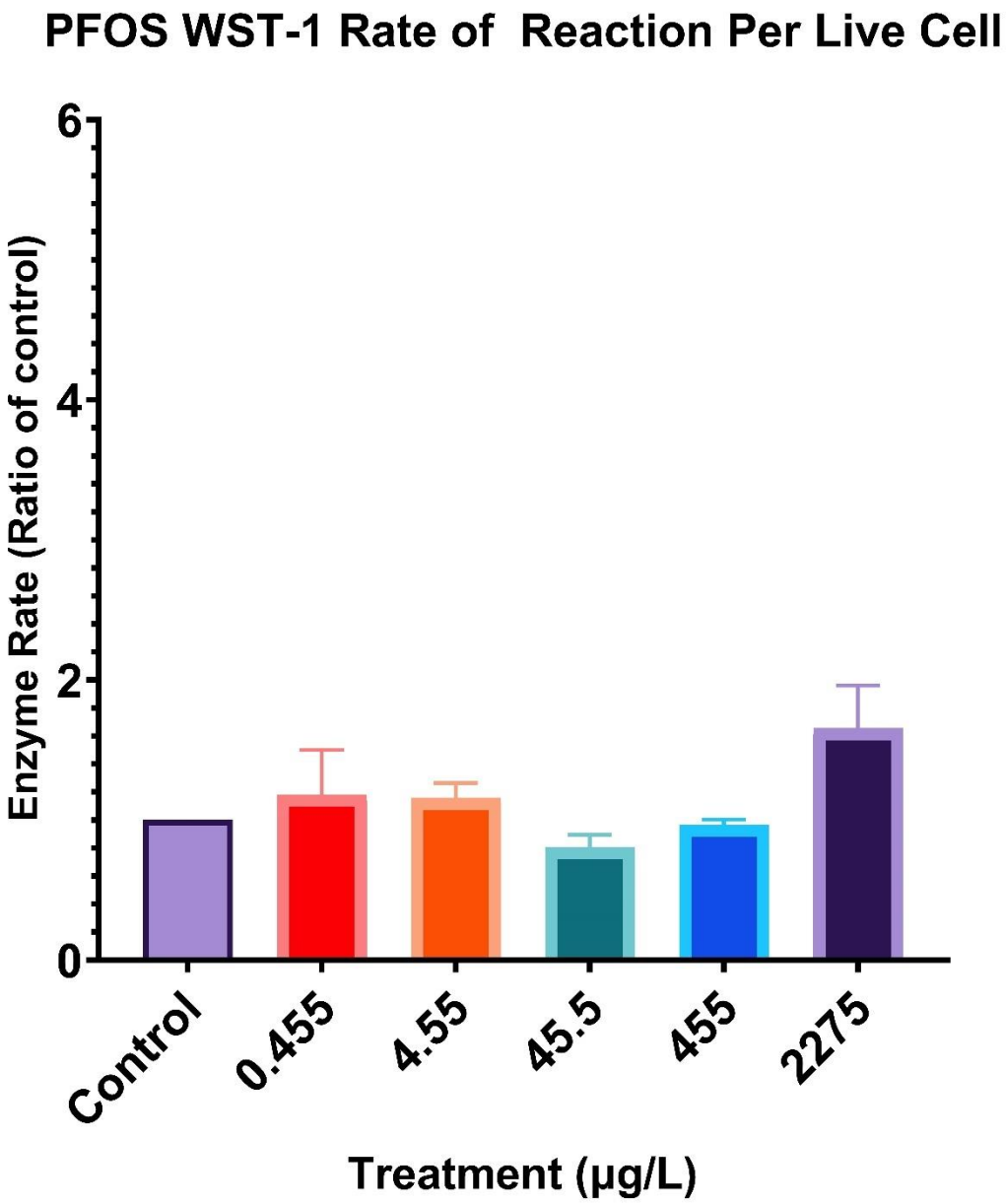


*Appendix 2:* Rates of mitochondrial dehydrogenase activity per live cell. Measurements were taken from hESCs exposed to PFOS for 6-days. Measurements were recorded over 2-hours. Values are given as ratios compared to control of each batch. Error bars represent standard error. Asterisks represent groups with significant difference when computed in an ANOVA by ranks (p-value<0.05). n=6.

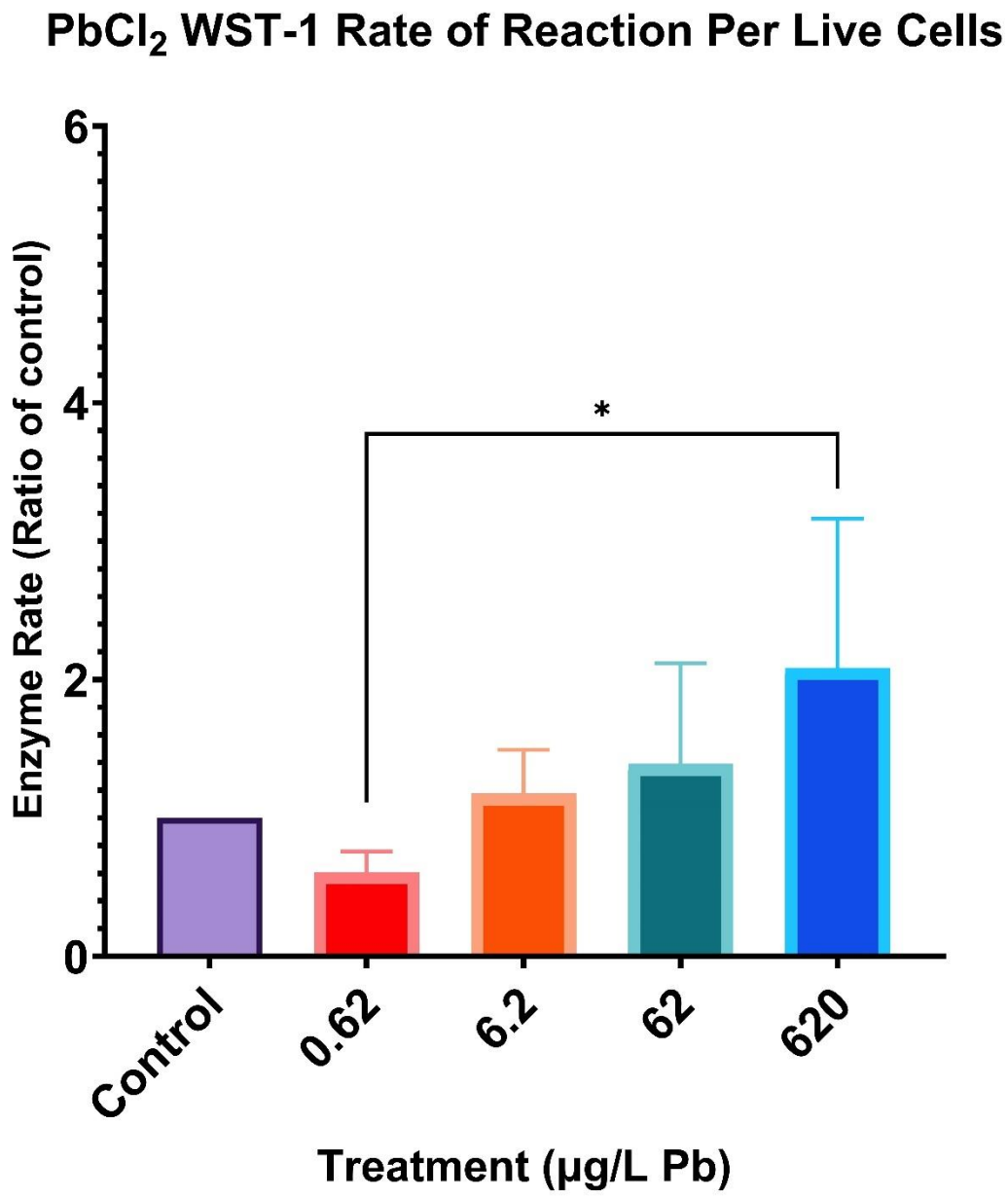


*Appendix 3:* Rates of mitochondrial dehydrogenase activity per live cell. Measurements were taken from hESCs exposed to $PbCl_2$ for 6-days. Measurements were recorded over 2-hours. Values given as ratios compared to control of each batch. Error bars represent standard error. Asterisks represent groups with significant difference when computed in an ANOVA by ranks (p-value<0.05). n=7.

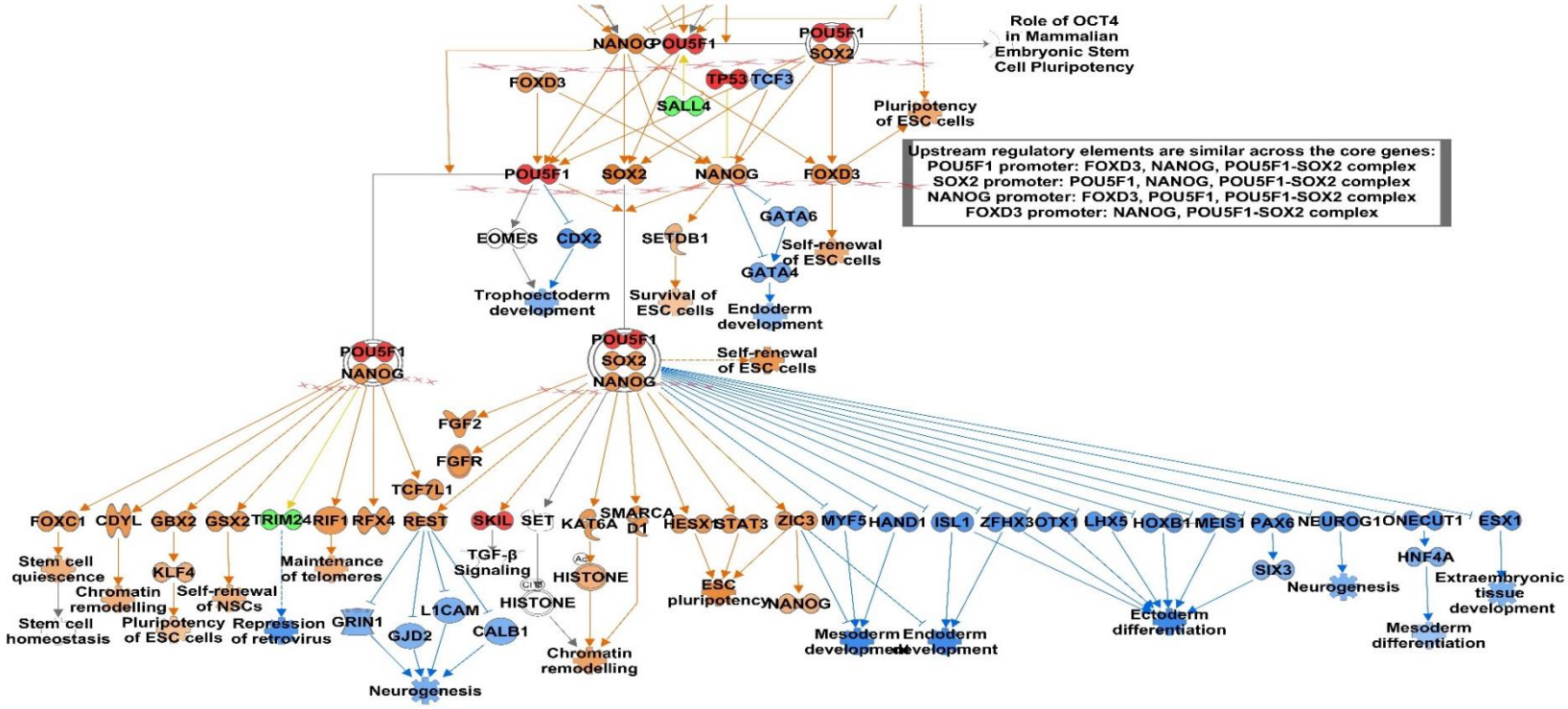


*Appendix 4*: The estimated activeated/deactivated major canonical pathways of Cluster 0. Pathway analysis is performed on Ingenuity Pathway Analysis (IPA). Red icons indicate significantly upregulated genes. Green icons indicate significantly down regulated genes. Orange and blue icons indicate predicted  activeated, and predicted inhibited genes/effects respectivley.

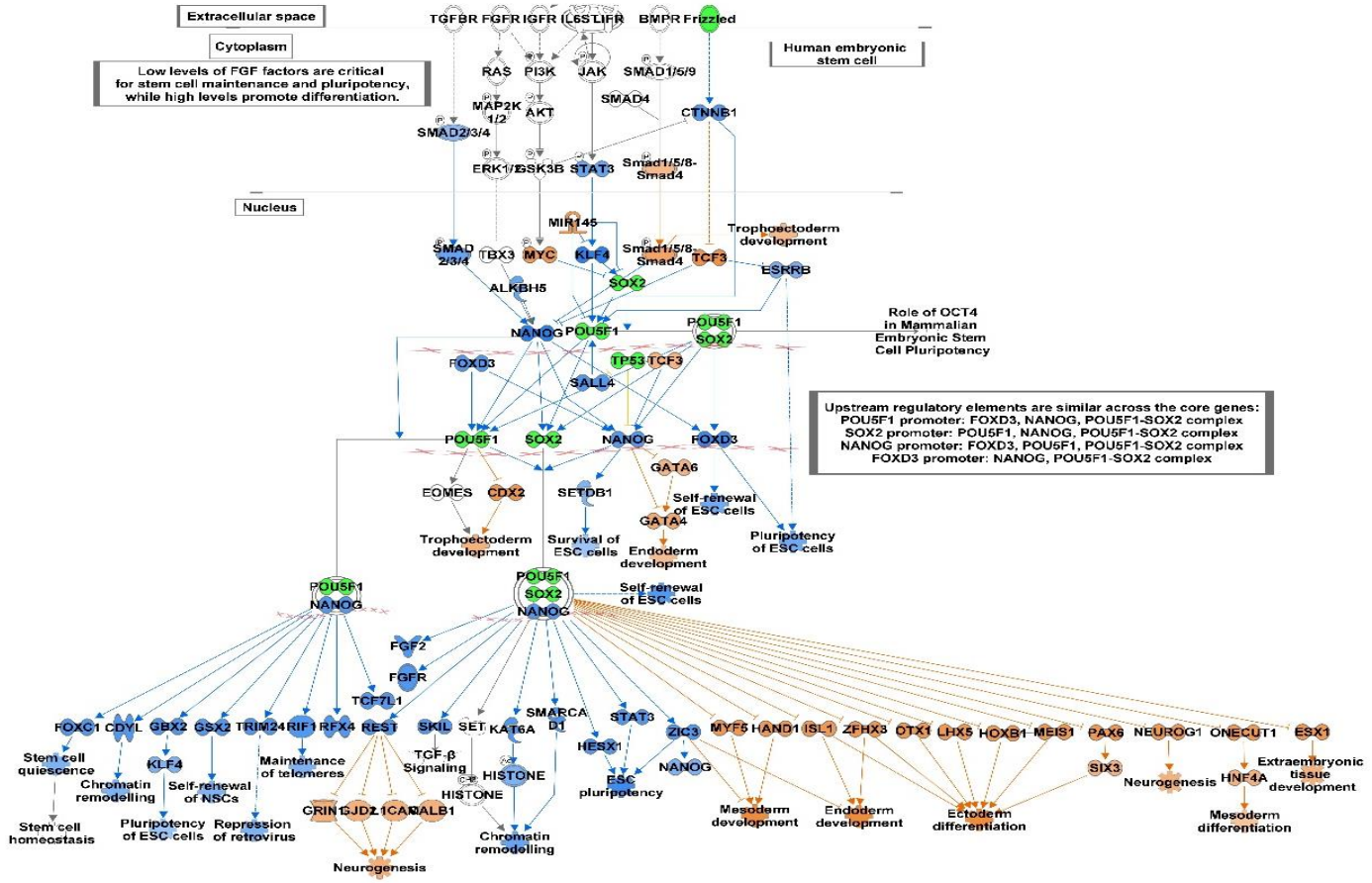


*Appendix 5*: The estimated activeated/deactivated major canonical pathways of Cluster 1. Pathway analysis is performed on IPA. Red icons indicate significantly upregulated genes. Green icons indicate significantly down regulated genes. Orange and blue icons indicate predicted activeated, and predicted inhibited genes/effects respectivley.

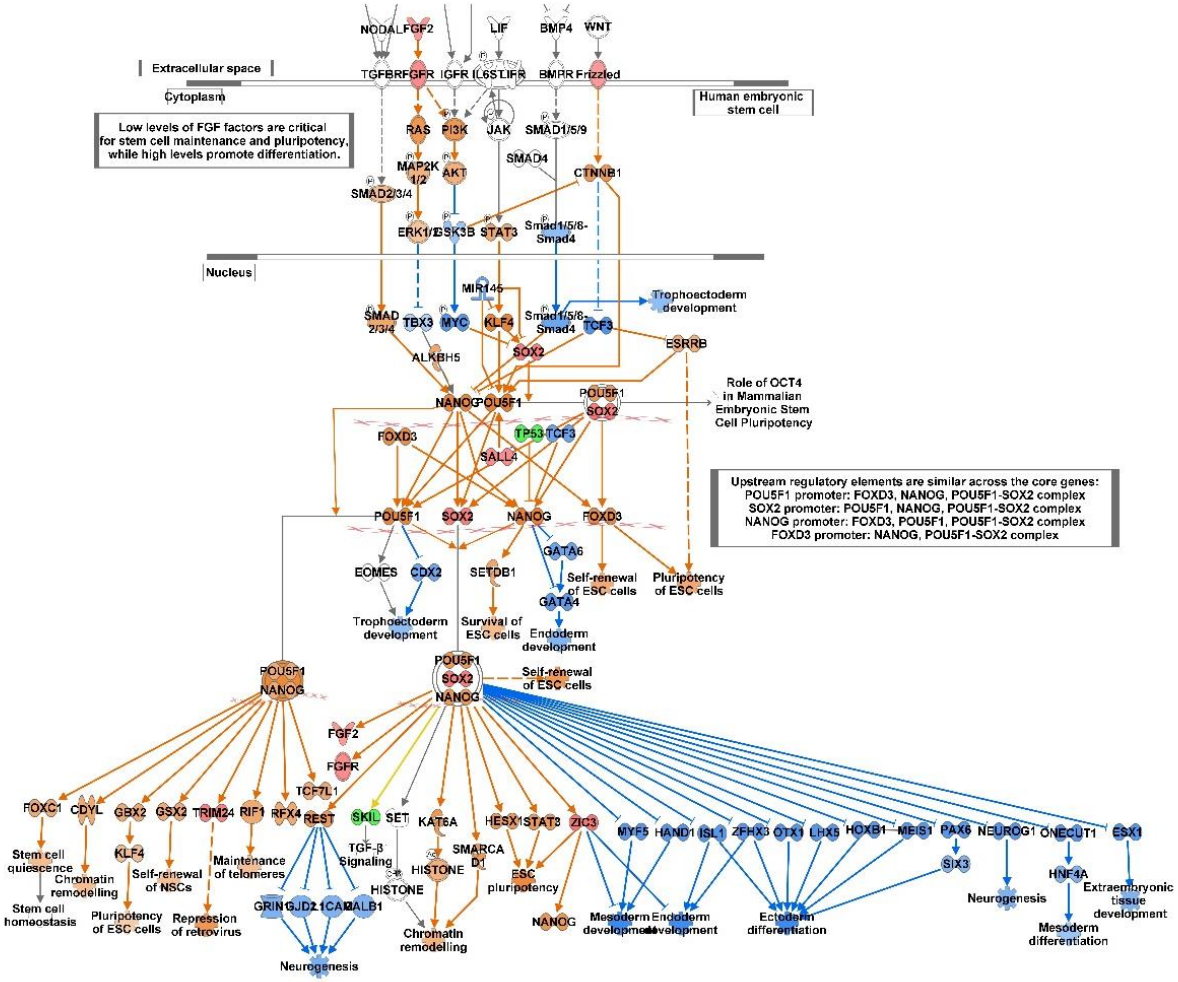


*Appendix 6*: The estimated activeated/deactivated major canonical pathways of Cluster 2. Pathway analysis is performed on IPA. Red icons indicate significantly upregulated genes. Green icons indicate significantly down regulated genes. Orange and blue icons indicate predicted activeated, and predicted inhibited genes/effects respectivley.

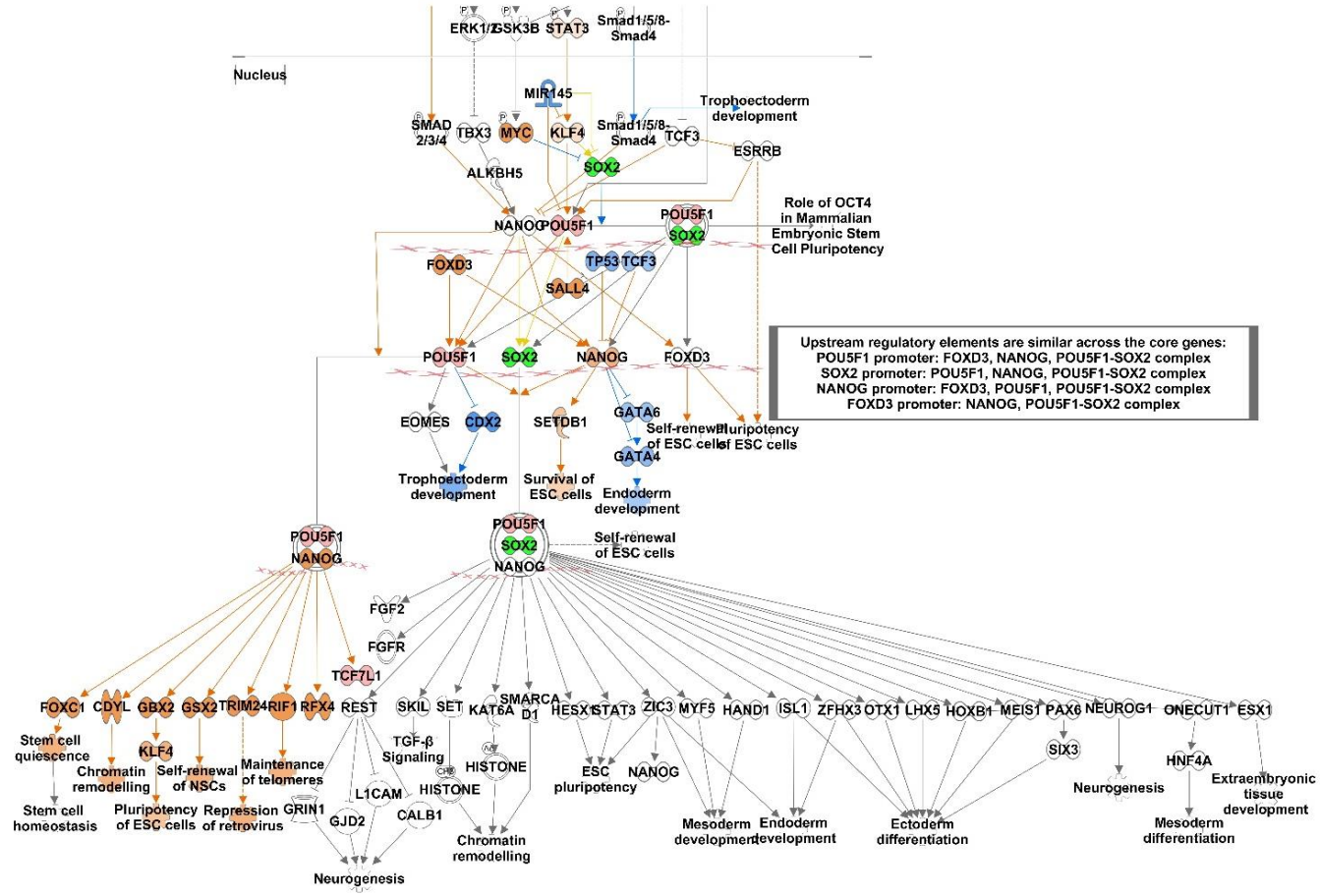


Appendix 7: The estimated activeated/deactivated major canonical pathways of Cluster 3. Pathway analysis is performed on IPA. Red icons indicate significantly upregulated genes. Green icons indicate significantly down regulated genes. Orange and blue icons indicate predicted activeated, and predicted inhibited genes/effects respectivley.

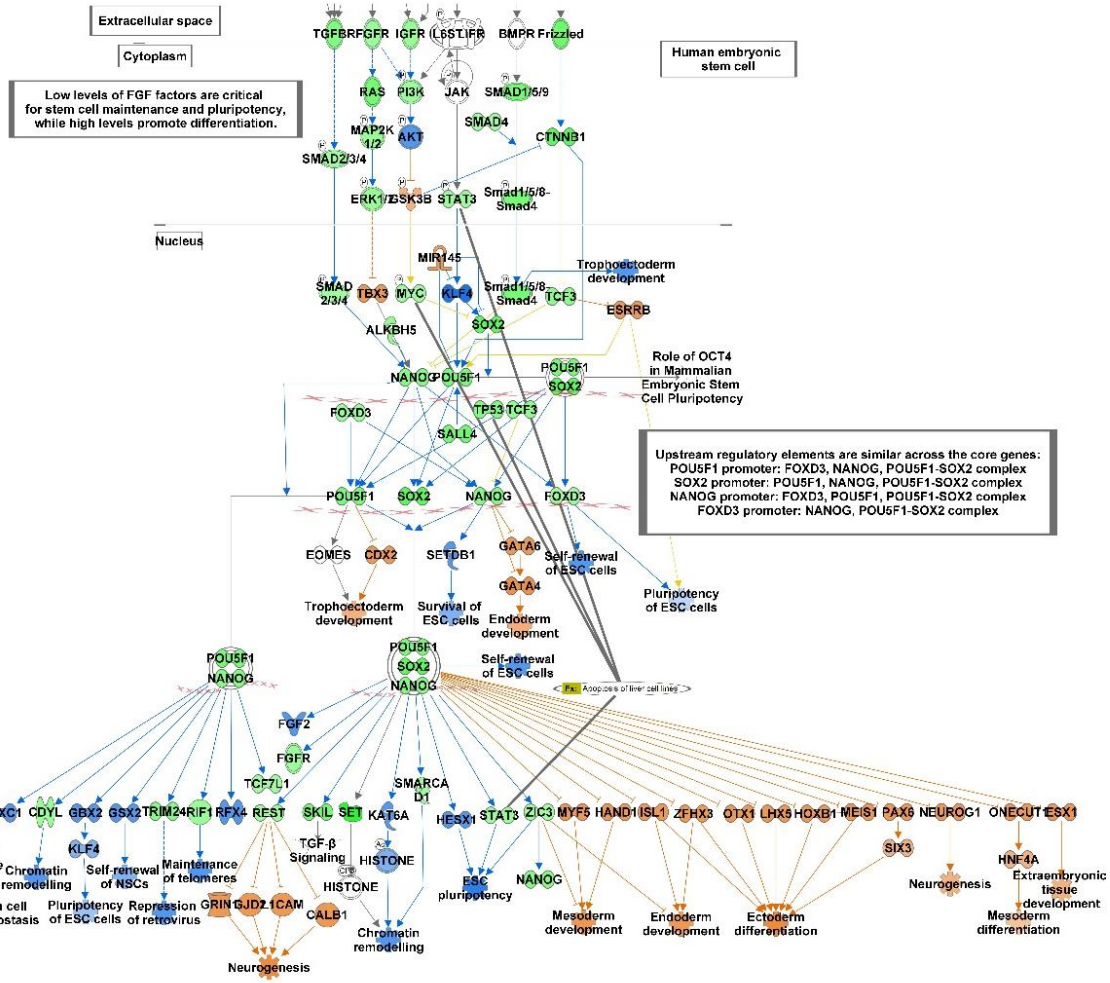


*Appendix 8*: The estimated activeated/deactivated major canonical pathways of Cluster 4. Pathway analysis is performed on IPA. Red icons indicate significantly upregulated genes. Green icons indicate significantly down regulated genes. Orange and blue icons indicate predicted activeated, and predicted inhibited genes/effects respectivley.

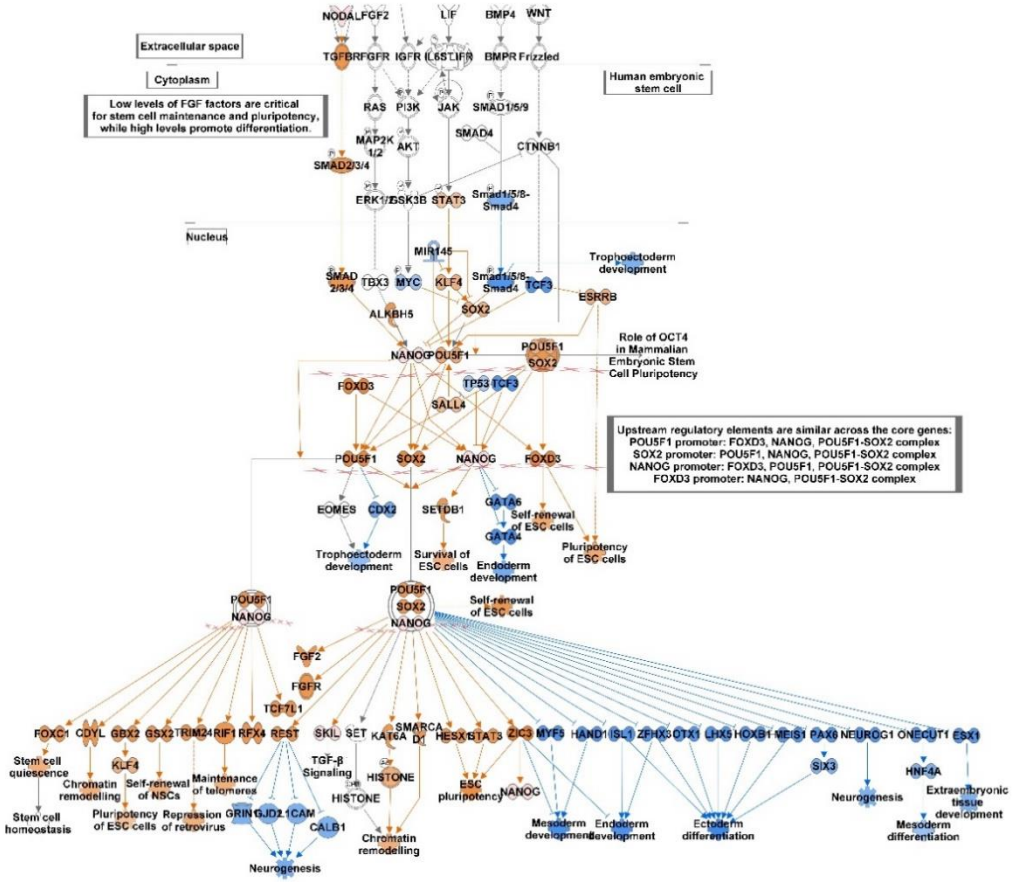


*Appendix 9:* The estimated activeated/deactivated major canonical pathways of Cluster 5. Pathway analysis is performed on IPA. Red icons indicate significantly upregulated genes. Green icons indicate significantly down regulated genes. Orange and blue icons indicate predicted activeated, and predicted inhibited genes/effects respectivley.

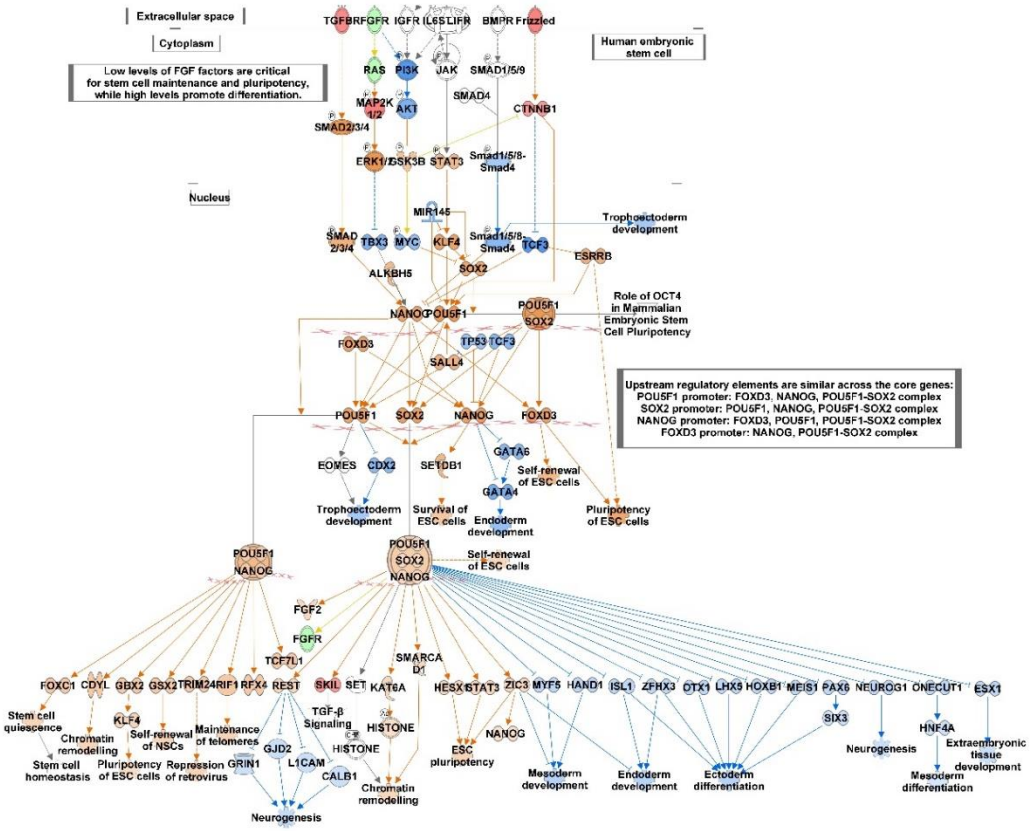


*Appendix 10*: The estimated activeated/deactivated major canonical pathways of Cluster 6. Pathway analysis is performed on IPA. Red icons indicate significantly upregulated genes. Green icons indicate significantly down regulated genes. Orange and blue icons indicate predicted activeated, and predicted inhibited genes/effects respectivley.

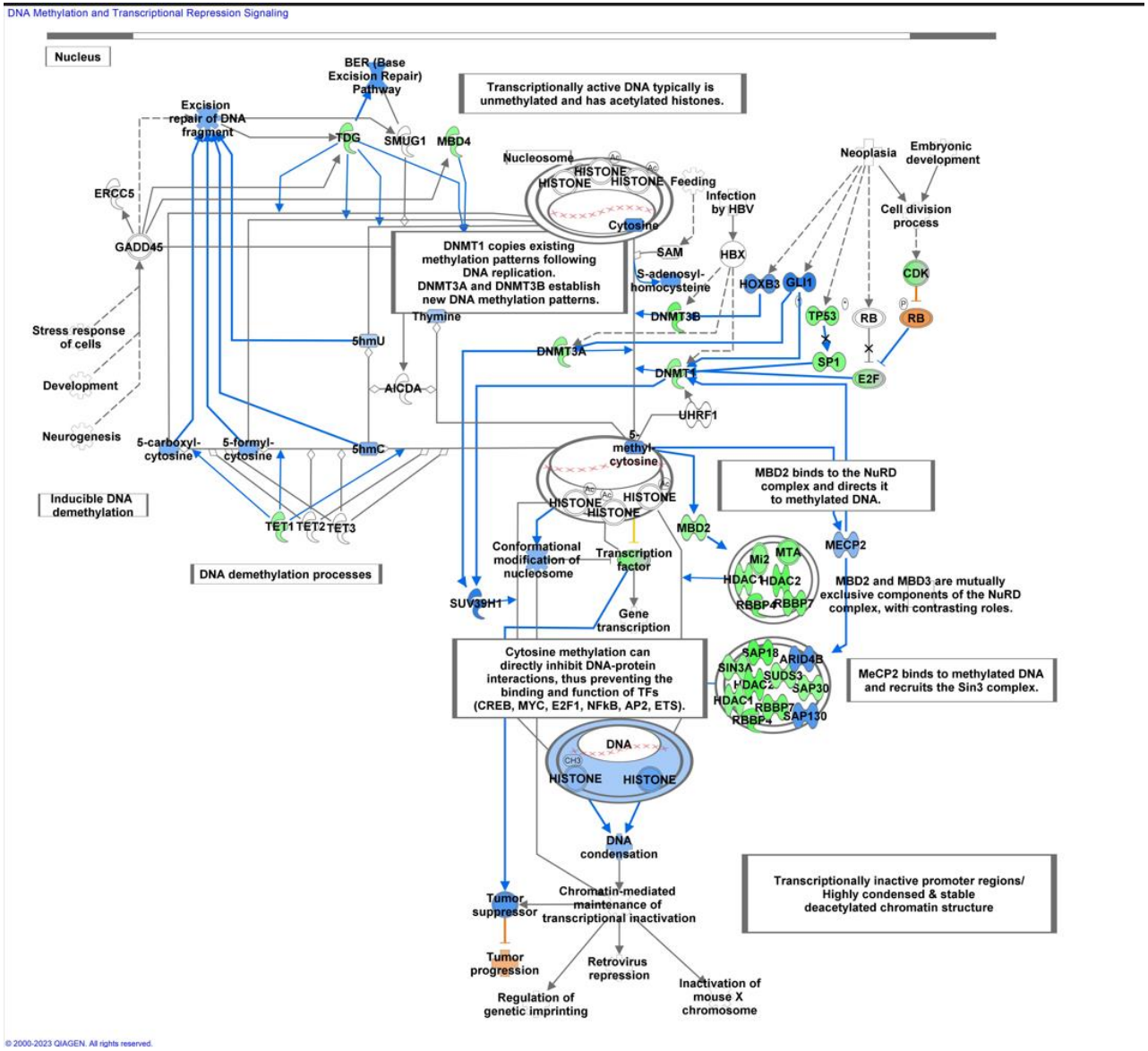


*Appendix 11:* The role of DNA methylation and transcrptional repression signalling pathway in X-chromasome inactivation of cluster 4 hESCs. Pathway analysis is performed on IPA. Red icons indicate significantly upregulated genes. Green icons indicate significantly down regulated genes. Orange and blue icons indicate predicted activeated, and predicted inhibited genes/effects respectivley.